

論文 / 著書情報
Article / Book Information

題目(和文)	炭素担持金属触媒を用いたバイオマス由来ポリオールの水素化脱酸素による有用化学物質合成に関する研究
Title(English)	Study on Hydrodeoxygenation of Biomass Derived Polyols to Value-Added Chemicals on Carbon-Supported Metal Catalyst
著者(和文)	Wang Weican
Author(English)	Weican Wang
出典(和文)	学位:博士(工学), 学位授与機関:東京工業大学, 報告番号:甲第12208号, 授与年月日:2022年9月22日, 学位の種別:課程博士, 審査員:多湖 輝興,山中 一郎,下山 裕介,山口 猛央,松本 秀行
Citation(English)	Degree:Doctor (Engineering), Conferring organization: Tokyo Institute of Technology, Report number:甲第12208号, Conferred date:2022/9/22, Degree Type:Course doctor, Examiner:,,,,
学位種別(和文)	博士論文
Type(English)	Doctoral Thesis



Tokyo Tech

Study on Hydrodeoxygenation of Biomass-Derived Polyols to Value-Added Chemicals on Carbon-Supported Metal Catalyst

By

Weican Wang

A thesis submitted to the
Faculty of the Graduate School of the
Tokyo Institute of Technology in partial fulfillment
of the requirements for the degree of
Doctor-Engineering

Department of Chemical Science and Engineering

Tokyo Institute of Technology

Tokyo, 2022

Acknowledgments

My acknowledgement and gratitude go to the following people:

I would like to first thank my advisor, Prof. Teruoki Tago, for the opportunity to perform this work in the Tago Laboratory at Tokyo Institute of Technology. I am very grateful to have been a member of the Tago group. Also, I've always appreciated your excellent personal and professional support. I would not have made it here without your optimism, advice, and support.

I'd also like to thank Dr. Hiroyasu Fujitsuka for your patient help. Your constructive suggestions always can show a clear path to me in the maze of research. I will always be grateful to you for not only teaching me so much about this work but also for teaching me the methodology of science research.

I would like to thank Dr. Kentaro Kimura, all current students (Mr. Goto, Mr. Zhang, Ms. Arayawate, Mr. Saika, Mr. Abiru, Ms. Endo, Mr. Kanomata, Mr. Kojima, Mr. Takahashi, Mr. Asami, Mr. Iizuka, Mr. Sakanushi, Ms. Nakatani, Ms. Yokosawa, Mr. Awano, Mr. Tsuchiya, and Mr. Tan) and all OBs and OGs (Mr. Kakagawa, Mr. Doike, Mr. Ding, Ms. Yamaji, Mr. Imaizumi, Mr. Tsurusako, Ms. Natnicha, Mr. Ye, Mr. Sato, Mr. Saito, Mr. Sano, and Ms. Nakatani) of Tago work group. Those wonderful times I have here will be my forever precious memories that I would never forget.

To my family, I want to thank my father and mother for always supporting me. Leaving homeland and studying abroad are always not easy, especially during this COVID pandemic period. I really appreciate you for your respecting and supporting my decisions. I would not be here without you.

Thank Ms. Fan Li (a.k.a. Don Donkey) for all the supports over the last few years. You know, you are always the special one to me.

Contents

1. Introduction.....	1
1.1 Background: road to carbon neutral.....	1
1.2 Biomass-derived compounds and its utilization.....	2
1.2.1 Lignocellulose.....	2
1.2.1 Starch	6
1.2.3 Bio-oils.....	7
1.2.4 Biomass-derived polyols.....	8
1.3 Importance of reducing oxygen contents in biomass conversion.....	10
1.4 Transformation of polyols into value-added chemicals via catalytic hydrodeoxygenation (HDO).....	11
1.4.1 Types of HDO catalyst.....	11
1.4.2 Types of HDO reaction system	17
1.4.3 Sources of H ₂ molecules	18
1.5 Motivation for this work	20
1.6 Objective of this work.....	22
1.7 Scope of this work.....	23
References.....	25
2. Synthesis of carbon-supported Cu catalysts using ion-exchange resin.....	34
2.1 Introduction.....	34
2.2 Experimental	35
2.2.1 Materials.....	35
2.2.2 Preparation of carbon-supported Cu catalysts using the ion-exchange resin method	35
2.2.3 Preparation of carbon-supported Cu catalysts by the impregnation method.....	37
2.2.4 Catalyst characterization	37
2.3 Results and discussion	40
2.3.1 Effects of catalyst preparation methods on catalyst properties	40
2.3.2 Effects of Mg addition on catalyst properties	46
2.4 Conclusions.....	53
References.....	54
3. Conversion of C ₃ polyol to value-added diols over carbon-supported metal catalysts	56
3.1 Introduction.....	56
3.2 Experimental	56
3.2.1 Materials.....	56
3.2.2 Catalytic reaction test.....	57

Study on Hydrodeoxygenation of Biomass-Derived Polyols to Value-Added Chemicals on Carbon-Supported Metal Catalyst
Weican Wang

3.3 Results and discussion	58
3.3.1 Effects of catalyst preparation methods and support on the catalytic performance of C3 HDO	58
3.3.2 Optimization of the C3 polyol HDO reaction conditions over Cu@C.....	60
3.3.3 Effect of Mg addition on catalytic performance of C3 HDO over MgCu@C catalysts.....	65
3.3.4 Catalyst stability tests for C3 polyol HDO.....	69
3.3.5 Insight into the reaction mechanism of C3 polyol HDO over Cu@C and MgCu@C....	71
3.4 Conclusions.....	74
References.....	76
4. Conversion of C4 polyol to value-added diols over carbon-supported metal catalysts	78
4.1 Introduction.....	78
4.2 Experimental.....	79
4.2.1 Materials.....	79
4.2.2 Catalytic reaction test.....	80
4.3 Results and discussion	82
4.3.1 Effects of catalyst preparation methods and supports on the catalytic performance of C4 HDO	82
4.3.2 Effects of Mg addition on catalytic performance of C4 HDO	86
4.3.3 Optimization of the C4 polyol HDO reaction conditions over Cu@C.....	89
4.3.4 Insight into the erythritol HDO pathway and mechanism over Cu@C.....	94
4.4 Conclusion	99
References.....	101
5. Conclusions and perspectives	102
Appendix 1. Effects of active metal species on C3 polyol HDO	107
A.1 Experimental.....	107
A.1.1 Materials.....	107
A.1.2 Preparation of carbon-supported bimetallic M-Cu (M = Ni, Co, Mg, Zn, Ru) catalysts by using the ion-exchange resin method.....	107
A.1.3. Catalytic reaction test.....	108
A.2 Results and discussion.....	109
A.2.1 Catalysts characterization.....	错误!未定义书签。
A.2.2 Reactivity test.....	错误!未定义书签。
List of publications	112

1. Introduction

1.1 Background: road to carbon neutral

The utilization of fossil fuels such as coal, crude oil, and natural gas has been surged since the 20th century. Nowadays, fossil fuels provide more than three quarter of the world's energy and major materials for the development of human society [1]. However, fossil-derived feedstocks are nonrenewable and human society will face a crisis of diminishing petroleum in the coming decades. Moreover, other issues such as environmental pollution and global warming are also concerned due to the excess CO₂ emission from petroleum utilization. In this regard, the utilization of biomass as alternatives to petrochemicals will be essential to solve the problem of carbon emissions and the diminishing of fossil fuels in the coming decades, because biomass is the readily available renewable carbon-based resource on earth [2]. By integrating conversion processes and equipment in a biorefinery facility, biomass can be converted into bioproducts and/or energy (**Figure 1.1**) [1]. The major utilization approaches of biomass including directly combustion to generate heat/power, thermochemical conversion to produce gases or liquids, biochemical conversion, and chemical conversion to produce various of chemicals. Particularly, catalytic conversion strategies that use biomass as feedstock to produce value-added chemicals have been widely studied in recent years, due to their wide operating conditions, high efficiency, and high economic potential [3]. Therefore, the replacement of petroleum-derived chemicals with renewable biomass materials using catalytic processes has been a major driving force for the evolution of the modern chemical industry.

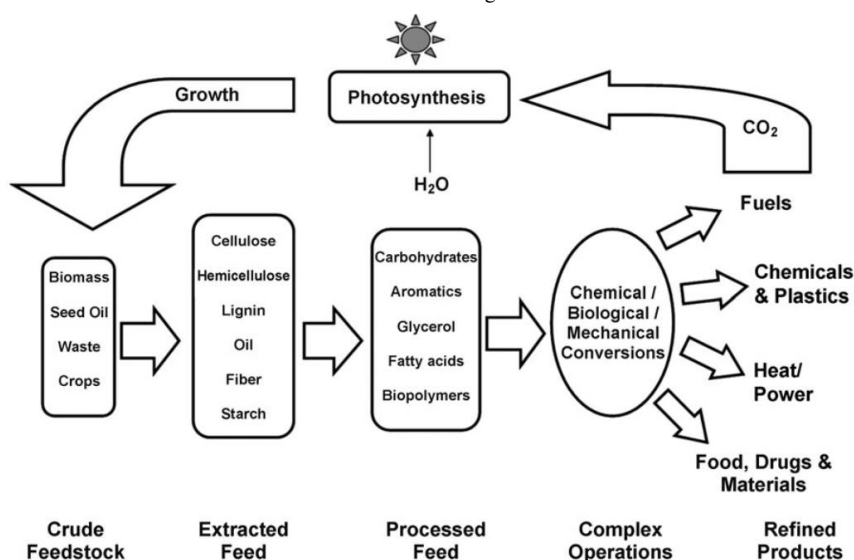


Figure 1.1: Sustainable conversion from crude biomass feedstocks to bioproducts and/or energy [1].

1.2 Biomass-derived compounds and its utilization

In general, biomass is defined as all organic matter, including crops, food, plants, and framing and forestry residues, which can be used as a source of energy. The complexity and variability of biomass should be also considered in developing conversion processes. Before the subsequent conversion to chemicals and/or bioenergy, pretreatment of biomass is a key step for the disintegration of the components. In general, pretreatments of biomass include physical pretreatment (milling, extrusion, microwave, ultrasound, ...), chemical pretreatment (acid, alkali, organosolv, ammonia fiber explosion, ...) and other physicochemical approaches. By employing these approaches, biomass can be disintegrated into individual components such as lignocellulose, oils, polyols, and the utilization of these components is discussed below.

1.2.1 Lignocellulose

Lignocellulosic biomass is the most abundant biomass material on the earth, which is produced with an amount of approximately 10-50 billion tons per year [4]. Lignocellulosic biomass can be obtained from various sources such as grass (e.g., corn stalk and wheat straw), softwood (white pine

and larch) and hardwood (Camphor and Birch). Considering the availability and security of the food supply, lignocellulosic biomass is an ideal feedstock for the production of chemicals and fuels. As shown in **Figure 1.2**, lignocellulose consists of three main biopolymer components: cellulose (40-50%), hemicellulose (20-30%), and lignin (10-35%) [5]. Each of the main components of lignocellulose can be converted to value-added chemical and/or biofuels (**Table 1.1**).

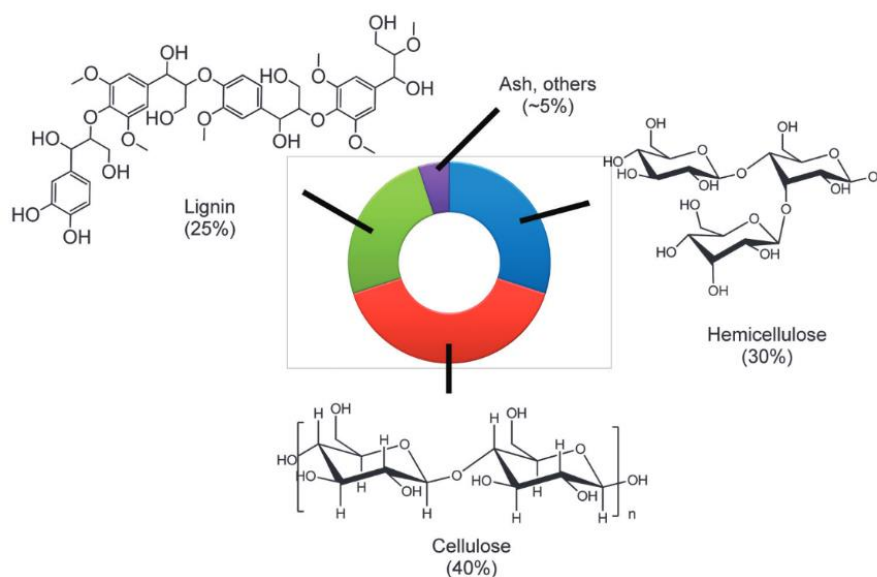


Figure 1.2: Proportion of cellulose, hemicellulose, and lignin as lignocellulose components [5].

The most abundant component in lignocellulose, i.e. cellulose, is a natural polymer of repeating D-glucose units. Cellulose has high mechanical strength and chemical stability due to intra- and intermolecular hydrogen bonds formed by hydroxyl groups in pyranose rings [2]. Therefore, to convert cellulose into biochemicals and/or biofuels, high-temperature processes such as pyrolysis and gasification are commonly applied [6]. The products of pyrolysis and gasification are mixtures of gases, oils, and solid residues that can be converted to fuels and chemicals [7]. Since cellulose is a kind of polysaccharide, it can also be transformed to its carbohydrate monomer and subsequently transformed to other platform chemicals through hydrolysis processes [8].

In contrast to cellulose, hemicellulose is a heterogeneous group of branched polysaccharides that consists of many different sugar monomers arranged in a random and amorphous structure [6].

The structural elements of hemicellulose include glucose, galactose, mannose, xylose, arabinose, and glucuronic acid. The degree of polymerization of hemicellulose is 50-200 monomers, which is much lower than that of cellulose. Compared to cellulose, hemicellulose is amorphous with little physical strength, and it can be readily hydrolyzed by dilute acids or bases.

Lignin is the third major component of lignocelluloses, which is a complex and recalcitrant phenolic macromolecule comprising phenylpropane type units [9]. The phenylpropane monomers of lignin can be categorized as guaiacyl, syringyl, and *p*-hydroxyphenyl. The specific monomer composition depends on the type of feedstock. Due to the presence of both guaiacyl and syringyl units, the hardwood lignin has higher methoxyl content, compared to the softwood lignin, which is composed of guaiacyl units only [10]. Like other biomasses, lignin can be valorized using three potential strategies [11]. First, lignin can be directly gasified or pyrolyzed to small-molecule compounds, which can be used to produce value-added chemicals using technology developed for petroleum feedstocks [12]. The second strategy is to remove the functional groups present in the lignin monomers to produce simple aromatic compounds such as phenol, benzene, toluene, and xylene [7]. In the third strategy, lignin is converted directly to valuable chemicals in a one-pot fashion, which is best suited for the production of fine chemicals with a high degree of functionality, such as vanillin [13].

Table 1.1: A summary of platform chemicals produced by chemical conversion of lignocellulosic biomass [14].

Fractions	Platform chemicals	Secondary chemicals	End-use products
Polysaccharides (Cellulose and hemicellulose)	C6, C5 Sugar alcohols (xylitol, arabitol, sorbitol, etc.)	Ethylene glycol, propylene glycol, hydroxyfuran, sugar acids	Green solvent, plastic, cosmetics, detergent, pharmaceuticals
	C3,C2 alcohols (1, 2- propylene glycol, ethylene glycol, and ethanol, etc.)	propylene ester of fatty acids, pyruvic acid, latic acid	Wetting agent, fuels, plastic, solvent, resin,
	C3 acids (propionic, malonic, 3-Hydroxy propionate, latic acid)	Propionyl acrylate, pharmaceutical intermediates and reagents, acrylates, acryl amides, propylene glycol, acrylic polymers	Water purification, dust control, gas purification, cleaners and detergents, coating, insulation, preservatives, fertilizers, pesticides, flocculants, chelators, insulation, packaging
	Levulinic acid	3-amino levulinate, succinates 2- methyltetrahydrofuran, 1,4-diols, γ -valerolactone	Molded plastics, packaging, fuels, oxygenates, resins, adhesives, insulating agents, coatings
	Furfurals	Furan Derivatives	Fuels, oxygenates, textiles, resin, adhesive, insulator agents, coatings
	Gluconic acid	Gluconolactones, esters	Cosmetics and pharmaceuticals
Lignin	Lignin monomers	Benzene, toluene, xylenes, polyols, phenols	Dyestuff, plastic, fuel, solvent, drug, paint, material applications, phenol formaldehyde resins, polyurethane foams, vanillin

1.2.1 Starch

Starch is the second most abundant organic compound on earth and could act as an effective biomass feedback for chemical production [15]. Nowadays, a large share of starch crops harvested is not only consumed as food or feed, but also a significant proportion is also used for numerous industrial applications [16].

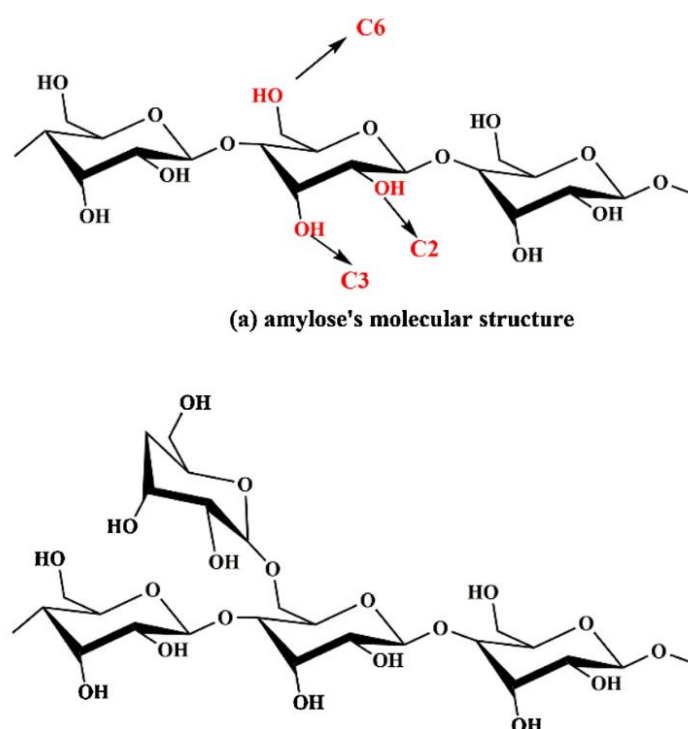


Figure 1.3: The multiscale structure of starch: (a) amylose's molecular structure and (b) molecular structure of amylopectin [17].

Starch can also be classified as a kind of polysaccharide because it is a naturally occurring blend of amylose and amylopectin (**Figure 1.3**). Amylose (M_w 10^5 – 10^6 g/mol) consists of long linear chains of glucopyranose units linked together with α -(1,4) linkages, while amylopectin (M_w 10^7 – 10^9 g/mol) contains much shorter branched chains formed with D-glucopyranose units. The ratio of amylose to amylopectin varies from 1:4 to 1:2 for standard starches [15]. Unlike cellulose, starch can undergo an easy deconstruction of its backbone to monomeric sugars because hydrolysis of α -glycosidic linkages in starch is favored over β -glycosidic linkages as in cellulose. Therefore, starch

biomass is a readily available and inexpensive feedstock for the production of simple sugars such as glucose and maltose, which can be converted to biofuels and / or important platform chemicals such as 5-hydroxymethylfurfural (HMF), 2, 5-diformylfuran (DFF), 2, 5-furandicarboxylic acid (FDCA), 2, 5-dimethylfuran (DMF), levulinic acid (LA) and sorbitol [16]. These platform chemicals can be used as possible alternatives to petroleum-based building blocks used in the commercial production of high-potential synthetic chemicals [18].

1.2.3 Bio-oils

Bio-oils are derived from biomass such as edible and non-edible vegetable oils, animal waste, microorganisms, algae, and recycled cooking greases. At present, edible vegetable oils are mainly produced bio-oils with an amount of 0.12 billion tons per year [19]. Palm oil has been reported to account for 33% of the world's production of edible vegetable oils, with soybean oil at 27% [20]. Relevant lipid classes related to bio-oils include triacylglycerols and related compounds (diacylglycerols, monoacylglycerols), hydrocarbons, ketones, alcohols, cholesterol, sterols, wax esters, free fatty acid, glycerol-phospholipids, glycerol-glycolipids, ether lipids and sphingolipids [21].

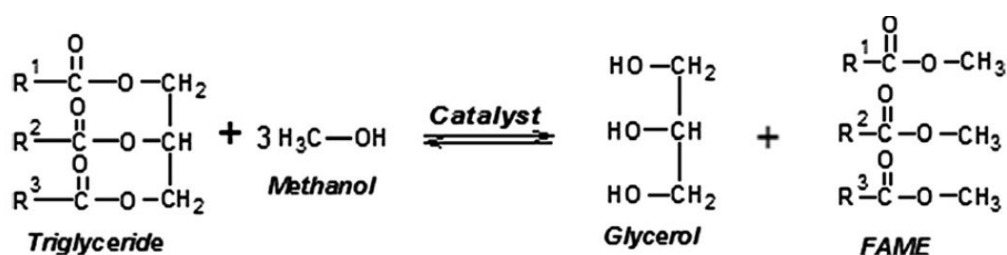


Figure 1.4: Overall transesterification reactions of triglyceride with methanol (R^1 , R^2 and R^3 are fatty acid chains) [22].

Bio-oils have been investigated as alternative feedstocks for fuels in the past decade. The main advantages of using bio-oils are that it has negligible sulfur, nitrogen, and metal contents and is carbon neutral. The use of bio-oils would mean recycling mobile carbon in contrast to the

mobilization of fixed carbon resulting from the combustion of fossil fuels. However, bio-oils are poor direct substitutes for fuels due to their high viscosity, high oxygen content, low heating values, and low volatility [23]. To valorize bio-oils into efficient substituents for diesel fuels, a transesterification process can be used to convert the key fraction in bio-oil triglycerides into fatty acid methyl esters (FAME, also known as biodiesel) as shown in **Figure 1.4** [22]. Compared to the original bio-oils, FAME has higher combustion efficiency, excellent lubricity, and comparable fuel properties as compared to petroleum-based diesel [24]. A common blend of 20% biodiesel with 80% petroleum-derived diesel (the B20 biodiesel) is widely implemented throughout the world [25]. However, the production of FAME from bio-oils also gives the unavoidable by-product, glycerol. As glycerol is a kind of biomass-derived polyol and is highly functionalized, the potential conversion of glycerol into beneficial chemicals also has gained intensive attention, which will be discussed in Section 1.1.5.

1.2.4 Biomass-derived polyols

Polyols are organic compounds containing at least two hydroxyl groups that are active for diverse organic reactions. Biomass-derived polyols, such as glycerol (C3), erythritol (C4), xylitol (C5), mannitol (C6), and sorbitol (C6), have similar chemical structures as each carbon is attached with a hydroxyl group (-OH), which can be easily derived from abundantly available biomass feedstocks [26]. The origin of biomass-derived polyols can be classified into sugars platform and bio-oils platform. C5-6 Polyols such as xylitol (C5) and sorbitol (C6) can be produced by catalytic hydrogenation of five or six carbon sugars directly obtained from crops or by hydrolysis of lignocellulosic biomass (cellulose and hemicellulose) [26–29]. Similarly, C4 polyols (namely, erythritol and threitol) can be produced by fermenting with various biomass feedstocks derived from glucose and sucrose [28]. On the other hand, the simplest biomass-derived polyol glycerol (C3) has been mass produced from biooils by transesterification/esterification reactions as a byproduct in the biodiesel industry [30].

Traditionally, biomass-derived polyols are important materials in the food industry, intermediates in the pharmaceutical industry, monomers in the polymer industry, and additives in the cosmetics industry [31]. In new biomass-based energy strategies, the valorization of these platform polyols has also been considered an option to produce value-added chemicals that provide alternative routes to conventional petrochemical-based pathways [32]. Compared to fossil materials, biomass-derived polyols are highly functionalized because of the existence of hydroxyl groups. Thus, in order to convert polyols into value-added chemicals, chemical processes that can selectively remove some of the functionalities are desired. For example, glycerol can be converted to value added chemicals such as C3 diols (1,2-propanediol and 1,3-propanediol), organic acid C3 (lactic acid), and aromatics via various reaction routes, as shown in **Figure 1.5**.

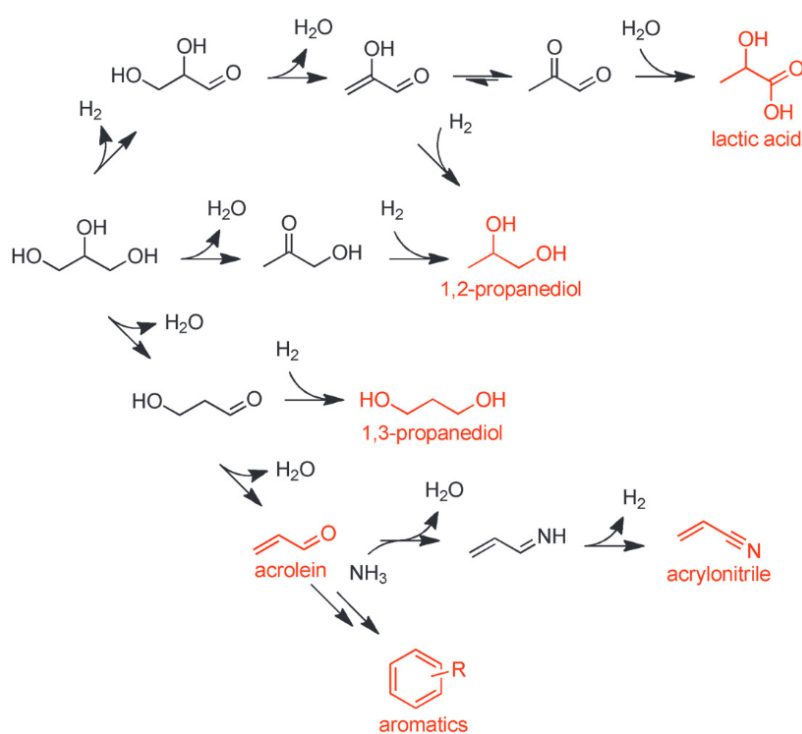


Figure 1.5: Examples of dehydrated products from glycerol [29].

1.3 Importance of reducing oxygen contents in biomass conversion

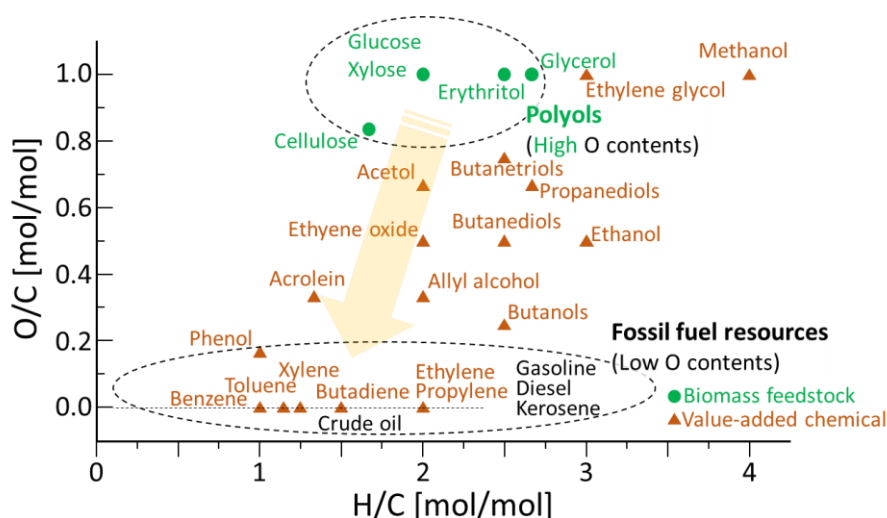
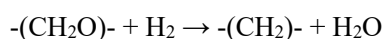


Figure 1.6: Production of value-add chemicals from biomass feedstocks [33].

As described above, biomass-derived feedstocks, such as polyols, acquire much superior oxygen contents compared to gas, coal, and crude oil obtained from petroleum resources (Figure 1.6). Therefore, it is highly desirable to selectively remove oxygen content to make it equivalent to petroleum as raw materials for value-added chemicals [34]. This process can be achieved by using an efficient technology, which is known as catalytic hydrodeoxygenation (HDO). In this process, extra oxygen contents in organic compounds are removed in the form of water by using hydrogen (gaseous hydrogen or hydrogen donors) in combination with a suitable metal catalyst. The general reaction stoichiometry of HDO may be schematically represented by [35]:



where $-(\text{CH}_2\text{O})-$ represents the carbohydrate in the biomass-derived compounds. In this process, the oxygen compounds are selectively removed without cracking the initial C-C bonds, which make the HDO processes a suitable approach for reducing the O/C ratio in biomass-derived compounds

1.4 Transformation of polyols into value-added chemicals via catalytic hydrodeoxygenation (HDO)

In this study, the catalytic HDO processes discussed are based on heterogeneous catalysts. Key factors in catalytic HDO process include: (1) types of catalyst; (2) reaction phase; and (3) hydrogen source. The pros and cons of these different reaction systems are summarized in **Table 1.2**, and will be further discussed in the next sections.

Table 1.2: Pros and Cons of different HDO reaction systems

	Pros	Cons
Catalyst type		
Noble metal catalysts	High activity	High price
	High stability	Selectivity to C-C cleavage
Transition metal catalysts	Low price	Low activity
	Selectivity to C-O cleavage	Low stability
Reaction phase		
Liquid phase	Low energy consumes	Low H ₂ solubility
Vapor phase	Feasible temperature control	High energy consumes
Source of H ₂		
External H ₂	Simple operation	Low H ₂ solubility
		Flammability problems
In site generated H ₂	High H ₂ availability Safer inert conditions	Extra operation steps

1.4.1 Types of HDO catalyst

The catalysts used for HDO reaction are typically classified into two categories based on the type of active metal used: transition metal catalysts and noble metal catalysts.

1.4.1.1 Noble metal catalysts

Noble metals, such as platinum (Pt), are known to activate hydrogen molecules. Thus, Pt-based catalysts are frequently applied for HDO of biomass-derived compounds. Checa et al. reported a

higher glycerol HDO activity of the Pt/ZnO catalyst compared to those of other noble metal catalysts. Glycerol conversion decreased in the order Pt > Rh > Pd > Au. The effects of the support of Pt-based catalysts were also investigated, the Pt-ZnO catalyst exhibited better catalytic performance than the support of SnO₂, ZrO₂, and TiO₂ due to its stronger metal-support interaction. Furthermore, the roles of Pt and support in the HDO reaction of glycerol were reported by Gandarias et al. [36]. The support (amorphous silico alumina) mainly acid sites involved in the dehydration of glycerol to acetol, while subsequent hydrogenation of acetol to 1,2-propanediol occurs at the Pt sites. Similar to Pt/alumina catalysts, HDO of polyols can be achieved by using other Pt catalysts with solid acid support, such as ZrO₂. Pt/solid base catalysts also catalyze HDO reactions. In the case of glycerol HDO, another reaction route is proposed for Pt/solid base catalysts (**Figure 1.7**, Route 2). Yuan et al. reported that the conversion of glycerol to 1,2-propanediol follows the route of dehydrogenation-dehydration-hydrogenation over Pt/hydrotalcite catalysts, which showed high activity and selectivity to 1,2-propanediol under mild conditions.

Ru is another well-known active component for activating hydrogen molecules, and Ru-based catalysts are also widely used in the HDO of polyols. In the early study by Montassier et al., Ru/active carbon (Ru/AC) showed considerable catalytic activity toward HDO polyols [37]. The combination of Ru/AC with acidic co-catalysts (liquid acids or acidic ion-exchange resins) is reported to be effective for simultaneous dehydration and hydrogenation, which subsequently improved the catalytic performance for HDO. However, the utilization of co-catalysts can cause some issues which make them less preferred. For instance, combining Ru/AC with liquid acids such as H₂SO₄ and HCl shows low dehydration activity and poor selectivity to the target product (1,2-propanediol) in the HDO of glycerol. Using acidic ion-exchange resin as a co-catalyst of Ru/AC can improve the catalyst performance but the low thermal stability and the poisoning effects of sulfur compounds in resin remain as challenges for the Ru/AC + solid acid system. Thus, using acidic supports such as gamma-Al₂O₃, SiO₂, and ZrO₂ is another possible approach to achieve both high activity and thermal resistance for HDO of polyols.

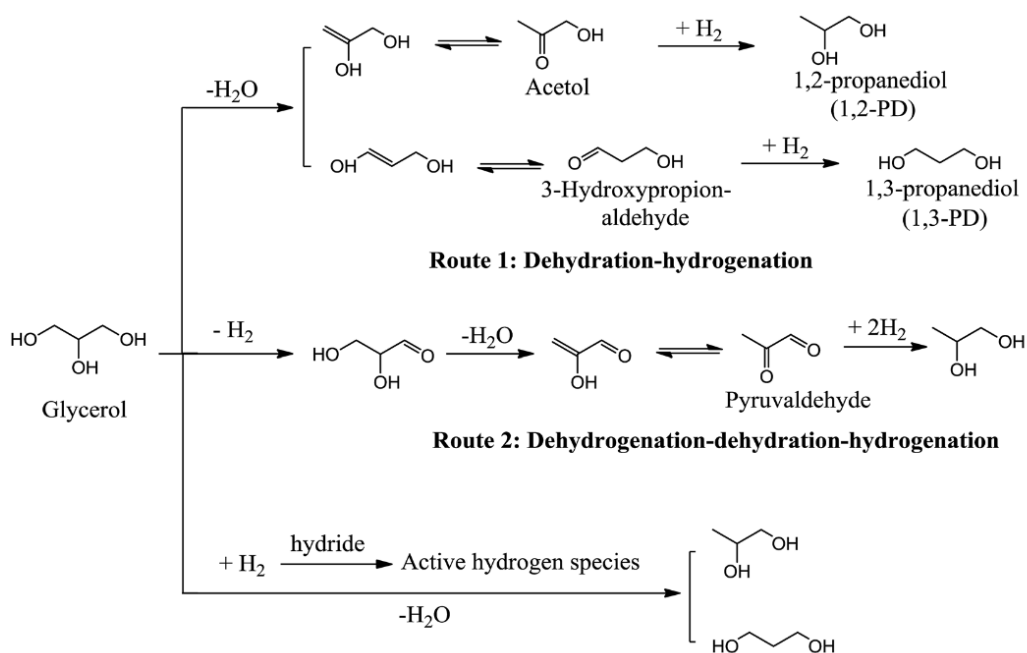


Figure 1.7: Proposed mechanisms of glycerol hydrogenolysis to produce propanediols [38].

1.4.1.2 Transition-metal-based catalysts

In the latest research, transition-metal-based catalysts have received increasing attention as a result of their low cost and high availability compared with noble-metal catalysts. Among the transition metals, Cu is the most frequently utilized metal component, because of its relatively lower price and lower ability to cleave C-C bonds compared to noble metals, and its relatively higher HDO activity among the transition metals. The catalytic performance of Cu-based catalysts depends on various parameters, i.e., the species of supports, preparation methods, catalyst additives, and HDO reaction conditions.

Cu/SiO₂ catalysts with various types of silica, such as hexagonal mesoporous silica, commercial silica gel, SBA-15, and delaminated hectorite, have been applied in HDO to produce value-added diols [39–43]. To disperse Cu nanoparticles on SiO₂ surface, significant approaches have been developed, including impregnation [40], precipitation [44], sol-gel [45], and ammonia evaporation hydrothermal method [46]. Generally, the catalytic performance of Cu/SiO₂ catalysts depends not only on the number of active Cu sites, but also on the ratio of Cu⁰/Cu⁺ due to the different functions of Cu⁰ and Cu⁺ sites in polyols HDO. Zhu et al. synthesized a robust Cu/SiO₂

catalyst using the ammonia evaporation hydrothermal method and applied the catalyst to glycerol HDO [46]. The TOF value of Cu/SiO₂ catalysts improved steadily with increasing Cu⁺/(Cu⁰ + Cu⁺) ratio, reaching a summit in the case of Cu⁺/(Cu⁰ + Cu⁺) = 0.39, and further declined with increasing ratio. The authors explained these results by proposing that Cu⁰ sites acted as the primary active sites for hydrogen activation and that Cu⁺ sites play a role to facilitate the absorbance and stabilization of the hydroxy group of glycerol. Furthermore, it was also speculated that Cu⁺ sites favored the dehydration step to produce intermediate acetol from glycerol, which subsequently hydrogenated at Cu⁰ sites to produce 1,2-propanediol. A recent analysis by Shan et al. highlights that Cu-O-Si-O structures are the primary active sites for glycerol dehydration to acetol, and Lewis acid sites derived from Cu-O-Si-O structures are a crucial prerequisite for excellent HDO performance [47]. Vasilidou et al. investigated the deactivation behavior of Cu/SiO₂ catalysts, suggesting that the deactivation of Cu/SiO₂ catalysts is commonly attributed to Cu aggregation or collapse of the mesoporous network [39].

Cu/Al₂O₃ catalysts have also been reported to be effective catalysts for polyols HDO. In the case of C3 polyol HDO, Cu/Al₂O₃ catalysts can show much higher activity and selectivity than commercial copper chromite catalysts commonly used, which is believed to be attributed to the promotion effects on the formation of reaction intermediates on support acid sites. Dmitriev et al. performed an experiment to optimize the reaction conditions of glycerol HDO in the presence of 50% Cu/Al₂O₃ in a fixed bed continuous-downflow reactor. At optimal conditions (250 °C, 5MPa H₂, superficial liquid velocity = 0.55 m³m⁻²h⁻¹) the selectivity to 1,2-propanediol reached around 91.5% with a glycerol conversion of 80-95% [48]. However, in the case of HDO C4-6 polyols, cleavage of C-C is more likely to occur on Cu/Al₂O₃ catalysts. Jin et al. reported that over a highly active Cu/CaO-Al₂O₃ catalyst, C-C cleavage of C3 polyols molecules is restrained while it is more likely to occur in the case of C4-6 polyols molecules [49], which is probably due to the degradation over solid acid sites on catalyst supports [50,51]. Although the metal-support interaction is relatively strong in Cu/Al₂O₃ catalysts, Cu aggregation remains a main challenge to achieve high

catalyst stability. The study by Liu et al. offers a method of adding a non-metallic oxide, boron oxide, to improve the stability of a Cu/Al₂O₃ catalyst and it exhibited an excellent catalytic performance during an over 120 h experimental run without obvious deactivation [52].

Cu-based catalysts supported on basic carriers such as MgO, ZnO, and hydrotalcites are also promising catalysts for production value-added diols from polyols via HDO. A 20%Cu/MgO catalysts prepared by a co-precipitation method was reported by Balaraju et al., which showed better catalytic performance to produce 1,2-propanediol from glycerol under mild reactions compared with conventional Cu-based catalysts prepared by the impregnation method [53]. A high selectivity toward 1,2-propanediol of 92% was obtained with 50% glycerol conversion at 200 °C under 40 bar H₂ for 8 h in an autoclave. The superior performance of the Cu/MgO catalysts was obtained due to the presence of bifunctional acidic and/or basic sites and the presence of strong metal–support synergetic interaction [54]. To further increase the conversion of glycerol on Cu/MgO catalysts, Yuan et al. added a small amount of NaOH to the reaction mixture to promote the attack of hydroxyl in the basic solution [55]. After the addition of NaOH, the conversion of glycerol increased from 58.4% to 82.0% at 180 °C under 3 MPa H₂ for 20 h. Similar to Cu / MgO catalysts, Cu/ZnO catalysts also showed good catalytic performance with polyols HDO [53], and the particle size of MgO or ZnO was found to have a significant influence on catalytic activity [55,56].

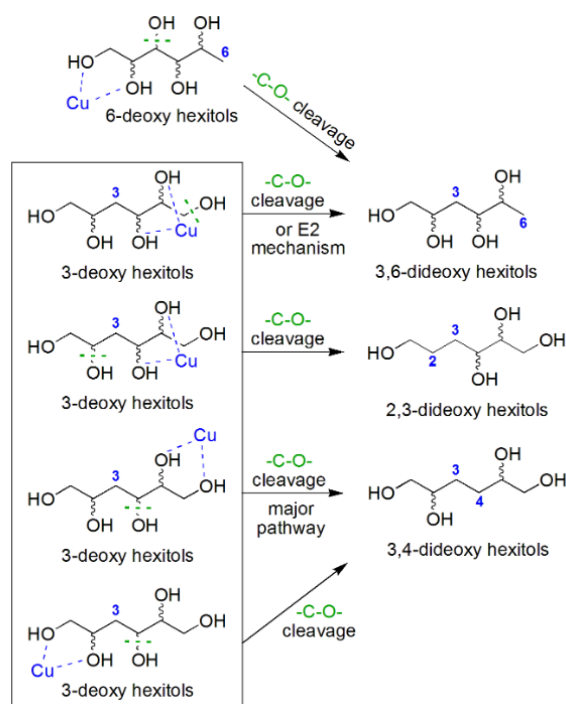


Figure 1.8: Selective -C-O- bond cleavage of 3-deoxy and 6-deoxy hexitols over Raney-Cu [57].

One of the catalytic characters of Cu-based catalyst in HDO is that diols with vicinal -OH groups are selectively produced from diols. In the case of C3 polyol HDO, 1,2-propanediol is selectively produced. As discussed above, this conversion can be explained by the dehydration-hydrogenation mechanisms which is a kinetically favored route over Cu-based catalysts. However, this mechanism can not well explain the formation of vicinal diols from polyols with longer C-C bonds such as sorbitol. Kühne et al. proposed a mechanism involves adsorption via vicinal OH-groups with cleavage of an adjacent OH-group or an OH-group with one methylene group distance, which leads to only three possible dideoxy products (**Figure 1.8**) [57]. This mechanism was found to be work well with C5 and C6 polyols as their deoxygenated products. These contradicting findings by Kühne et al. show that Cu catalysts with the same composition are able to catalyze different -C-O- bond cleavage pathways.

In addition to Cu-based catalysts, Ni- and Co-based catalysts are also active for catalyzing the HDO reactions of polyols. In general, the number of research related to Ni- and Co-based catalysts is lower than that related to Cu-based catalysts because of the lower selectivity towards HDO

products. A 63.0% glycerol conversion was achieved in RANEY Ni under mild reaction conditions of 1 MPa H₂ and 463 K, while the selectivity towards 1,2-propanediol was only 77.0% [58]. A carbothermal reduced Ni/AC catalyst prepared by Yu et al. gave 63.2% conversion of glycerol with 77.4% selectivity for 1,2-propanediol at 200 °C under 5 MPa H₂ after 24 h [59]. Likewise, a series of Co/ZnO catalysts prepared by the coprecipitation method showed the highest selectivity for 1,2-propanediol of 80% with a conversion of 70.0% glycerol at 180 °C under 4 MPa H₂ after 8 h [60].

1.4.2 Types of HDO reaction system

HDO reaction systems can be classified into several types according to their reactor configuration, the phase in which the HDO reaction taken into place, and the source of hydrogen atoms.

1.4.2.1 Liquid phase HDO

In most cases, HDO reactions of polyol are conducted in the liquid phase using a batch reactor charged with high-pressure H₂ gas. Most of the studies cited and discussed above were performed under these conditions. On the other hand, continuous processes were also investigated by some researchers because the continuous mode has its advantage in commercialization and keeping the catalyst stability. Rode et al. provides a detailed comparison between batch and continuous processes in the liquid phase [61]. The HDO of glycerol was studied as a model reaction, and modified Cu-Cr catalysts were used. This work revealed that by changing from batch to continuous process, the reaction rate was evidently accelerated (conversion increased from 34 to 65%), and the formation of undesired C-C cracking products was also suppressed due to the lower contact time. The difference in reaction rate in the batch and continuous reactors was assumed to be due to competition between hydrogen and glycerol molecules over the active sites in batch mode. Furthermore, the catalysts used in the continuous system showed high stability; no obvious deactivation occurred during 800 h time on stream. The work by Hao et al. also reported a stable

conversion from glycerol to 1,2-propanediol over a Cu-H₄SiW₁₂O₄₀/Al₂O₃ catalyst in a continuous flow reactor in the liquid phase [62]. Both glycerol conversion and HDO product selectivity were maintained at initial levels for over 250 h without catalyst deactivation.

1.4.2.2 Vapor phase HDO

Converting polyols to value-added chemicals via HDO reactions in the vapor phase is less preferred because of the high energy cost for evaporating polyols. In their 2009 study, Akiyama et al. performed the vapor phase HDO reaction of glycerol over copper metal catalysts at ambient hydrogen pressure [63]. This work presented an efficient process during which glycerol was converted into a dehydration intermediate (hydroxyacetone) at ca. 200 °C, and the following hydrogenation into HDO products was completed at approximately 120 °C. This process provided a feasible method to solve the trade-off problem between the dehydration step and the hydrogenation step in the 2-step HDO mechanism, where the dehydration step requires relatively high reaction temperatures [64], and the hydrogenation step favors low temperatures [65].

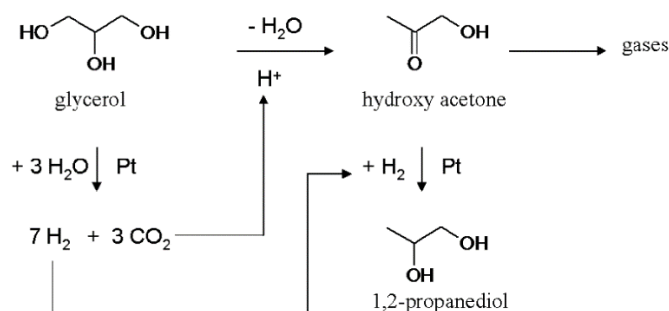


Figure 1.8: Main pathways for the conversion of glycerol into 1,2-propanediol via bifunctional catalysis with Pt/NaY [66].

1.4.3 Sources of H₂ molecules

The conversion of polyols to value-added chemicals via HDO requires the presence of hydrogen. Thus, catalytic HDO reaction systems can also be classified depending on the origin of hydrogen: externally added hydrogen type and in situ generated hydrogen type. Conventionally,

high pressure gas is used to provide hydrogen molecules for the HDO reaction. However, the use of molecular hydrogen suffers from its low solubility and flammability problems. In order to overcome these issues, HDO processes using in situ generated hydrogen was suggested. Two major strategies have been investigated to achieve this idea: to generate hydrogen by reforming the polyol reactant (aqueous phase reforming, APR) [66]; and to generate hydrogen by transfer reactions by adding a donor hydrogen compound (catalytic transfer hydrogenation, CTH) [67]. Polyol APR reactions have been studied over various types of active metals, including Pt [68,69], Ru [70], Ni [70–72] and Cu [71,72]. In the case of CTH, hydrogen molecules are obtained from externally added alcohol hydrogen donors, such as methanol [73], ethanol [74,75], and 2-propanol [76]. In addition, formic acid has attracted considerable attention from researchers as a promising hydrogen donor for polyols HDO due to its potential as a H₂ carrier and as a means of using CO₂ [73,77,78]. Given these points, the in-situ hydrogen generation system was considered as an attractive alternative for polyol HDO, because it can overcome the efficiency issues of gaseous hydrogen and allows operation under inert conditions.

1.5 Motivation for this work

Based on the reports and discussion above, it has become clear that developing renewable alternatives to petrochemicals, such as biomass, will be essential to solve the problem of carbon emissions and the diminishing of fossil fuels in the coming decades [79,80]. In particular, the conversion of biomass-derived polyols has been considered an attractive approach to produce value-added chemicals due to their high abundance and remarkable sustainability [81–83]. In particular, several studies have focused on the conversion of C3-4 polyols to produce C3-4 diols, which are widely used as important chemical building blocks and monomers in the synthesis of polymer resin [84,85].

As discussed above, the conversion of biomass-derived polyols to the corresponding diols can be achieved by selectively removing oxygen atoms in glycerol by hydrodeoxygenation (HDO) [86,87]. Generally, the HDO reaction of C3 polyol (glycerol) into the corresponding propanediols (PrD) is carried out over metal catalysts under a pressurized H₂ atmosphere [88]. Noble metal catalysts, including Pt [89], Pd [90], Ru [92,93] and Rh [94]-based catalysts, have been studied for the conversion of glycerol to PrD. In the same way, previous studies on the HDO reaction of erythritol (C4) are carried out mainly with noble metal catalysts, such as Ru, Rh, Re, Pd, Ir, and their alloys [84,91–96]. However, noble metal catalysts have some inevitable disadvantages, such as high cost and low selectivity towards HDO products due to their ability to cleave C-C bonds [97,98]. Therefore, cheaper transition metal-based catalysts have received increasing attention for polyol HDO in recent research [58,60,73,99,100]. Among these catalysts based on non-noble metals, the Cu-based catalyst is one of the most promising candidates in polyol HDO due to its relatively lower price and lower ability to cleave C-C bonds than noble metals, and relatively higher HDO activity among non-noble metals [46,101–103].

However, there are still challenges to be solved in Cu-based catalysts for polyol HDO. One of the critical problems is Cu aggregation due to the low Hüttig temperature of Cu (approximately

407 K). The sintering of Cu particles during catalyst synthesis and pretreatment leads to a low metal dispersion and a larger Cu particle size, causing the limited activities of Cu catalysts [102,104]. The aggregation of active metal particles during the reaction also causes poor stability and short lifetime of Cu catalysts [105]. Furthermore, side reactions such as oligomerization and degradation can occur over solid acid sites on catalyst supports [50,106]. To suppress side reactions, high hydrogen pressures (>2 MPa) can be applied while incurring extra cost because of the handling of pressurized hydrogen. Thus, catalysts with inert support which can show high activity and selectivity under relatively lower hydrogen pressures would be compatible choices to improve product selectivity. Thus, the development of novel Cu catalysts with highly dispersed stable Cu nanoparticles and inert support is supposed to be an effective approach to achieve a highly effective conversion of biomass.

In previous work by our group, a novel synthesis method was reported using metal-loaded ion-exchange resin as precursors [107,108]. Carbon-supported Pt, Pd, Ni, and Pt-Ni alloy catalysts with high metal dispersion (particle size of 2.3–3.8 nm observed by transmission electron microscopy) and high metal loading (>10 wt%) were prepared by this method. Because the ion-exchange resin can be ionized in a basic solution, the formation of stable metal ions in the solution is required. As Cu forms $\text{Cu}(\text{NH}_3)_2^+$ cations in concentrated ammonia solutions, similar to Pt and Ni, this preparation method can be applied to prepare carbon-supported Cu catalysts, which could be promising candidates for catalyzing the HDO reaction of biomass-derived polyols.

When the potential and challenges of selective HDO reactions for the transformations of polyols to value-added commodities are considered, comprehensive research on the HDO of polyols is necessary. Therefore, to develop new biomass valorization processes, several efforts would be made in this work to achieve efficient conversion of C3-4 polyols into diols. In particular, the development of cheap, highly active, and stable catalysts; optimization of reaction parameters and better understanding of the major and side HDO reaction pathways need to be further investigated to obtain high HDO products yield.

1.6 Objective of this work

The overall objective of this work is to develop a highly effective conversion process from biomass-derived polyols to value-added chemicals (diols) via catalytic hydrodeoxygenation (HDO). Cu-based catalysts have been shown to be promising catalysts for this process, yet the low metal dispersion and stability caused by Cu agglomeration have remained as a main challenge. New catalyst synthesis methods were developed in this work to prepare novel Cu-based catalysts, and characterizations were conducted to investigate structure-property relations of these catalysts. Reaction tests were carried out over these catalysts to study structure-activity relationships, using C3 and C4 polyols as model reactants, as well as to probe reaction mechanism of polyols. Furthermore, optimization of reaction conditions was performed to improve the yield of desired value-added HDO products (diols). These results were used to evaluate the potential for HDO of biomass-derived polyol compounds over the prepared catalysts. The insight gained from these experiments may be used to design improved Cu-based catalysts and reaction scheme for of biomass-derived polyols as well as other renewable resources to produce value-added chemicals and / or fuels.

1.7 Scope of this work

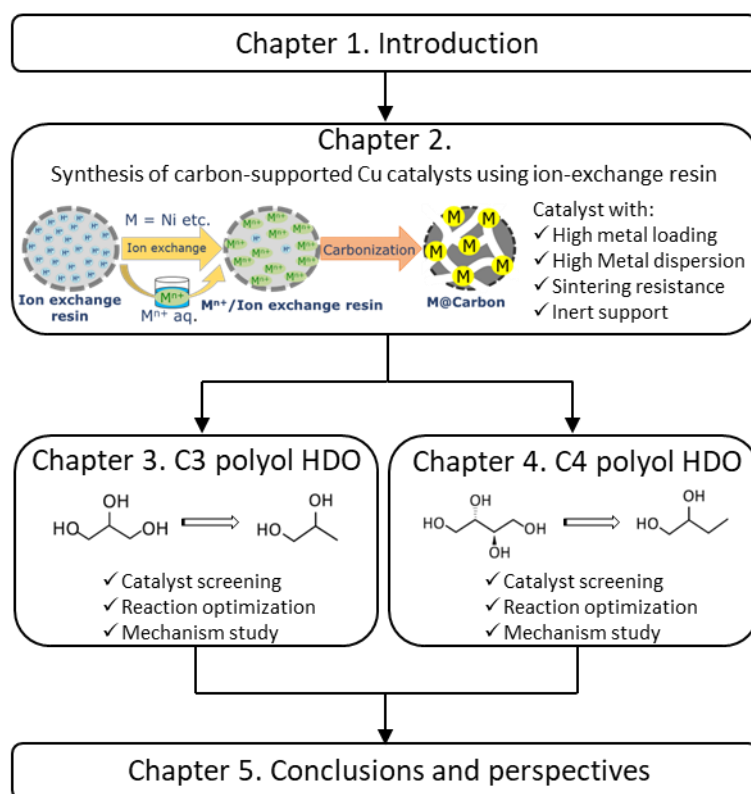


Figure 1.9: Flowchart of this work.

The flowchart of this work is illustrated in **Figure 1.9**. **Chapter 2** of this thesis is dedicated to preparing novel Cu-based catalysts which can show high activity for polyols HDO. The desired properties of the catalyst include high metal dispersion, high metal loading, and high resistance to sintering. These properties can lead to high activity and stability for catalyzing HDO reactions. In this regard, a novel method was modified to prepare carbon-supported Cu catalysts using ion-exchange resin as carbon precursor. Comparison of catalyst properties between prepared novel carbon-supported Cu catalyst and conventional Cu catalysts prepared by impregnation method on different support (activated carbon, SiO₂, Al₂O₃) was performed. In addition, to further improve the metal dispersion and sintering resistance, addition of a second metal specie (Mg) as additive was applied. A better understanding of structure-property relations for Cu-based catalyst could be obtained in this chapter.

Chapter 3 focused on applying the prepared Cu catalysts to the catalytic HDO of the C3 polyol

with simplest molecule structure (glycerol) to produce C3 diols. The activity tests of prepared Cu catalysts were conducted to screen effective catalysts for HDO. In particular, correlations between catalyst physicochemical properties and catalytic performance were addressed. Then, the reaction parameters (temperature, H₂ pressure, reaction time) should be optimized to achieve higher HDO product yield. For the catalysts which showed best performance among the prepared catalyst, reusability tests were conducted to investigate its stability. In addition, better understanding of the mechanisms involved in the catalyst was addressed to further optimize the catalyst and reaction conditions to increase the yield of the C3 diol products.

Chapter 4 reports on a detailed investigation of the conversion of larger-molecule polyol via catalytic HDO over prepared Cu-based catalysts. The results detailed in chapter 2 and 3 suggest that carbon-supported monometallic Cu and Mg-Cu bimetallic catalysts were effective for C3 HDO, thus these catalysts were applied for C4 polyol (erythritol). Similar to the case of C3 polyol conversion, screening of catalysts should be performed, and the catalyst structure-activity relationship should be addressed. Then the effects of the reaction conditions were investigated to optimize the reaction to obtain a higher C4 diol yield. Furthermore, because HDO products obtained from C4 polyols are more complicated than in the case of C3 polyol, the reaction pathways and mechanisms should be carefully checked for possible further optimization of reaction conditions to increase the yield of value-added C4 diols.

Finally, **Chapter 5** summarized the work performed in the previous chapters and concludes with final through on the conversion of biomass-derived polyols via catalytic HDO over Cu-based catalysts. It also discussed how these processes can be further improved to advance the feasibility of effective valorization of biomass-derived platform chemicals.

References

- [1] J.N. Chheda, G.W. Huber, J.A. Dumesic, Liquid-Phase Catalytic Processing of Biomass-Derived Oxygenated Hydrocarbons to Fuels and Chemicals, *Angew. Chem. Int. Ed.* 46 (2007) 7164–7183. <https://doi.org/10.1002/anie.200604274>.
- [2] J.-P. Lange, Lignocellulose Liquefaction to Biocrude: A Tutorial Review, *ChemSusChem*. 11 (2018) 997–1014. <https://doi.org/10.1002/cssc.201702362>.
- [3] K. Kohli, R. Prajapati, B.K. Sharma, Bio-Based Chemicals from Renewable Biomass for Integrated Biorefineries, *Energies*. 12 (2019) 233. <https://doi.org/10.3390/en12020233>.
- [4] S. Haghghi Mood, A. Hossein Golfeshan, M. Tabatabaei, G. Salehi Jouzani, G.H. Najafi, M. Gholami, M. Ardjmand, Lignocellulosic biomass to bioethanol, a comprehensive review with a focus on pretreatment, *Renew. Sustain. Energy Rev.* 27 (2013) 77–93. <https://doi.org/10.1016/j.rser.2013.06.033>.
- [5] C. Xu, R.A.D. Arancon, J. Labidi, R. Luque, Lignin depolymerisation strategies: towards valuable chemicals and fuels, *Chem. Soc. Rev.* 43 (2014) 7485–7500. <https://doi.org/10.1039/C4CS00235K>.
- [6] A. Yamaguchi, N. Mimura, M. Shirai, O. Sato, Cascade Utilization of Biomass: Strategy for Conversion of Cellulose, Hemicellulose, and Lignin into Useful Chemicals, *ACS Sustain. Chem. Eng.* 7 (2019) 10445–10451. <https://doi.org/10.1021/acssuschemeng.9b00786>.
- [7] Q. Bu, H. Lei, A.H. Zacher, L. Wang, S. Ren, J. Liang, Y. Wei, Y. Liu, J. Tang, Q. Zhang, R. Ruan, A review of catalytic hydrodeoxygenation of lignin-derived phenols from biomass pyrolysis, *Bioresour. Technol.* 124 (2012) 470–477. <https://doi.org/10.1016/j.biortech.2012.08.089>.
- [8] S. Sreekantan, A.A. Kirali, B. Marimuthu, Enhanced one-pot selective conversion of cellulose to ethylene glycol over NaZSM-5 supported metal catalysts, *New J. Chem.* (2021). <https://doi.org/10.1039/D1NJ03257G>.
- [9] K. Ye, Y. Liu, S. Wu, J. Zhuang, A review for lignin valorization: Challenges and perspectives in catalytic hydrogenolysis, *Ind. Crops Prod.* 172 (2021) 114008. <https://doi.org/10.1016/j.indcrop.2021.114008>.
- [10] Q. Liu, S. Wang, Y. Zheng, Z. Luo, K. Cen, Mechanism study of wood lignin pyrolysis by using TG–FTIR analysis, *J. Anal. Appl. Pyrolysis.* 82 (2008) 170–177. <https://doi.org/10.1016/j.jaap.2008.03.007>.
- [11] J. Zakzeski, P.C.A. Bruijninx, A.L. Jongerijs, B.M. Weckhuysen, The Catalytic Valorization of Lignin for the Production of Renewable Chemicals, *Chem. Rev.* 110 (2010) 3552–3599. <https://doi.org/10.1021/cr900354u>.
- [12] A. Agarwal, M. Rana, J.-H. Park, Advancement in technologies for the depolymerization of lignin, *Fuel Process. Technol.* 181 (2018) 115–132. <https://doi.org/10.1016/j.fuproc.2018.09.017>.
- [13] R. Nie, H. Yang, H. Zhang, X. Yu, X. Lu, D. Zhou, Q. Xia, Mild-temperature hydrodeoxygenation of vanillin over porous nitrogen-doped carbon black supported nickel

- nanoparticles, *Green Chem.* 19 (2017) 3126–3134. <https://doi.org/10.1039/C7GC00531H>.
- [14] Z. Yuan, W. Dai, S. Zhang, F. Wang, J. Jian, J. Zeng, H. Zhou, Heterogeneous strategies for selective conversion of lignocellulosic polysaccharides, *Cellulose*. 29 (2022) 3059–3077. <https://doi.org/10.1007/s10570-022-04434-8>.
- [15] R.F. Tester, J. Karkalas, X. Qi, Starch—composition, fine structure and architecture, *J. Cereal Sci.* 39 (2004) 151–165. <https://doi.org/10.1016/j.jcs.2003.12.001>.
- [16] S. Roy Goswami, M.-J. Dumont, V. Raghavan, Starch to value added biochemicals, *Starch - Stärke*. 68 (2016) 274–286. <https://doi.org/10.1002/star.201500058>.
- [17] X. Wang, L. Huang, C. Zhang, Y. Deng, P. Xie, L. Liu, J. Cheng, Research advances in chemical modifications of starch for hydrophobicity and its applications: A review, *Carbohydr. Polym.* 240 (2020) 116292. <https://doi.org/10.1016/j.carbpol.2020.116292>.
- [18] R.-J. van Putten, J.C. van der Waal, E. de Jong, C.B. Rasrendra, H.J. Heeres, J.G. de Vries, Hydroxymethylfurfural, A Versatile Platform Chemical Made from Renewable Resources, *Chem. Rev.* 113 (2013) 1499–1597. <https://doi.org/10.1021/cr300182k>.
- [19] M. Al-Sabawi, J. Chen, S. Ng, Fluid Catalytic Cracking of Biomass-Derived Oils and Their Blends with Petroleum Feedstocks: A Review, *Energy Fuels*. 26 (2012) 5355–5372. <https://doi.org/10.1021/ef3006417>.
- [20] M.M. Gui, K.T. Lee, S. Bhatia, Feasibility of edible oil vs. non-edible oil vs. waste edible oil as biodiesel feedstock, *Energy*. 33 (2008) 1646–1653. <https://doi.org/10.1016/j.energy.2008.06.002>.
- [21] W.W. Christie, *Lipid analysis: isolation, separation, identification, and structural analysis of lipids*, Oily Press, Bridgwater, England, 2003.
- [22] K. de Boer, P.A. Bahri, Supercritical methanol for fatty acid methyl ester production: A review, *Biomass Bioenergy*. 35 (2011) 983–991. <https://doi.org/10.1016/j.biombioe.2010.11.037>.
- [23] S. Gea, Y.A. Hutapea, A.F.R. Piliang, A.N. Pulungan, R. Rahayu, J. Layla, A.D. Tikoalu, K. Wijaya, W.D. Saputri, A Comprehensive Review of Experimental Parameters in Bio-oil Upgrading from Pyrolysis of Biomass to Biofuel Through Catalytic Hydrodeoxygenation, *BioEnergy Res.* (2022). <https://doi.org/10.1007/s12155-022-10438-w>.
- [24] A. Gharehghani, M. Mirsalim, R. Hosseini, Effects of waste fish oil biodiesel on diesel engine combustion characteristics and emission, *Renew. Energy*. 101 (2017) 930–936. <https://doi.org/10.1016/j.renene.2016.09.045>.
- [25] S.S. Chen, T. Maneerung, D.C.W. Tsang, Y.S. Ok, C.-H. Wang, Valorization of biomass to hydroxymethylfurfural, levulinic acid, and fatty acid methyl ester by heterogeneous catalysts, *Chem. Eng. J.* 328 (2017) 246–273. <https://doi.org/10.1016/j.cej.2017.07.020>.
- [26] O. Gómez-Jiménez-Aberasturi, J.R. Ochoa-Gómez, New approaches to producing polyols from biomass, *J. Chem. Technol. Biotechnol.* 92 (2017) 705–711. <https://doi.org/10.1002/jctb.5149>.
- [27] P. Furtwengler, L. Avérous, Renewable polyols for advanced polyurethane foams from diverse biomass resources, *Polym. Chem.* 9 (2018) 4258–4287. <https://doi.org/10.1039/C8PY00827B>.
- [28] X. Liu, X. Wang, S. Yao, Y. Jiang, J. Guan, X. Mu, Recent advances in the production of polyols

from lignocellulosic biomass and biomass-derived compounds, *RSC Adv.* 4 (2014) 49501–49520. <https://doi.org/10.1039/C4RA06466F>.

[29] J. ten Dam, U. Hanefeld, *Renewable Chemicals: Dehydroxylation of Glycerol and Polyols*, *ChemSusChem.* 4 (2011) 1017–1034. <https://doi.org/10.1002/cssc.201100162>.

[30] S. Bagheri, N.M. Julkapli, W.A. Yehye, Catalytic conversion of biodiesel derived raw glycerol to value added products, *Renew. Sustain. Energy Rev.* 41 (2015) 113–127. <https://doi.org/10.1016/j.rser.2014.08.031>.

[31] H. Schiweck, A. Bär, R. Vogel, E. Schwarz, M. Kunz, C. Dusautois, A. Clement, C. Lefranc, B. Lüssem, M. Moser, S. Peters, Sugar Alcohols, in: *Ullmanns Encycl. Ind. Chem.*, American Cancer Society, 2012. https://doi.org/10.1002/14356007.a25_413.pub3.

[32] B. Yin, X. Jin, G. Zhang, H. Yan, W. Zhang, X. Liu, M. Liu, C. Yang, J. Shen, Catalytic Transfer Hydrogenolysis of Bio-Polyols to Renewable Chemicals over Bimetallic PtPd/C Catalysts: Size-Dependent Activity and Selectivity, *ACS Sustain. Chem. Eng.* 8 (2020) 5305–5316. <https://doi.org/10.1021/acssuschemeng.0c00524>.

[33] 中川航司, イオン交換樹脂を前駆体とした炭素担持金属触媒による C4, C5 ポリオール類の水素化脱酸素反応系の構築, 東京工業大学, 2019.

[34] Y. Weng, T. Wang, S. Qiu, C. Wang, L. Ma, Q. Zhang, L. Chen, Y. Li, F. Sun, Q. Zhang, Aqueous-Phase Hydrodeoxygenation of Biomass Sugar Alcohol into Renewable Alkanes over a Carbon-Supported Ruthenium with Phosphoric Acid Catalytic System, *ChemCatChem.* 9 (2017) 774–781. <https://doi.org/10.1002/cctc.201601470>.

[35] K.D. Maher, D.C. Bressler, Pyrolysis of triglyceride materials for the production of renewable fuels and chemicals, *Bioresour. Technol.* 98 (2007) 2351–2368. <https://doi.org/10.1016/j.biortech.2006.10.025>.

[36] I. Gandarias, P.L. Arias, S.G. Fernández, J. Requies, M. El Doukkali, M.B. Güemez, Hydrogenolysis through catalytic transfer hydrogenation: Glycerol conversion to 1,2-propanediol, *Catal. Today.* 195 (2012) 22–31. <https://doi.org/10.1016/j.cattod.2012.03.067>.

[37] C. Montassier, J.C. Ménézo, L.C. Hoang, C. Renaud, J. Barbier, Aqueous polyol conversions on ruthenium and on sulfur-modified ruthenium, *J. Mol. Catal.* 70 (1991) 99–110. [https://doi.org/10.1016/0304-5102\(91\)85008-P](https://doi.org/10.1016/0304-5102(91)85008-P).

[38] Y. Wang, J. Zhou, X. Guo, Catalytic hydrogenolysis of glycerol to propanediols: a review, *RSC Adv.* 5 (2015) 74611–74628. <https://doi.org/10.1039/C5RA11957J>.

[39] E.S. Vasiliadou, A.A. Lemonidou, Investigating the performance and deactivation behaviour of silica-supported copper catalysts in glycerol hydrogenolysis, *Appl. Catal. Gen.* 396 (2011) 177–185. <https://doi.org/10.1016/j.apcata.2011.02.014>.

[40] E.S. Vasiliadou, T.M. Eggenhuisen, P. Munnik, P.E. de Jongh, K.P. de Jong, A.A. Lemonidou, Synthesis and performance of highly dispersed Cu/SiO₂ catalysts for the hydrogenolysis of glycerol, *Appl. Catal. B Environ.* 145 (2014) 108–119. <https://doi.org/10.1016/j.apcatb.2012.12.044>.

[41] E.S. Vasiliadou, A.A. Lemonidou, Kinetic study of liquid-phase glycerol hydrogenolysis over

- Cu/SiO₂ catalyst, *Chem. Eng. J.* 231 (2013) 103–112. <https://doi.org/10.1016/j.cej.2013.06.096>.
- [42] M.D. González, P. Salagre, R. Mokaya, Y. Cesteros, Tuning the acidic and textural properties of ordered mesoporous silicas for their application as catalysts in the etherification of glycerol with isobutene, *Catal. Today*. 227 (2014) 171–178. <https://doi.org/10.1016/j.cattod.2013.10.029>.
- [43] S. Zhu, X. Gao, Y. Zhu, Y. Zhu, H. Zheng, Y. Li, Promoting effect of boron oxide on Cu/SiO₂ catalyst for glycerol hydrogenolysis to 1,2-propanediol, *J. Catal.* 303 (2013) 70–79. <https://doi.org/10.1016/j.jcat.2013.03.018>.
- [44] Z. Huang, F. Cui, H. Kang, J. Chen, X. Zhang, C. Xia, Highly Dispersed Silica-Supported Copper Nanoparticles Prepared by Precipitation–Gel Method: A Simple but Efficient and Stable Catalyst for Glycerol Hydrogenolysis, *Chem. Mater.* 20 (2008) 5090–5099. <https://doi.org/10.1021/cm8006233>.
- [45] S. Panyad, S. Jongpatiwut, T. Sreethawong, T. Rirksomboon, S. Osuwan, Catalytic dehydroxylation of glycerol to propylene glycol over Cu–ZnO/Al₂O₃ catalysts: Effects of catalyst preparation and deactivation, *Catal. Today*. 174 (2011) 59–64. <https://doi.org/10.1016/j.cattod.2011.03.029>.
- [46] S. Zhu, X. Gao, Y. Zhu, W. Fan, J. Wang, Y. Li, A highly efficient and robust Cu/SiO₂ catalyst prepared by the ammonia evaporation hydrothermal method for glycerol hydrogenolysis to 1,2-propanediol, *Catal. Sci. Technol.* 5 (2015) 1169–1180. <https://doi.org/10.1039/C4CY01148A>.
- [47] J. Shan, H. Liu, K. Lu, S. Zhu, J. Li, J. Wang, W. Fan, Identification of the dehydration active sites in glycerol hydrogenolysis to 1,2-propanediol over Cu/SiO₂ catalysts, *J. Catal.* 383 (2020) 13–23. <https://doi.org/10.1016/j.jcat.2019.12.032>.
- [48] G.S. Dmitriev, I.S. Melchakov, V.O. Samoilov, D.N. Ramazanov, L.N. Zanaevskii, Synthesis of 1,2-Propylene Glycol in a Continuous Down-Flow Fixed-Bed Reactor With Cu/Al₂O₃ Catalyst, *ChemistrySelect*. 7 (2022) e202104257. <https://doi.org/10.1002/slct.202104257>.
- [49] X. Jin, J. Shen, W. Yan, M. Zhao, P.S. Thapa, B. Subramaniam, R.V. Chaudhari, Sorbitol Hydrogenolysis over Hybrid Cu/CaO–Al₂O₃ Catalysts: Tunable Activity and Selectivity with Solid Base Incorporation, *ACS Catal.* 5 (2015) 6545–6558. <https://doi.org/10.1021/acscatal.5b01324>.
- [50] W. Suprun, M. Lutecki, T. Haber, H. Papp, Acidic catalysts for the dehydration of glycerol: Activity and deactivation, *J. Mol. Catal. Chem.* 309 (2009) 71–78. <https://doi.org/10.1016/j.molcata.2009.04.017>.
- [51] B. Kühne, H. Vogel, R. Meusinger, S. Kunz, M. Kunz, Mechanistic study on –C–O– and –C–C– hydrogenolysis over Cu catalysts: identification of reaction pathways and key intermediates, *Catal. Sci. Technol.* 8 (2018) 755–767. <https://doi.org/10.1039/C7CY02426F>.
- [52] C. Liu, Y. Shang, S. Wang, X. Liu, X. Wang, J. Gui, C. Zhang, Y. Zhu, Y. Li, Boron oxide modified bifunctional Cu/Al₂O₃ catalysts for the selective hydrogenolysis of glucose to 1,2-propanediol, *Mol. Catal.* 485 (2020) 110514. <https://doi.org/10.1016/j.mcat.2019.110514>.
- [53] M. Balaraju, K. Jagadeeswaraiyah, P.S.S. Prasad, N. Lingaiah, Catalytic hydrogenolysis of biodiesel derived glycerol to 1,2-propanediol over Cu–MgO catalysts, *Catal. Sci. Technol.* 2 (2012)

- 1967–1976. <https://doi.org/10.1039/C2CY20059G>.
- [54] N.N. Pandhare, S.M. Pudi, P. Biswas, S. Sinha, Selective Hydrogenolysis of Glycerol to 1,2-Propanediol over Highly Active and Stable Cu/MgO Catalyst in the Vapor Phase, *Org. Process Res. Dev.* 20 (2016) 1059–1067. <https://doi.org/10.1021/acs.oprd.6b00110>.
- [55] Z. Yuan, J. Wang, L. Wang, W. Xie, P. Chen, Z. Hou, X. Zheng, Biodiesel derived glycerol hydrogenolysis to 1,2-propanediol on Cu/MgO catalysts, *Bioresour. Technol.* 101 (2010) 7088–7092. <https://doi.org/10.1016/j.biortech.2010.04.016>.
- [56] M. Balaraju, V. Rekha, P.S. Sai Prasad, R.B.N. Prasad, N. Lingaiah, Selective Hydrogenolysis of Glycerol to 1, 2 Propanediol Over Cu–ZnO Catalysts, *Catal. Lett.* 126 (2008) 119–124. <https://doi.org/10.1007/s10562-008-9590-6>.
- [57] B.B. Kühne, Investigations on the selective deoxygenation of sugar alcohols over heterogeneous catalysts, n.d.
- [58] A. Perosa, P. Tundo, Selective Hydrogenolysis of Glycerol with Raney Nickel †, *Ind. Eng. Chem. Res.* 44 (2005) 8535–8537. <https://doi.org/10.1021/ie0489251>.
- [59] W. Yu, J. Xu, H. Ma, C. Chen, J. Zhao, H. Miao, Q. Song, A remarkable enhancement of catalytic activity for KBH₄ treating the carbothermal reduced Ni/AC catalyst in glycerol hydrogenolysis, *Catal. Commun.* 11 (2010) 493–497. <https://doi.org/10.1016/j.catcom.2009.12.009>.
- [60] V. Rekha, C. Sumana, S.P. Douglas, N. Lingaiah, Understanding the role of Co in Co–ZnO mixed oxide catalysts for the selective hydrogenolysis of glycerol, *Appl. Catal. Gen.* 491 (2015) 155–162. <https://doi.org/10.1016/j.apcata.2014.10.042>.
- [61] C.V. Rode, A.A. Ghalwadkar, R.B. Mane, A.M. Hengne, S.T. Jadkar, N.S. Biradar, Selective Hydrogenolysis of Glycerol to 1,2-Propanediol: Comparison of Batch and Continuous Process Operations, *Org. Process Res. Dev.* 14 (2010) 1385–1392. <https://doi.org/10.1021/op1001897>.
- [62] S.-L. Hao, W.-C. Peng, N. Zhao, F.-K. Xiao, W. Wei, Y.-H. Sun, Hydrogenolysis of glycerol to 1,2-propanediol catalyzed by Cu-H₄SiW₁₂O₄₀/Al₂O₃ in liquid phase, *J. Chem. Technol. Biotechnol.* 85 (2010) 1499–1503. <https://doi.org/10.1002/jctb.2456>.
- [63] M. Akiyama, S. Sato, R. Takahashi, K. Inui, M. Yokota, Dehydration–hydrogenation of glycerol into 1,2-propanediol at ambient hydrogen pressure, *Appl. Catal. Gen.* 371 (2009) 60–66. <https://doi.org/10.1016/j.apcata.2009.09.029>.
- [64] S. Sato, M. Akiyama, K. Inui, M. Yokota, Selective Conversion of Glycerol into 1,2-Propanediol at Ambient Hydrogen Pressure, *Chem. Lett.* 38 (2009) 560–561. <https://doi.org/10.1246/cl.2009.560>.
- [65] L. Huang, Y.-L. Zhu, H.-Y. Zheng, Y.-W. Li, Z.-Y. Zeng, Continuous production of 1,2-propanediol by the selective hydrogenolysis of solvent-free glycerol under mild conditions, *J. Chem. Technol. Biotechnol.* 83 (2008) 1670–1675. <https://doi.org/10.1002/jctb.1982>.
- [66] E. D’Hondt, S.V. de Vyver, B.F. Sels, P.A. Jacobs, Catalytic glycerol conversion into 1,2-propanediol in absence of added hydrogen, *Chem. Commun.* (2008) 6011–6012. <https://doi.org/10.1039/B812886C>.

- [67] M.G. Musolino, L.A. Scarpino, F. Mauriello, R. Pietropaolo, Selective transfer hydrogenolysis of glycerol promoted by palladium catalysts in absence of hydrogen, *Green Chem.* 11 (2009) 1511–1513. <https://doi.org/10.1039/B915745J>.
- [68] C. Pendem, P. Gupta, N. Chaudhary, S. Singh, J. Kumar, T. Sasaki, A. Datta, R. Bal, Aqueous phase reforming of glycerol to 1,2-propanediol over Pt-nanoparticles supported on hydrotalcite in the absence of hydrogen, *Green Chem.* 14 (2012) 3107–3113. <https://doi.org/10.1039/C2GC36019E>.
- [69] I. Gandarias, P.L. Arias, J. Requies, M.B. Güemez, J.L.G. Fierro, Hydrogenolysis of glycerol to propanediols over a Pt/ASA catalyst: The role of acid and metal sites on product selectivity and the reaction mechanism, *Appl. Catal. B Environ.* 97 (2010) 248–256. <https://doi.org/10.1016/j.apcatb.2010.04.008>.
- [70] D. Roy, B. Subramaniam, R.V. Chaudhari, Aqueous phase hydrogenolysis of glycerol to 1,2-propanediol without external hydrogen addition, *Catal. Today.* 156 (2010) 31–37. <https://doi.org/10.1016/j.cattod.2010.01.007>.
- [71] R.B. Mane, C.V. Rode, Simultaneous glycerol dehydration and in situ hydrogenolysis over Cu–Al oxide under an inert atmosphere, *Green Chem.* 14 (2012) 2780–2789. <https://doi.org/10.1039/C2GC35661A>.
- [72] Z. Gao, C. Li, Y. Shao, G. Gao, Q. Xu, H. Tian, S. Zhang, X. Hu, Sequence of Ni/SiO₂ and Cu/SiO₂ in dual catalyst bed significantly impacts coke properties in glycerol steam reforming, *Int. J. Hydrog. Energy.* 46 (2021) 26367–26380. <https://doi.org/10.1016/j.ijhydene.2021.05.140>.
- [73] I. Gandarias, P.L. Arias, S.G. Fernández, J. Requies, M. El Doukkali, M.B. Güemez, Hydrogenolysis through catalytic transfer hydrogenation: Glycerol conversion to 1,2-propanediol, *Catal. Today.* 195 (2012) 22–31. <https://doi.org/10.1016/j.cattod.2012.03.067>.
- [74] S. Xia, L. Zheng, L. Wang, P. Chen, Z. Hou, Hydrogen-free synthesis of 1,2-propanediol from glycerol over Cu–Mg–Al catalysts, *RSC Adv.* 3 (2013) 16569–16576. <https://doi.org/10.1039/C3RA42543F>.
- [75] M.G. Musolino, L.A. Scarpino, F. Mauriello, R. Pietropaolo, Selective transfer hydrogenolysis of glycerol promoted by palladium catalysts in absence of hydrogen, *Green Chem.* 11 (2009) 1511–1513. <https://doi.org/10.1039/B915745J>.
- [76] I. Gandarias, P.L. Arias, J. Requies, M. El Doukkali, M.B. Güemez, Liquid-phase glycerol hydrogenolysis to 1,2-propanediol under nitrogen pressure using 2-propanol as hydrogen source, *J. Catal.* 282 (2011) 237–247. <https://doi.org/10.1016/j.jcat.2011.06.020>.
- [77] J. Yuan, S. Li, L. Yu, Y. Liu, Y. Cao, Efficient catalytic hydrogenolysis of glycerol using formic acid as hydrogen source, *Chin. J. Catal.* 34 (2013) 2066–2074. [https://doi.org/10.1016/S1872-2067\(12\)60656-1](https://doi.org/10.1016/S1872-2067(12)60656-1).
- [78] I. Gandarias, J. Requies, P.L. Arias, U. Armbruster, A. Martin, Liquid-phase glycerol hydrogenolysis by formic acid over Ni–Cu/Al₂O₃ catalysts, *J. Catal.* 290 (2012) 79–89. <https://doi.org/10.1016/j.jcat.2012.03.004>.
- [79] B. Valle, A. Remiro, N. García-Gómez, A.G. Gayubo, J. Bilbao, Recent research progress on

bio-oil conversion into bio-fuels and raw chemicals: a review, *J. Chem. Technol. Biotechnol.* 94 (2019) 670–689. <https://doi.org/10.1002/jctb.5758>.

[80] M. Besson, P. Gallezot, C. Pinel, Conversion of Biomass into Chemicals over Metal Catalysts, *Chem. Rev.* 114 (2014) 1827–1870. <https://doi.org/10.1021/cr4002269>.

[81] A.M. Ruppert, K. Weinberg, R. Palkovits, Hydrogenolysis Goes Bio: From Carbohydrates and Sugar Alcohols to Platform Chemicals, *Angew. Chem. Int. Ed.* 51 (2012) 2564–2601. <https://doi.org/10.1002/anie.201105125>.

[82] K. Tomishige, Y. Nakagawa, M. Tamura, Production of Diols from Biomass, in: Z. Fang, R.L. Smith, X. Qi (Eds.), *Prod. Platf. Chem. Sustain. Resour.*, Springer Singapore, Singapore, 2017: pp. 343–373. https://doi.org/10.1007/978-981-10-4172-3_11.

[83] G.M. Lari, G. Pastore, M. Haus, Y. Ding, S. Papadokonstantakis, C. Mondelli, J. Pérez-Ramírez, Environmental and economical perspectives of a glycerol biorefinery, *Energy Environ. Sci.* 11 (2018) 1012–1029. <https://doi.org/10.1039/C7EE03116E>.

[84] L. Liu, J. Cao, Y. Nakagawa, M. Betchaku, M. Tamura, M. Yabushita, K. Tomishige, Hydrodeoxygenation of C4–C6 sugar alcohols to diols or mono-alcohols with the retention of the carbon chain over a silica-supported tungsten oxide-modified platinum catalyst, *Green Chem.* (2021). <https://doi.org/10.1039/D1GC01486B>.

[85] J.B. Restrepo, C.D. Paternina-Arboleda, A.J. Bula, 1,2—Propanediol Production from Glycerol Derived from Biodiesel's Production: Technical and Economic Study, *Energies.* 14 (2021) 5081. <https://doi.org/10.3390/en14165081>.

[86] T. Gabrysch, M. Muhler, B. Peng, The kinetics of glycerol hydrodeoxygenation to 1,2-propanediol over Cu/ZrO₂ in the aqueous phase, *Appl. Catal. Gen.* 576 (2019) 47–53. <https://doi.org/10.1016/j.apcata.2019.03.001>.

[87] W. Wang, K. Nakagawa, T. Yoshikawa, T. Masuda, E. Fumoto, Y. Koyama, T. Tago, H. Fujitsuka, Selective aqueous phase hydrodeoxygenation of erythritol over carbon-supported Cu catalyst prepared from ion-exchange resin, *Appl. Catal. Gen.* 619 (2021) 118152. <https://doi.org/10.1016/j.apcata.2021.118152>.

[88] M. Pagliaro, R. Ciriminna, H. Kimura, M. Rossi, C. Della Pina, From Glycerol to Value-Added Products, *Angew. Chem. Int. Ed.* 46 (2007) 4434–4440. <https://doi.org/10.1002/anie.200604694>.

[89] W. Oberhauser, C. Evangelisti, R.P. Jumde, R. Psaro, F. Vizza, M. Bevilacqua, J. Filippi, B.F. Machado, P. Serp, Platinum on carbonaceous supports for glycerol hydrogenolysis: Support effect, *J. Catal.* 325 (2015) 111–117. <https://doi.org/10.1016/j.jcat.2015.03.003>.

[90] F. Mauriello, A. Vinci, C. Espro, B. Gumina, M.G. Musolino, R. Pietropaolo, Hydrogenolysis vs. aqueous phase reforming (APR) of glycerol promoted by a heterogeneous Pd/Fe catalyst, *Catal. Sci. Technol.* 5 (2015) 4466–4473. <https://doi.org/10.1039/C5CY00656B>.

[91] K. Chen, M. Tamura, Z. Yuan, Y. Nakagawa, K. Tomishige, One-Pot Conversion of Sugar and Sugar Polyols to n-Alkanes without C–C Dissociation over the Ir-ReO_x/SiO₂ Catalyst Combined with H-ZSM-5, *ChemSusChem.* 6 (2013) 613–621. <https://doi.org/10.1002/cssc.201200940>.

- [92] Y. Amada, H. Watanabe, Y. Hirai, Y. Kajikawa, Y. Nakagawa, K. Tomishige, Production of Biobutanediols by the Hydrogenolysis of Erythritol, *ChemSusChem*. 5 (2012) 1991–1999. <https://doi.org/10.1002/cssc.201200121>.
- [93] M. Gu, L. Liu, Y. Nakagawa, C. Li, M. Tamura, Z. Shen, X. Zhou, Y. Zhang, K. Tomishige, Selective Hydrogenolysis of Erythritol over Ir–ReO_x/Rutile-TiO₂ Catalyst, *ChemSusChem*. 14 (2021) 642–654. <https://doi.org/10.1002/cssc.202002357>.
- [94] N. Ota, M. Tamura, Y. Nakagawa, K. Okumura, K. Tomishige, Hydrodeoxygenation of Vicinal OH Groups over Heterogeneous Rhenium Catalyst Promoted by Palladium and Ceria Support, *Angew. Chem. Int. Ed.* 54 (2015) 1897–1900. <https://doi.org/10.1002/anie.201410352>.
- [95] A. Said, D. Da Silva Perez, N. Perret, C. Pinel, M. Besson, Selective C–O Hydrogenolysis of Erythritol over Supported Rh-ReO_x Catalysts in the Aqueous Phase, *ChemCatChem*. 9 (2017) 2768–2783. <https://doi.org/10.1002/cctc.201700260>.
- [96] A. Sadier, N. Perret, D. Da Silva Perez, M. Besson, C. Pinel, Effect of carbon chain length on catalytic C O bond cleavage of polyols over Rh-ReO_x/ZrO₂ in aqueous phase, *Appl. Catal. Gen.* 586 (2019) 117213. <https://doi.org/10.1016/j.apcata.2019.117213>.
- [97] T. Miyazawa, Y. Kusunoki, K. Kunimori, K. Tomishige, Glycerol conversion in the aqueous solution under hydrogen over Ru/C + an ion-exchange resin and its reaction mechanism, *J. Catal.* 240 (2006) 213–221. <https://doi.org/10.1016/j.jcat.2006.03.023>.
- [98] E. Maris, W. Ketchie, M. Murayama, R. Davis, Glycerol hydrogenolysis on carbon-supported PtRu and AuRu bimetallic catalysts, *J. Catal.* 251 (2007) 281–294. <https://doi.org/10.1016/j.jcat.2007.08.007>.
- [99] V. Rekha, N. Raju, C. Sumana, N. Lingaiah, Continuous Hydrogenolysis of Glycerol to 1,2-Propanediol Over Bi-metallic Ni–Ag Supported on γ -Al₂O₃ Catalysts, *Catal. Lett.* 147 (2017) 1441–1452. <https://doi.org/10.1007/s10562-017-2052-2>.
- [100] B.C.M. Morales, B.A.O. Quesada, Conversion of glycerol to hydroxyacetone over Cu and Ni catalysts, *Catal. Today*. 372 (2021) 115–125. <https://doi.org/10.1016/j.cattod.2020.11.025>.
- [101] R.J. Chimentão, P. Hirunsit, C.S. Torres, M.B. Ordoño, A. Urakawa, J.L.G. Fierro, D. Ruiz, Selective dehydration of glycerol on copper based catalysts, *Catal. Today*. 367 (2021) 58–70. <https://doi.org/10.1016/j.cattod.2020.09.031>.
- [102] N. Azri, R. Irmawati, U.I. Nda-Umar, M.I. Saiman, Y.H. Taufiq-Yap, Effect of different supports for copper as catalysts on glycerol hydrogenolysis to 1,2-propanediol, *J. King Saud Univ. - Sci.* 33 (2021) 101417. <https://doi.org/10.1016/j.jksus.2021.101417>.
- [103] R.B. Mane, A.M. Hengne, A.A. Ghalwadkar, S. Vijayanand, P.H. Mohite, H.S. Potdar, C.V. Rode, Cu:Al Nano Catalyst for Selective Hydrogenolysis of Glycerol to 1,2-Propanediol, *Catal. Lett.* 135 (2010) 141–147. <https://doi.org/10.1007/s10562-010-0276-5>.
- [104] A. Bouriakova, P.S.F. Mendes, B. Katryniok, J. De Clercq, J.W. Thybaut, Co-metal induced stabilization of alumina-supported copper: impact on the hydrogenolysis of glycerol to 1,2-propanediol, *Catal. Commun.* 146 (2020) 106134. <https://doi.org/10.1016/j.catcom.2020.106134>.

Study on Hydrodeoxygenation of Biomass-Derived Polyols to Value-Added Chemicals on Carbon-Supported Metal Catalyst

Weican Wang

- [105] C. Montassier, J.M. Dumas, P. Granger, J. Barbier, Deactivation of supported copper based catalysts during polyol conversion in aqueous phase, *Appl. Catal. Gen.* 121 (1995) 231–244. [https://doi.org/10.1016/0926-860X\(94\)00205-3](https://doi.org/10.1016/0926-860X(94)00205-3).
- [106] J. Ji, Y. Xu, Y. Liu, Y. Zhang, A nanosheet Ru/WO₃ catalyst for efficient conversion of glucose to butanediol, *Catal. Commun.* 144 (2020) 106074. <https://doi.org/10.1016/j.catcom.2020.106074>.
- [107] S. Hanprerakriengkrai, H. Fujitsuka, K. Nakagawa, H. Nakagawa, T. Tago, Preparation of carbon supported Pt-Ni alloy nanoparticle catalyst with high metal loading using cation exchange resin and its application for hydrogen production, *Chem. Eng. J.* 377 (2019) 120276. <https://doi.org/10.1016/j.cej.2018.10.213>.
- [108] H. Fujitsuka, K. Nakagawa, S. Hanprerakriengkrai, H. Nakagawa, T. Tago, Hydrogen Production from Formic Acid Using Pd/C, Pt/C, and Ni/C Catalysts Prepared from Ion-Exchange Resins, *J. Chem. Eng. Jpn.* 52 (2019) 423–429. <https://doi.org/10.1252/jcej.18we251>.

2. Synthesis of carbon-supported Cu catalysts using ion-exchange resin

2.1 Introduction

The development of novel Cu catalysts with highly dispersed stable Cu nanoparticles is supposed to be an effective approach to achieve a highly effective conversion of C3-4 polyol HDO to diols. In previous work by our group, a novel synthesis method was reported using metal-loaded ion-exchange resin as precursors [1,2]. Carbon-supported Pt, Pd, Ni, and Pt-Ni alloy catalysts with high metal dispersion (particle size of 2.3–3.8 nm observed by transmission electron microscopy) and high metal loading (>10 wt%) were prepared by this method. Because the ion-exchange resin can be ionized in a basic solution, the formation of stable metal ions in the solution is required. As Cu forms $\text{Cu}(\text{NH}_3)_2^+$ cations in concentrated ammonia solutions, similar to Pt and Ni, this preparation method can be applied to prepare carbon-supported Cu catalysts, which could be promising candidates for catalyzing the HDO reaction of biomass-derived polyols.

In addition, to further improve the metal dispersion and activity of Cu-based catalysts, other metals can be applied as additives and/or promoters. Such additives can be noble metals including Pt [3], Pd [4], and Ru [5], as well as cheaper non-noble metals including Co [6,7], Mg [8,9], and Ni [3]. A recent study by Kumar et al. involved the promotional effects of Mg^{2+} species in bimetallic Cu-Mg/SiO₂ catalysts on the selective production of 1,2-PrD from glycerol [8]. A decrease in crystallite size from 39.31 to 14.60 nm was achieved by tuning the Cu/Mg weight from 3/1 to 1/2, and the turnover frequency increased from 79.20 to 93.15 h⁻¹. Thus, to achieve effective polyols HDO over Cu-based catalysts, preparing bimetallic Cu-based catalysts by using the ion-exchange resin method can be another promising solution.

2.2 Experimental

2.2.1 Materials

All chemicals were used without further purification. $\text{Cu}(\text{NO}_3)_2 \cdot 3\text{H}_2\text{O}$ (98%), $\text{Mg}(\text{NO}_3)_2 \cdot 6\text{H}_2\text{O}$ (98%), and ammonia aqueous solution (28wt%) were purchased from FUJIFILM Wako Pure Chemical Ltd., Japan. DIAION WK-11 ion exchange resin (weakly acidic cation-exchange type, total exchange capacity: 4.3 mEq/g-resin, mean particle size: 620 μm) was purchased from Mitsubishi Chemical Corp., Japan. Activated carbon support (Norit® RX3 EXTRA) was purchased from Sigma-Aldrich Japan. Amorphous SiO_2 (JRC-SIO-12) and Al_2O_3 (JRC-ALO-07) were provided by the Catalysis Society of Japan.

2.2.2 Preparation of carbon-supported Cu catalysts using the ion-exchange resin method

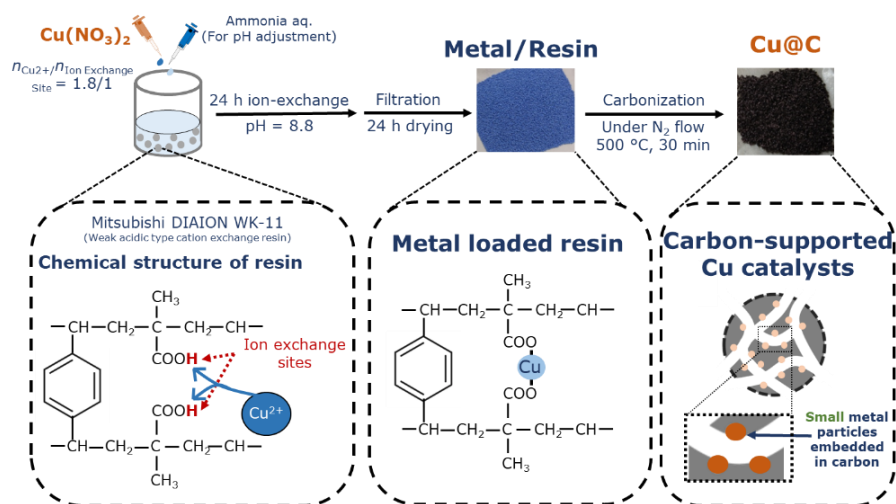


Figure 2.1: Schematic diagram of carbon-supported monometallic Cu catalyst ($\text{Cu}@C$) preparation using ion-exchange resin as a carbon precursor.

The preparation method of $\text{Cu}@C$ catalysts was modified from the method described in previous reports [1,2,10–12]. The weakly acidic cation-exchange resin, Mitsubishi DIAION WK-11, contain methacrylic acid moieties as ion-exchange sites and was used as the carbon source, while $\text{Cu}(\text{NO}_3)_2 \cdot 3\text{H}_2\text{O}$ was used as the Cu precursor. First, the Cu-loaded resin was prepared by ion exchange; 5 g of WK-11 was added to 100 mL of distilled water, and then 100 mL of

Study on Hydrodeoxygenation of Biomass-Derived Polyols to Value-Added Chemicals on Carbon-Supported Metal Catalyst
Weican Wang

$\text{Cu}(\text{NO}_3)_2$ solution (0.4 mol/L) was added dropwise to the resin solution at room temperature with stirring. In this case, the ratio of metal ions in solution to the theoretical ion exchange capacity of the resin was set at 180% mEq/mEq to realize a high metal loading. Then, the pH of the solution was adjusted to 8.8 using an aqueous ammonia solution, and the time the pH reached 8.8 was taken as the starting time of the ion exchange. The pH value was adjusted to 8.8 at 2 h and 4 h after the commencement of ion exchange. After 24 h of ion exchange, the Cu-loaded resin was collected by filtration and dried at room temperature overnight. The Cu@C catalysts were obtained by treating the Cu-loaded resin at 500 °C for 30 min under N_2 flow. The monometallic catalyst obtained was denoted Cu@C

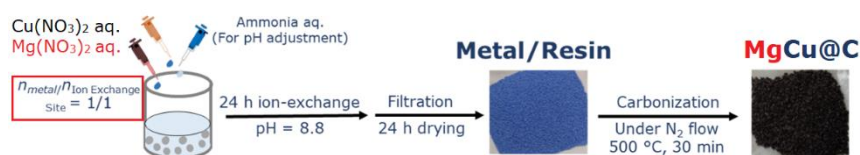


Figure 2.2: Schematic diagram of carbon-supported bimetallic $\text{M}_m\text{Cu}_n\text{@C}$ catalyst preparation using ion-exchange resin as a carbon precursor.

For the synthesis of bimetallic MgCu@C catalyst, metal precursors ($\text{Cu}(\text{NO}_3)_2$ and $\text{Mg}(\text{NO}_3)_2$) were dissolved in an aqueous solution with the designed molar ratio, then the metal solution (0.2 mol/L) was mixed with the calculated amount of WK-11 resin. The ratio of metal ions (Cu^{2+} and Mg^{2+}) in solution to the theoretical ion exchange capacity of the resin was adjusted to 100% mEq/mEq to obtain metal-loaded resin with a designed Cu/Mg ratio. The obtained bimetallic catalyst was denoted as $\text{Mg}_m\text{Cu}_n\text{@C}$, where m/n was the nominal molar ratio of Mg to Cu.

2.2.3 Preparation of carbon-supported Cu catalysts by the impregnation method

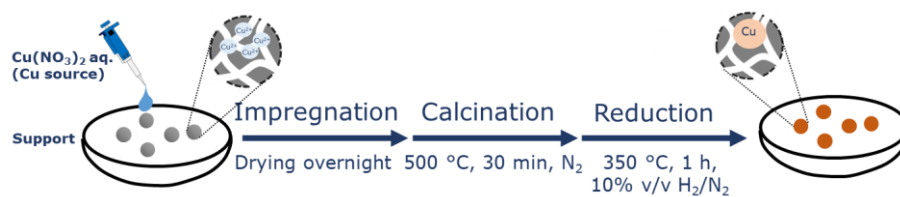


Figure 2.3: Schematic diagram of the preparation of supported monometallic Cu catalysts using the impregnation method.

The reference Cu catalysts supported on activated carbon (Cu/AC), alumina (Cu/Al₂O₃), and silica (Cu/SiO₂) were prepared by an impregnation method. Before impregnation, the supports were ground into particles with diameter ranging from 300 to 850 μm, then calcined in an N₂ atmosphere at 500 °C for 1 h to remove impurities on the support surface. After calcination of the support, a predetermined amount of Cu(NO₃)₂ solution was added and mixed with the support in a flask. After this treatment, the solvent was removed at 60 °C and 15 kPa for 1 h and the sample was dried at 110 °C in an oven overnight. Finally, the dried sample was then calcined again under an N₂ atmosphere at 500 °C for 1 h.

2.2.4 Catalyst characterization

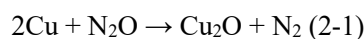
The metal loading of the prepared carbon supported catalysts was estimated using a thermogravimetric analyzer (Thermo plus Evo2 TG8120, Rigaku Corp., Japan). The sample was heated to 900 °C at a heating rate of 10 °C/min in a N₂ flow, then the feed gas was changed to air to combust the carbon support. The metal weight in the sample was calculated by assuming that the carbon content was fully combusted during measurement, and the remaining ashes were metal oxides (CuO and MgO). Metal compositions in the samples were measured using inductively coupled plasma-optical emission spectrometry (ICP-OES; 5100 VDV, Agilent Technologies Inc., Japan).

The N₂ adsorption-desorption isotherms at 77 K were collected using a high-precision

volumetric gas adsorption analyzer (BELSORP MINI X, MicrotracBEL Corp., Japan). The samples were degassed prior to the measurement under 10 Pa vacuum at 150 °C for at least 12 h.

The X-ray diffraction (XRD) patterns were recorded using an X-ray diffractometer (Smart Lab XRD, Rigaku Corp., Japan). Before measurement, the sample was reduced at 350 °C in 10% H₂/N₂ flow for 1 h. XRD measurement was performed using Cu K α radiation ($\lambda = 1.5418 \text{ \AA}$) operated at 40 kV and 45 mA, 0.02 ° step and 10 °/min scan speed. The diffraction peak observed at $2\theta = 44.3^\circ$ which corresponds to Cu (1 1 1) facet was employed to calculate the mean crystallite size (d_{XRD}) of metal particles using the Scherrer equation ($d = k\lambda/\beta_L \cos\theta$) [13], where k is the Debye-Scherrer constant (0.9), θ is the Bragg angle, and β_L is the half-width of the diffraction peak.

The exposed metal surface area was measured by N₂O titration using a catalyst analyzer (BELCAT II, MicrotracBEL Corp., Japan). The sample was first reduced at 350 °C in 50% H₂/He flow for 1 h and then cooled to 50 °C in He flow. N₂O titration was carried out by injecting 4.67% N₂O/He gas in pulse form at 50 °C. During N₂O titration, only surface Cu atoms were oxidized to Cu₂O by N₂O as the reaction equation below, and therefore surface Cu atoms can be estimated from the amount of N₂O consumed [5].



Pulse circulation stopped when the maximum pulse number of 10 or the last 3 pulses reached equilibrium (equilibrium rate < 1.2%). N₂O uptake and N₂ formation were determined by a thermal conductivity detector (TCD) equipped with a separation column. For MgCu@C catalysts, it was assumed that all N₂O uptake was consumed by Cu atoms. The surface area of the Cu metal was calculated according to Equation 2 :

$$S_{\text{N}_2\text{O}} = \frac{2n_{\text{N}_2\text{O}} \times \sigma_m}{m} = \frac{V_{\text{N}_2\text{O}} \times \frac{2}{22414} \times N_A \times \sigma_m}{m} \quad (2-2)$$

where $n_{\text{N}_2\text{O}}$ was the consumed N₂O atoms, $V_{\text{N}_2\text{O}}$ was the volume of the consumed N₂O gas at 1 atm and 0 °C, N_A was the Avogadro constant and σ_m was the cross-sectional atomic area of Cu (0.0680 nm² / atom) and m was the weight of the sample.

The morphology and average particle size (d_{TEM}) of the samples were analyzed by transmission electron microscopy (TEM) images. Before measurement, the sample was reduced at 350 °C in 10% H₂/N₂ flow for 1 h. TEM analysis was performed with a H-7650 Zero.A microscope (Hitachi High-Technologies Corp., Japan) operated at 120 kV. The mean particle sizes of the samples were estimated by calculating the number of mean diameters of the observed particles using ImageJ software. The geometric surface area (S_{TEM}) was calculated under the assumption that all Cu particles were spherical with the diameter of d_{TEM} .

The state of Mg in the catalysts was investigated by using X-ray photoelectron spectrometry (XPS), energy dispersive X-ray spectroscopy (EDS) in scanning transmission electron microscopy (STEM), and CO₂-temperature programmed desorption. The XPS spectra were acquired in a JPS-9010 (JEOL Ltd., Japan) electron spectrometer. The non-monochromatized Al-K α X-ray source was operated at 25 kV and 12 mA. Before data acquisition, the sample was reduced at 350 °C in 10% H₂/N₂ flow for 1 h and then degassed for 12 h under vacuum to minimize surface contamination. For energy calibration, a carbon 1s photoelectron line of 285 eV was used. The STEM-EDS mapping was obtained by using a STEM (JEM-2100F, JEOL Ltd., Japan) equipped with EDS (JED-2300T; JEOL Ltd., Japan). The acceleration voltage of the TEM observation was set at 200 kV. The CO₂-TPD profile was acquired using the catalyst analyzer (BELCAT II; MicrotracBEL Corp., Japan) directly connected to a quadrupole mass spectrometer (BELMASS; MicrotracBEL Corp., Japan). 100 mg of the sample was placed in the reactor tube and heated in helium flow to 350 °C and pretreated in 50 % H₂/He flow at 350 °C for 1 h. The sample was then cooled to 50 °C in helium flow and the gas flow was changed to CO₂ for 30 min. Finally, the sample was heated from 50 °C to 650 °C at 10 °C/min with recording the signal intensity of CO₂ ($m/z = 44$).

2.3 Results and discussion

2.3.1 Effects of catalyst preparation methods on catalyst properties

Metal loading, metal ratio, BET surface area, metal particle size, and metal surface area of synthesized monometallic Cu-based catalysts are presented in **Table 2.1**.

Table 2.1: Properties of the prepared monometallic Cu catalysts.

Catalyst	Cu@C	Cu/AC	Cu/SiO ₂	Cu/Al ₂ O ₃
Metal loading [wt%]	66.9	17.5	15.0 ^a	15.0 ^a
BET surface area [m ² /g _{cat}]	119	1106	66	147
Mean metal particle size; d_{XRD} [nm]	17.4	27.7	35.3	40.2
d_{TEM} [nm]	14.9	22.8	40.5	52.8
Geometric Cu surface area; S_{TEM}^b [m ² /g]	30.2	9.2	2.5	1.9
Accessible Cu surface area; $S_{N_2O}^c$ [m ² /g]	2.26	0.04	0.60	2.49
S_{N_2O} / S_{TEM} [%]	7.5	0.4	24.0	130.8

^a Nominal value

^b Calculated from d_{TEM} .

^c Calculated by N₂O titration.

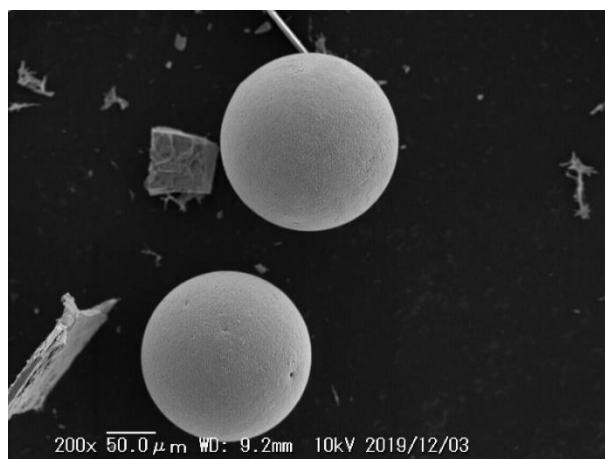


Figure 2.4: SEM image of Cu@C.

The prepared Cu@C catalyst was spherical with diameters of 200–600 μm (**Figure 2.4**), suggesting that the shape of the initial resin was maintained during the carbonization process. The high metal loading of Cu@C (66.9 wt%) was due to the high ion-exchange capability of the resin

and the high Cu concentration used during catalyst preparation.

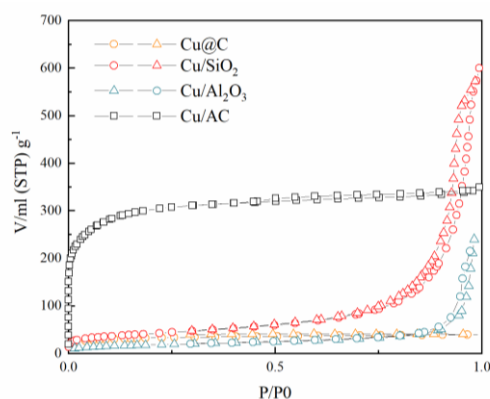


Figure 2.5: N₂ adsorption-desorption isotherms of prepared monometallic Cu catalysts.

As shown in **Figure 2.5**, the BET surface areas of Cu/AC, Cu/SiO₂, and Cu/Al₂O₃ catalysts prepared impregnation method were close to the original support material, showing that the pore structures of the supports were remained after impregnation and calcination. On the other hand, the prepared Cu@C showed type I isotherms, indicating that Cu@C was rich in micropores, and the BET surface area of Cu@C was 119 m²/g. As reported in our previous research, the BET surface area of the initial WK-11 resin is 5.7 m²/g [1]. The micropore structures in Cu@C were developed during the carbonization process, where the functional groups of the resin decomposed and produced small molecular gases (CO, CO₂, and H₂O) within the melted resin, and the diffusion of these gases created micropores in the final catalysts.

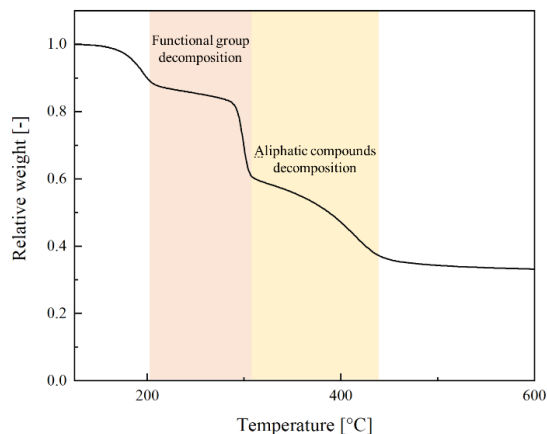


Figure 2.6: Thermogravimetric profile of Cu-loaded ion-exchange resin under N₂ atmosphere.
Heating rate = 10 °C/min.

As shown in **Figure 2.6**, the decomposition of functional groups on the ion-exchange resin and the generation of small molecular gases, such as CO, CO₂, and H₂O, proceeded at approximately 200–300 °C during carbonization process. In this step, ion-exchangeable functional groups were removed and therefore the acid sites of the carbon support disappeared. Furthermore, cleavage and recombination of carbon-carbon bonds in the resin with simultaneous production of tar (large aliphatic hydrocarbons and/or poly aromatic rings) proceeded at approximately 300 to 400 °C.

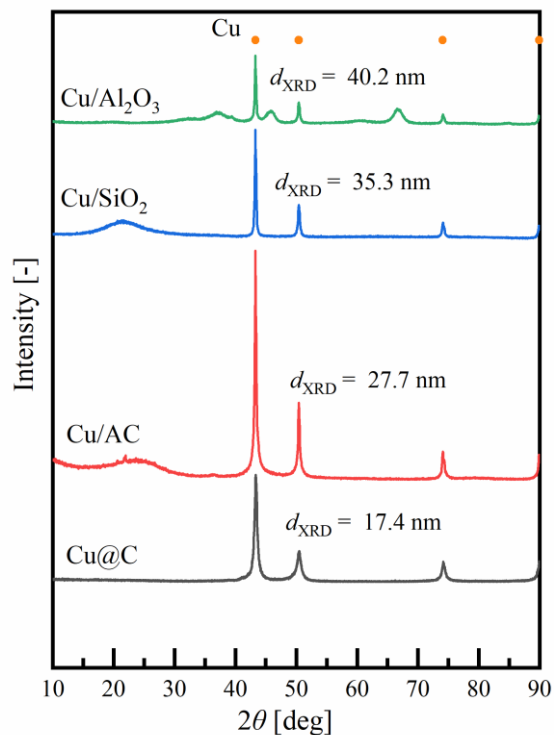


Figure 2.7: XRD patterns of fresh Cu based catalysts. Fresh catalysts were treated with H₂ at 350 °C for 1 h.

The crystal structure and particle size of Cu in the Cu@C and reference catalysts were investigated by XRD measurements. As shown in **Figure 2.7**, the diffraction peaks at around 44.3, 50.4, and 74.1° were corresponded to the (1 1 1), (2 0 0), and (2 0 2) crystal planes of metallic Cu phase (JCPDS 85–1326) [4], suggesting that Cu was successfully loaded on the supports in the metallic state for all catalysts. Diffraction peaks attributed to CuO and Cu₂O were not detectable in these samples. For all prepared Cu-based catalysts, the diffraction peaks with the highest relative intensity were observed at around $2\theta = 44.3^\circ$, and the crystalline sizes calculated from 44.3° were always 7–37 % larger than that of 50.4 and 74.1°. Therefore, these peaks observed 44.3° were applied to calculate the mean metal particles (d_{TEM}).

The particle size estimated from the XRD pattern (d_{XRD}) of Cu/AC, Cu/SiO₂, and Cu/Al₂O₃ was 27.7, 35.3, and 40.2 nm, respectively. In the XRD patterns of Cu/AC and Cu/Al₂O₃, intense sharp peaks and small broad peaks assigned to the metallic Cu phase were observed, suggesting that

the size of the metal particles in these catalysts was not uniform. The wide Cu particle size distribution of the Cu-based catalyst prepared by the impregnation method was ascribed to the severe aggregation of Cu particles because of the weak interactions between Cu and the supports during the preparation of the catalyst. On the contrary, the particle size of the Cu metal in Cu@C determined from the XRD patterns (d_{XRD}) was only 17.4 nm, which was smaller than other reference catalysts, despite the fact that Cu@C has a higher Cu loading.

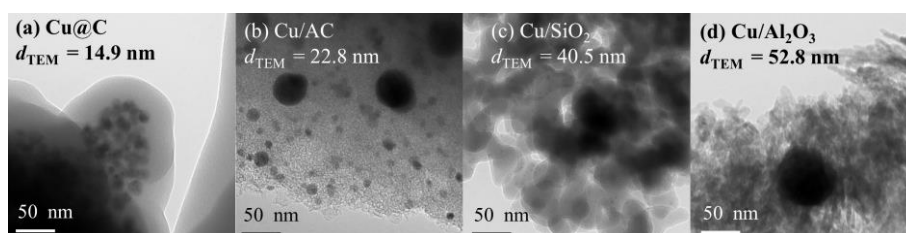


Figure 2.8: TEM images for reduced (a) Cu@C, (b) Cu/AC, (c) Cu/SiO₂, and (d) Cu/Al₂O₃.

The results of TEM observation supported the finding of XRD measurement. As shown in **Figure 2.8**, Cu particle size of Cu@C observed by TEM ($d_{TEM} = 14.9$ nm) was consistent with the d_{XRD} , indicating that the Cu particle size in Cu@C was almost uniform. In the case of Cu/AC, small Cu particles with diameter < 10 nm and large Cu particles with diameter > 50 nm were observed in Cu/AC, indicating that the Cu particles migrated over the support surface due to the high treatment temperature (calcined at 500 °C) and the weak interactions between the Cu particles and the supports [2]. As a result, large Cu particles formed by the aggregation, leading to low metal dispersion. Aggregated Cu particles were also observed in the Cu/SiO₂ and Cu/Al₂O₃ catalysts. The d_{TEM} of Cu/SiO₂ and Cu/Al₂O₃ was 40.5 and 52.8 nm, respectively. The low Cu dispersion indicated the low thermal stability of impregnation-prepared catalysts, which could be a disadvantage for catalytic activity.

The accessible Cu surface area of Cu@C estimated from N₂O titration (S_{N_2O}) was smaller than the geometric Cu surface area (S_{TEM}), indicating that the Cu particles were partially embedded in the carbon support and the entire surface of Cu particles was inaccessible to N₂O molecules. The

formation of Cu particles and the softening and melting of the resin occurred simultaneously during the carbonization step of the Cu@C preparation process. Cu particles in Cu@C were confined in the carbon support, inhibiting further aggregation of the Cu particles (Figure 2.9). Metal accessibility, which represents the ratio of accessible metal surface area to geometric area, was estimated to be 7.9%.

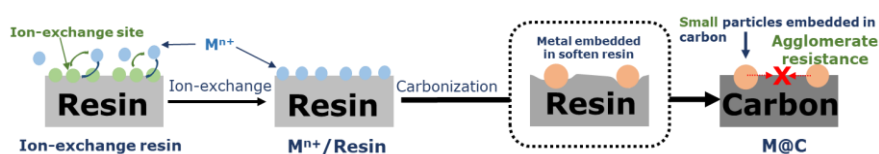


Figure 2.9: Confinement structure of Cu@C inhibiting further aggregation of Cu particles.

On the contrary, the accessible Cu surface areas of impregnation-prepared catalysts were found to depend on the support material. Cu/AC showed a small Cu surface area of $0.04 \text{ m}^2/\text{g}$, which is possibly due to the wide particle size distribution and the poisoning effects of impurities on the support. The SEM-EDS analysis (Figure 2.10) showed that Cu/AC contained sulfur (0.72 wt%) and chlorine (0.15 wt%) as impurities, which can have a strong interaction with Cu to form less reducible Cu particles that are not available for the measurement of N_2O titration. In the case of Cu/ SiO_2 and Cu/ Al_2O_3 , the accessible Cu surface areas were 0.60 and $2.49 \text{ m}^2/\text{g}$, respectively. The high Cu surface areas of Cu/ Al_2O_3 were likely derived from the high Cu surface accessibility. The ratio of the accessible Cu surface area to the geometric Cu surface area was even greater than 100%, indicating that almost all of the Cu surface was exposed and available for chemisorption.

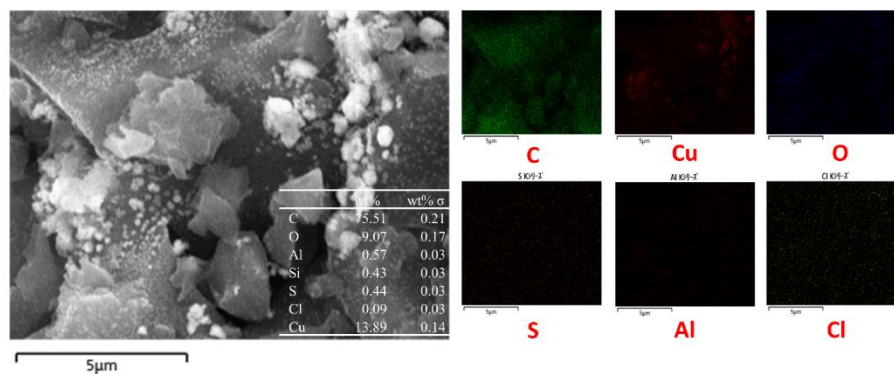


Figure 2.10: SEM-EDS and elemental mapping of Cu/AC

2.3.2 Effects of Mg addition on catalyst properties

Metal loading, metal ratio, BET surface area, metal particle size, and metal surface area of synthesized bimetallic MgCu@C catalysts are presented in **Table 2.2**.

Table 2.2: Properties of the Cu@C and MgCu@C catalysts.

Catalyst	Cu@C	Mg ₁ Cu ₁₅ @C	Mg ₁ Cu ₉ @C	Mg ₁ Cu ₄ @C
Cu loading [wt%]	66.9	57.8	56.5	52.0
Mg loading [wt%]	-	1.2	2.2	4.2
Cu/Mg ratio ^a [mol/mol]	-	17.8	10.3	4.7
BET surface area [m ² /g _{cat}]	119	76	129	12.5
Mean metal particle size; <i>d</i> _{XRD} ^b [nm]	17.4	16.5	15.0	11.6
<i>d</i> _{TEM} [nm]	14.9	13.5	12.5	10.0
Geometric Cu surface area; <i>S</i> _{TEM} ^c [m ² /g]	30.2	30.2	34.1	44.2
Accessible Cu surface area; <i>S</i> _{N₂O} ^d [m ² /g]	2.26	0.51	2.49	1.38
<i>S</i> _{N₂O} / <i>S</i> _{TEM} [%]	7.5	1.7	7.3	3.1

^a Measured by ICP-OES

^b Calculated from XRD diffraction peaks at around 44.3°

^c Calculated by *d*_{TEM}.

^d Calculated by N₂O titration.

As discussed above, the monometallic Cu@C catalyst showed a relatively high metal loading of 66.9 wt% due to the high ion exchange capacity of the high Cu concentration. Likewise, bimetallic MgCu@C catalysts prepared from ion exchange resin also showed high metal loadings (> 56 wt%). The bimetallic MgCu@C showed relatively lower metal loadings compared to those of

monometallic Cu@C because of the smaller molecular weight of magnesium and the smaller amount of loaded metal ions. During the preparation of MgCu@C, the ratio of the metal ions in solution to the theoretical ion-exchange capacity of the resin was set at 100% mEq/mEq. Because of the adsorption-desorption equilibrium of metal ions in solutions, metal ions were not fully loaded on resin, leading to a smaller actual ratio of loaded metal ions to ion-exchange capacity and the lower metal loading. The difference between Cu²⁺ and Mg²⁺ ions in the adsorption-desorption equilibrium also resulted in the slightly higher Cu/Mg molar ratio measured by ICP-OES listed in **Table 2.2**.

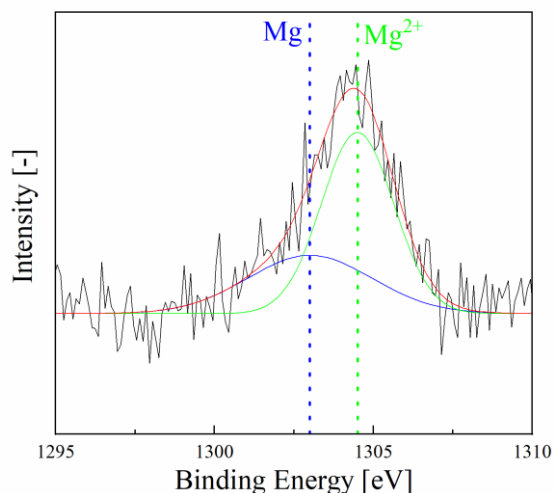


Figure 2.11: Mg 1s XPS spectra of the Mg₁Cu₉@C catalyst.

In addition, the Mg species in the MgCu@C catalysts were analyzed by XPS as shown in **Figure 2.11**. The Mg 1s peak at around binding energy = 1304.5 eV was corresponded to Mg²⁺ species and peak at 1303 eV was corresponded to metallic Mg. The larger surface area of the Mg²⁺ peak indicated that the major Mg species in MgCu@C catalysts was Mg²⁺. Furthermore, the surface atomic ratio of Cu/Mg calculated from XPS spectra using manufacture default element factor was 0.8/1 mol/mol, indicating that Mg species were highly dispersed over catalyst support and may partly cover on Cu surface, which leads to the significantly lower value compared with total Cu/Mg atomic ratio (10.3/1 mol/mol).

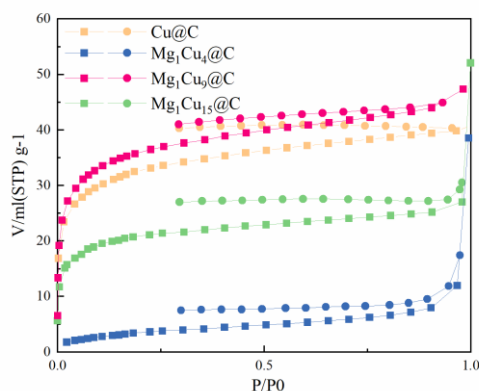


Figure 2.12: N₂ adsorption-desorption isotherms of Cu@C and MgCu@C catalysts

The N₂ adsorption-desorption isotherms of MgCu@C catalysts are shown in **Figure 2.12**. The Cu@C, Mg₁Cu₉@C, and Mg₁Cu₁₅@C catalysts showed type I isotherms corresponding to typical microporous materials. The micropore structures in these MgCu@C catalysts were developed during the carbonization process as in the original Cu@C catalyst. Therefore, the BET surface areas of these catalysts were significantly higher than the specific surface area of the original WK-11 resin (5.7 m²/g). However, the BET surface area of the Mg₁Cu₄@C catalyst was considerably lower than other catalysts prepared from ion exchange resin, which was only 12.5 m²/g. The Mg₁Cu₄@C catalysts showed type III isotherms corresponding to non-porous or macroporous materials, indicating that resin carbonization was insufficient. This result could be due to the high content of Mg²⁺ species on the surface of Mg₁Cu₄@C, which may inhibit the diffusion of gases from the inside of the resin.

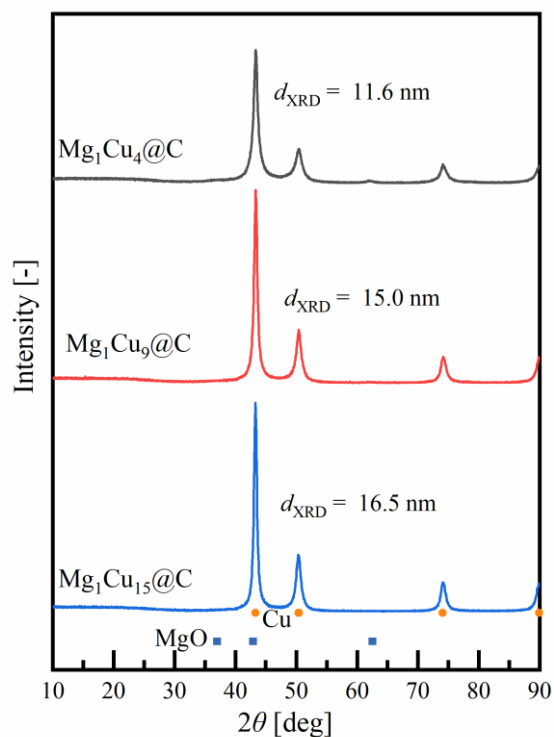


Figure 2.13: XRD patterns for the fresh MgCu@C catalysts. All samples were reduced at 350 °C in 10% H₂/N₂ flow for 1 h before the measurement.

The XRD patterns of reduced Cu@C and MgCu@C catalysts are presented in **Figure 2.13**. Diffraction peaks corresponding to metallic Cu are observed in all of the prepared catalysts. The diffraction peaks at around 44.3, 50.4, and 74.1° were corresponded to the (1 1 1), (2 0 0), and (2 0 2) crystal planes of metallic Cu phase (JCPDS 85–1326), and the diffraction peaks attributed to CuO and Cu₂O were not detectable in these samples. These results suggested that Cu was successfully load on carbon support in metallic phase. Additionally, no obvious diffraction peaks of Mg species could be observed, indicating that Mg species were highly dispersed on the MgCu@C catalysts.

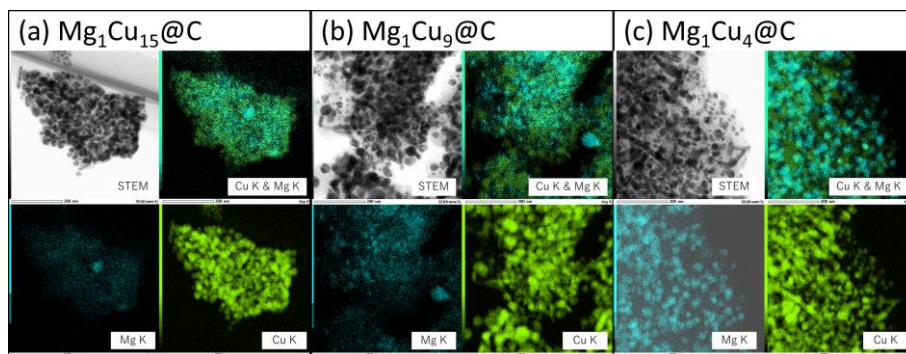


Figure 2.14: STEM-EDS images and element mapping of (a) $Mg_1Cu_{15}@C$, (b) $Mg_1Cu_9@C$, and (c) $Mg_1Cu_4@C$.

The results from XRD measurement were in accordance with the STEM-EDS images and element mapping of $MgCu@C$ catalysts (**Figure 2.14**). In the case of $Mg_1Cu_{15}@C$ and $Mg_1Cu_9@C$, Mg species were dispersed over the catalyst while Cu atoms tended to form agglomerated sphere particles, which explained the sharp diffraction peaks of Cu and no Mg diffraction peaks observed. On the other hand, for $Mg_1Cu_4@C$, whose Mg loading was 4.2 wt%, the dispersion of Mg was decreased as they tended to aggregate in specific areas. The overlapped element mapping images showed that Mg was located both in the Cu and near Cu areas. Combing the XPS analysis, these results suggested that Mg species were mainly Mg^{2+} species that highly dispersed over catalyst surface, and Mg^0 species may also existed in the form of Cu-Mg alloy.

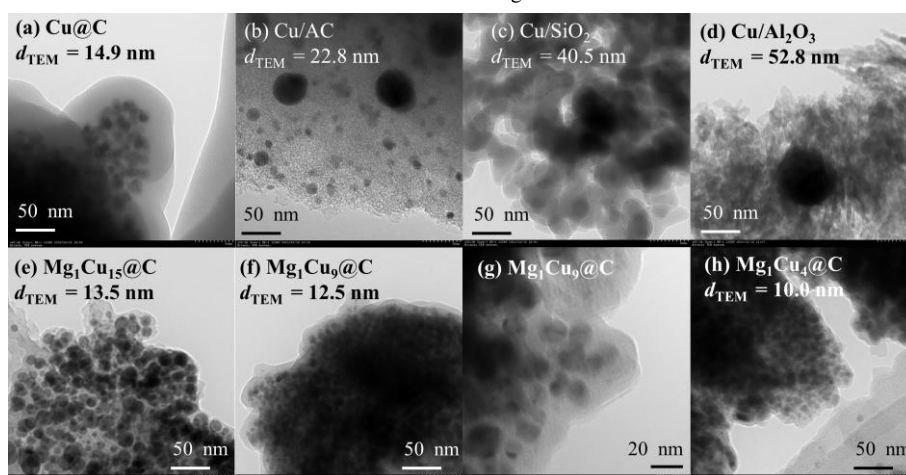


Figure 2.15: TEM images for reduced (a) Cu@C, (b) Cu/AC, (c) Cu/SiO₂, (d) Cu/Al₂O₃, (e) Mg₁Cu₁₅@C, (f, g) Mg₁Cu₉@C, and (h) Mg₁Cu₄@C.

Similar to Cu@C, MgCu@C catalysts showed small particle sizes and a uniform particle size distribution according to the XRD and TEM observations. As the amount of Mg added increased, the metal particle size decreased. As shown in **Figure 2.15**, the d_{TEM} of Mg₁Cu₁₅@C was 13.5 nm. The d_{TEM} of MgCu@C decreased to 12.5 nm when the Cu/Mg ratio was changed to 9/1 and was further decreased to 10.0 nm when the Cu/Mg ratio was further changed to 4/1. These results indicated that the addition of Mg was effective in decreasing the sizes of Cu particles. This increase in metal dispersion was probably due to the fact that Mg²⁺ species hindered the dissociation and surface diffusion of Cu atoms [14,15], which could be helpful in improving the catalytic activity of polyol HDO.

The accessible Cu surface areas of the MgCu@C samples were measured by N₂O titration. Mg₁Cu₉@C exhibited a higher Cu surface area of 2.49 m²/g compared to 2.26 m²/g of the Cu@C sample, which could be attributed to improved metal dispersion. On the contrary, the surface area of Cu decreased dramatically when the Cu/Mg ratio changed to 4/1 and 15/1. The ratios of the accessible Cu area ($S_{\text{N}_2\text{O}}$) to the surface area of geometric metal particles (S_{TEM}) in Mg₁Cu₄@C ($S_{\text{N}_2\text{O}}/S_{\text{TEM}} = 3.1\%$) and Mg₁Cu₁₅@C ($S_{\text{N}_2\text{O}}/S_{\text{TEM}} = 1.7\%$) were obviously lower than those of Cu@C ($S_{\text{N}_2\text{O}}/S_{\text{TEM}} = 7.5\%$) and Mg₁Cu₉@C ($S_{\text{N}_2\text{O}}/S_{\text{TEM}} = 7.3\%$). These values indicated that the larger moiety of Cu surfaces of Mg₁Cu₄@C and Mg₁Cu₁₅@C were covered by carbon support or Mg

species and thus not available for N_2O molecules. Together with the results of N_2 adsorption and STEM-EDS analysis, incomplete carbonization of the resin and increased Mg contents may be the reason for this negative effect.

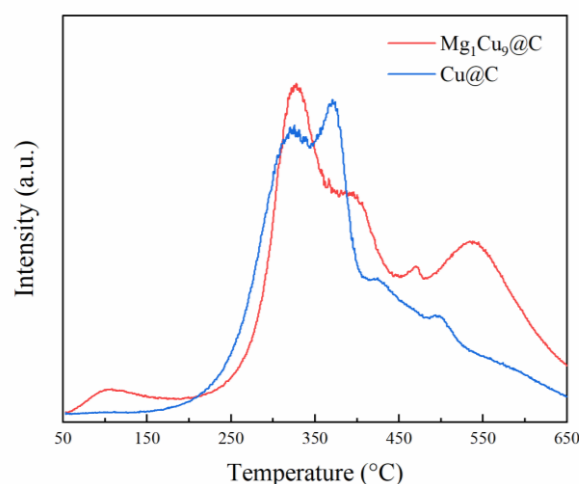


Figure 2.16: CO_2 -TPD profiles of reduced $Cu@C$ and $Mg_1Cu_9@C$.

To explore the basicity of the catalyst surface after Mg addition, the CO_2 -TPD of $Cu@C$ and $Mg_1Cu_9@C$ catalysts was studied. As shown in **Figure 2.16**, $Cu@C$ and $Mg_1Cu_9@C$ catalysts have CO_2 desorption peaks with close position at around 350 °C. However, the CO_2 desorption peaks of the $Mg_1Cu_9@C$ appeared at around 90 and 550 °C, which were not observed in $Cu@C$. In the CO_2 -TPD profile, the higher temperature of the CO_2 desorption peak means the stronger the basicity of the catalyst. Therefore, the addition of Mg strengthened the basicity of the monometallic $Cu@C$ catalyst. It was reported that base site in catalyst can promote the dehydration of polyols to form unsaturated intermediates [16]. Thus, the addition of basic Mg^{2+} species may have significant effects on the catalytic performance of polyols HDO.

2.4 Conclusions

From the above results, we concluded that the carbon-supported Cu@C catalyst with a small metal particle size ($d_{\text{TEM}} = 14.9 \text{ nm}$) was successfully prepared using an ion-exchange resin as the starting material. The higher dispersion of Cu on Cu@C was possibly due to the high dispersion of the Cu precursor on the ion-exchange resin. The high metal dispersion of Cu@C was believed to be ascribed to the confinement structure, which suppressed Cu sintering under hydrothermal reaction conditions. In particular, the high available Cu surface area ($2.3 \text{ m}^2/\text{g}$) and high metal loading ($>50 \text{ wt\% Cu}$ loading) of Cu@C indicated promising catalytic activity for catalyzing polyols HDO.

Furthermore, the addition of Mg to Cu@C further enhanced the metal dispersion of the catalyst. Characterization studies revealed that MgCu@C possessed even higher metal dispersion ($d_{\text{TEM}} < 15 \text{ nm}$) than Cu@C due to the Mg^{2+} species in the catalyst preventing dissociation and surface diffusion of Cu atoms during preparation. The addition of Mg species also enhanced the basicity of catalyst, which may have significant effects on the catalytic performance of polyols HDO.

References

- [1] S. Hanprerakriengkrai, H. Fujitsuka, K. Nakagawa, H. Nakagawa, T. Tago, Preparation of carbon supported Pt-Ni alloy nanoparticle catalyst with high metal loading using cation exchange resin and its application for hydrogen production, *Chem. Eng. J.* 377 (2019) 120276. <https://doi.org/10.1016/j.cej.2018.10.213>.
- [2] H. Fujitsuka, K. Nakagawa, S. Hanprerakriengkrai, H. Nakagawa, T. Tago, Hydrogen Production from Formic Acid Using Pd/C, Pt/C, and Ni/C Catalysts Prepared from Ion-Exchange Resins, *J. Chem. Eng. Jpn.* 52 (2019) 423–429. <https://doi.org/10.1252/jcej.18we251>.
- [3] S. Xia, Z. Yuan, L. Wang, P. Chen, Z. Hou, Hydrogenolysis of glycerol on bimetallic Pd-Cu/solid-base catalysts prepared via layered double hydroxides precursors, *Appl. Catal. Gen.* 403 (2011) 173–182. <https://doi.org/10.1016/j.apcata.2011.06.026>.
- [4] Y. Kang, X. Bu, G. Wang, X. Wang, Q. Li, Y. Feng, A Highly Active Cu–Pt/SiO₂ Bimetal for the Hydrogenolysis of Glycerol to 1,2-Propanediol, *Catal. Lett.* 146 (2016) 1408–1414. <https://doi.org/10.1007/s10562-016-1766-x>.
- [5] S. Zhu, X. Gao, Y. Zhu, W. Fan, J. Wang, Y. Li, A highly efficient and robust Cu/SiO₂ catalyst prepared by the ammonia evaporation hydrothermal method for glycerol hydrogenolysis to 1,2-propanediol, *Catal. Sci. Technol.* 5 (2015) 1169–1180. <https://doi.org/10.1039/C4CY01148A>.
- [6] W. Mondach, S. Chanklang, P. Somchuea, T. Witoon, M. Chareonpanich, K. Faungnawakij, H. Sohn, A. Seubsai, Highly efficient TiO₂-supported Co–Cu catalysts for conversion of glycerol to 1,2-propanediol, *Sci. Rep.* 11 (2021) 23042. <https://doi.org/10.1038/s41598-021-02416-7>.
- [7] N. Raju, V. Rekha, B. Abhishek, P.M. Kumar, C. Sumana, N. Lingaiah, Studies on continuous selective hydrogenolysis of glycerol over supported Cu–Co bimetallic catalysts, *New J. Chem.* 44 (2020) 3122–3128. <https://doi.org/10.1039/C9NJ04945B>.
- [8] P. Kumar, A.K. Shah, J.-H. Lee, Y.H. Park, U.L. Štangar, Selective Hydrogenolysis of Glycerol over Bifunctional Copper–Magnesium-Supported Catalysts for Propanediol Synthesis, *Ind. Eng. Chem. Res.* 59 (2020) 6506–6516. <https://doi.org/10.1021/acs.iecr.9b06978>.
- [9] S.M. Pudi, P. Biswas, S. Kumar, Selective hydrogenolysis of glycerol to 1,2-propanediol over highly active copper–magnesia catalysts: reaction parameter, catalyst stability and mechanism study, *J. Chem. Technol. Biotechnol.* 91 (2016) 2063–2075. <https://doi.org/10.1002/jctb.4802>.
- [10] A. Sharma, I. Saito, H. Nakagawa, K. Miura, Effect of carbonization temperature on the nickel crystallite size of a Ni/C catalyst for catalytic hydrothermal gasification of organic compounds, *Fuel.* 86 (2007) 915–920. <https://doi.org/10.1016/j.fuel.2006.11.001>.
- [11] A. Sharma, H. Nakagawa, K. Miura, Uniform dispersion of Ni nano particles in a carbon based catalyst for increasing catalytic activity for CH₄ and H₂ production by hydrothermal gasification, *Fuel.* 85 (2006) 2396–2401. <https://doi.org/10.1016/j.fuel.2006.04.007>.
- [12] A. Sharma, H. Nakagawa, K. Miura, A novel nickel/carbon catalyst for CH₄ and H₂ production from organic compounds dissolved in wastewater by catalytic hydrothermal gasification, *Fuel.* 85

Study on Hydrodeoxygenation of Biomass-Derived Polyols to Value-Added Chemicals on Carbon-Supported Metal Catalyst

Weican Wang

(2006) 179–184. <https://doi.org/10.1016/j.fuel.2005.04.035>.

[13] R. Jenkins, R. Snyder, Introduction to X-Ray Powder Diffractometry, John Wiley & Sons, 2012.

[14] M.D. Argyle, C.H. Bartholomew, Heterogeneous Catalyst Deactivation and Regeneration: A Review, *Catalysts*. 5 (2015) 145–269. <https://doi.org/10.3390/catal5010145>.

[15] Y. Dai, P. Lu, Z. Cao, C.T. Campbell, Y. Xia, The physical chemistry and materials science behind sinter-resistant catalysts, *Chem. Soc. Rev.* 47 (2018) 4314–4331. <https://doi.org/10.1039/C7CS00650K>.

[16] S. Basu, A.K. Sen, A Review on Catalytic Dehydration of Glycerol to Acetol, *ChemBioEng Rev.* n/a (n.d.). <https://doi.org/10.1002/cben.202100009>.

3. Conversion of C3 polyol to value-added diols over carbon-supported metal catalysts

3.1 Introduction

C3 polyol (i.e., glycerol) has been reported as one of the top 12 biomass-derived platform chemicals due to its potential of being a versatile building block [1]. Glycerol has been massively produced as a by-product of biodiesel production in the last decades [2]. Therefore, glycerol valorization is of great interest and can provide additional environmental and economic benefits to the biodiesel industry [3]. Various chemicals can be produced from glycerol, including propanediols, cyclic acetals, glycerol carbonates, glycerol esters, glycerol ethers, acrolein, and other value-add chemicals [4]. Among these chemicals, one of the HDO products converted from glycerol, 1,2-propanediol (1,2-PrD), is one of the promising chemicals that can be used in a wide variety of industrial applications, such as pharmaceuticals, detergents, polyester fibers, resins, aircraft deicing fluids, heat transfer liquids, and solvents [5]. In this chapter, the conversion of glycerol was performed over various Cu-based catalysts to produce value-added C3 diols.

3.2 Experimental

3.2.1 Materials

All chemicals were used without further purification. Glycerol (97%) and distilled water were purchased from FUJIFILM Wako Pure Chemical Ltd., Japan. 1,5-entanediol (97%) was purchased from Tokyo Chemical Industry CO., LTD., Japan.

3.2.2 Catalytic reaction test

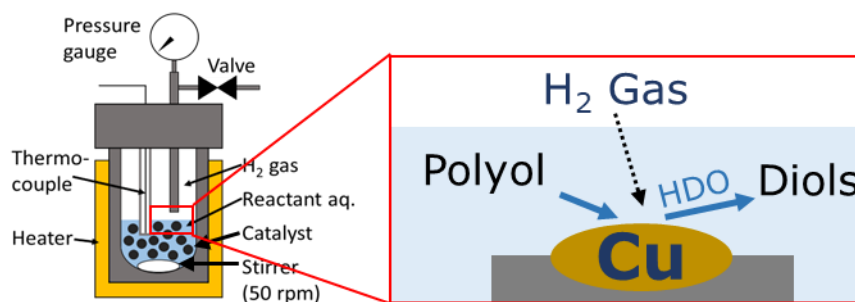


Figure 3.1: Reactor scheme of the Teflon-sealed stainless-steel batch reactor.

The liquid phase HDO of glycerol was performed in a 100 ml Teflon-sealed stainless-steel batch reactor (HIRO Corp., Japan, **Figure 3.1**). Before the reaction test, the prepared catalyst was reduced in 10% H₂/N₂ flow at 350 °C for 1 h, then ground into powder and sieved into diameters less than 100 μm. Typically, 20 g of 15 wt% polyol aqueous solution and a predetermined amount of catalyst were introduced into the reactor. The reactor was flushed with Ar gas for 3 times to purge out the remaining air, sequentially pressurized with H₂ and heated to the designed temperature. The time the reactor reached the designed temperature was taken as the starting time of the reaction. After the desired reaction time, the reactor was quenched in an ice bath to terminate the reaction. The gaseous phase products in the reactor were purged out by Ar gas and collected in a gasbag. The gaseous products were analyzed using a GC-2014 gas chromatograph (Shimadzu Co. Ltd., Japan) equipped with a TCD and a Porapak-Q column (GL Sciences Inc., Japan). The liquid products and the catalysts were separated by centrifugation and filtration. The compounds in the liquid samples were identified by a GC-2010 gas chromatograph (Shimadzu Co. Ltd., Japan) equipped with a DB-WAX column (Agilent Technologies Inc., Japan) and a Parvum 2 mass spectrometer (Shimadzu Co. Ltd., Japan). The identified liquid products were quantified using a GC-2014 gas chromatograph equipped with a DB-WAX column and a flame ionization detector (FID) using 1,5-pentanediol as internal standard. Components observed by GC-FID but could not be identified by GC-MS products were labelled “Unknown products” in the following figures and tables. The conversion of reactant

(X), product yield (Y_i), product selectivity (S_i), carbon balance (CB), and turnover frequency (TOF) were calculated according to the equations below, respectively:

$$X [\text{C-mol}\%] = \frac{\sum \text{mol of product carbon atoms}}{\text{mol of carbon atoms charged into reactor}} \times 100\% \quad (3-1)$$

$$Y_i [\text{C-mol}\%] = \frac{\text{mol of carbon atoms in } i}{\text{mol of carbon atoms charged into reactor}} \times 100\% \quad (3-1)$$

$$S_i [\text{C-mol}\%] = \frac{\text{mol of carbon atoms in } i}{\sum \text{mol of product carbon atoms}} \times 100\% \quad (3-2)$$

$$CB [\%] = \frac{\text{mol of carbon atoms recovered after reaction}}{\text{mol of carbon atoms in initial reactant}} \times 100\% \quad (3-3)$$

$$TOF [\text{h}^{-1}] = \frac{\text{mol of the converted reactant}}{\text{mol of Cu atoms on accessible surface} \times \text{Reaction time}} \quad (3-4)$$

where the number of Cu atoms accessible on the surface was estimated by N_2O titration.

3.3 Results and discussion

3.3.1 Effects of catalyst preparation methods and support on the catalytic performance of C3 HDO

First, the effects of different catalyst preparation methods and supports on the conversion of glycerol to 1,2-propanediol (1,2-PrD) were studied. Reaction tests on monometallic Cu catalysts were carried out at 180 °C under 1.2 MPa H_2 for 72 h, and the mass ratio of Cu to glycerol in the reactor was fixed at 0.05 $\text{g}_{\text{Cu}}/\text{g}_{\text{Glycerol}}$ for Cu@C, Cu/AC and Cu/ SiO_2 , and 0.03 $\text{g}_{\text{Cu}}/\text{g}_{\text{Glycerol}}$ for Cu/ Al_2O_3 to avoid the formation of slurry-like solutions.

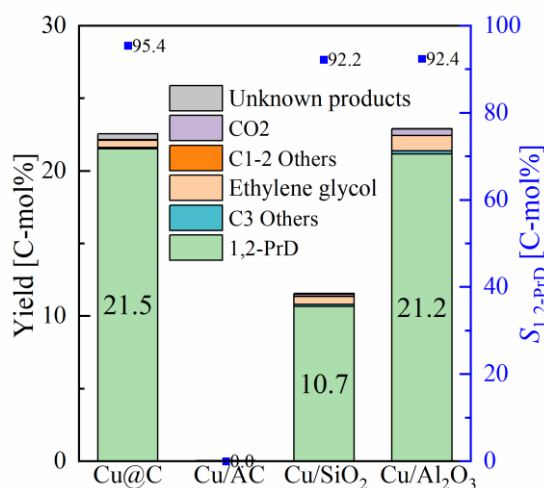


Figure 3.2: Product yields and selectivity to 1,2-PrD with the prepared Cu-based catalysts. (Reactant: 20 g of 15 wt% aqueous glycerol solution; catalyst loading: 0.05 g_{Cu}/g_{glycerol} for Cu@C, Cu/AC, and Cu/SiO₂, 0.03 g_{Cu}/g_{glycerol} for Cu/Al₂O₃; reaction temperature: 180 °C; reaction time: 72 h, initial H₂ pressure: 1.2 MPa).

Figure 3.2 shows the product yield and selectivity to 1,2-PrD over the prepared monometallic Cu catalysts. 1,2-PrD was selectively produced over Cu@C as the main HDO product with a yield ($Y_{1,2-PrD}$) of 21.5 C-mol% and a high selectivity ($S_{1,2-PrD}$) of 95.4 C-mol%. Other C₃ products (mono alcohol and propanoic acid) and cracking products (ethylene glycol, CO₂, and methanol) were also generated at small yields. Furthermore, hydroxyacetone was produced over Cu@C with a selectivity of 0.3 C-mol%. The existence of hydroxyacetone suggested that the HDO of glycerol over Cu@C could proceed via the dehydrogenation-hydrogenation route, which is further investigated in **Section 3.3.5**. The carbon balance for Cu@C was 100.4 %, indicating that compounds that could not be detected by GC, such as oligomerized products and highly oxygenated compounds, were not produced over Cu@C. These results suggest that the Cu@C catalyst was able to selectively remove a terminal -OH group in glycerol to produce value-added 1,2-PrD, and the high activity and selectivity could be attributed to the high Cu dispersion and the inert carbon support.

In contrast, carbon-supported Cu catalyst prepared from the impregnation method (Cu/AC) showed almost no activity for glycerol HDO. The $X_{glycerol}$ was only 0.1 C-mol% and no HDO

products were produced. The low Cu surface area measured by N_2O titration suggested that the low activity of Cu/AC may also be due to the poisoning effect of impurities on the activated carbon support.

In the case of the monometallic Cu catalyst supported on SiO_2 and Al_2O_3 , the main HDO product was 1,2-PrD and ethylene glycerol, CO_2 , hydroxyacetone, and other unknown products were produced. The glycerol conversion over Cu/ SiO_2 and Cu/ Al_2O_3 was 11.0 and 22.9 C-mol%, respectively. The TOF value of Cu/ SiO_2 and Cu/ Al_2O_3 was 3.33 and 3.23 h^{-1} , respectively. Close TOF values suggested that the difference in glycerol conversion between Cu/ SiO_2 and Cu/ Al_2O_3 was mainly due to the difference in the exposed surface area of Cu. Compared to Cu@C, Cu/ SiO_2 and Cu/ Al_2O_3 catalysts exhibited lower selectivities for 1,2-PrD and higher selectivities for cracking products. The selectivities towards 1,2-PrD were 95.4, 92.2, and 92.4 C-mol% over Cu@C, Cu/ SiO_2 , and Cu/ Al_2O_3 , respectively, while the selectivities toward C1-2 products were 2.3, 6.2, and 6.5 C-mol%, respectively. The interaction between the Cu and SiO_2 support has been reported to generate Lewis acid sites [6], which can be active sites to catalyze side reactions. Therefore, the higher selectivity to cracking products for Cu/ SiO_2 and Cu/ Al_2O_3 could be explained by the side reactions that occur on the silica and alumina supports.

Taken together, these findings demonstrated that the Cu@C catalyst prepared by the novel ion-exchange resin method showed catalytic activity higher than that of the carbon-supported catalysts prepared by the impregnation method and exhibited higher selectivity to the desired HDO product compared to that of other Cu catalysts prepared with different supports, which could be attributed to the highly dispersed Cu particles and the use of carbon support without solid acid sites.

3.3.2 Optimization of the C3 polyol HDO reaction conditions over Cu@C

3.3.2.1 Effects of hydrogen pressure on C3 polyol HDO over Cu@C

Because the HDO of glycerol was carried out in a batch reactor, the hydrogen pressure changed widely with reaction time. To optimize the reaction conditions of glycerol HDO, the effect of H_2

pressure must be determined. Thus, the effect of initial hydrogen pressure on the product yield and selectivity for the glycerol HDO reaction over Cu@C was investigated. The initial hydrogen pressure was varied from 0.6 to 1.2 MPa, and the selected ratio of the amount of metal in the catalyst to the amount of the reactant was 0.2 gCu/g_{glycerol}. For all the experiments, the hydrogen gas remained after 24 h reaction; hence, the glycerol reaction proceeded throughout the reaction period.

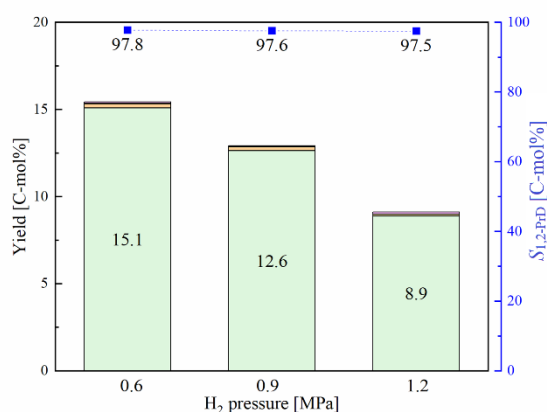
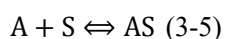


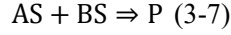
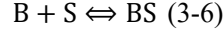
Figure 3.3: Effect of H₂ pressure on product yields. (Reactant: 20 g of 15 wt% aqueous glycerol solution, catalyst loading: 0.2 g_{Cu}/g_{glycerol}, reaction temperature: 180 °C, reaction time: 24 h, initial H₂ pressure: 0.6–1.2 MPa)

As shown in **Figure 3.3**, the yield of HDO product (1,2-PrD) were 15.1, 12.6, and 8.9 C-mol% at initial pressures of 0.6, 0.9, and 1.2 MPa, respectively. The slight decrease in glycerol conversion and HDO product yield with H₂ pressure was attributed to competitive adsorption of glycerol and hydrogen, which is consistent with the literature [7]. For Cu catalysts using support possessing solid acid sites such as Cu/SiO₂ and Cu/Al₂O₃, hydroxyl group in glycerol and hydrogen are likely to be adsorbed on the solid acid and Cu metal. Therefore, the competitive adsorption of H₂ and the reactant was not generally observed. On the contrary, the prepared Cu@C catalyst did not possess solid acid sites and Cu surface was the only catalytic active site involved in the reaction. Thus, both reactants (glycerol and H₂) compete for the same active sites (Cu surface) to proceed reaction, where the reaction can be represented by the Langmuir-Hinshelwood mechanism [8]:



Study on Hydrodeoxygenation of Biomass-Derived Polyols to Value-Added Chemicals on Carbon-Supported Metal Catalyst

Weican Wang



where A, B, AS, BS, and P are glycerol, H₂, glycerol adsorbed on Cu surface, H₂ adsorbed on Cu surface, and HDO products (1,2-PrD and H₂O), respectively. In this case, the rate law can be written as:

$$r = kC_{AS}C_{BS} = k\theta_B C_S \theta_A C_S \quad (3-8)$$

where C_{AS}, C_{BS} are the surface concentration of Cu sites occupied by glycerol and H₂, respectively; C_S is the concentration of all Cu sites; θ_A and θ_B are the fraction of Cu sites occupied by glycerol and H₂, respectively; k is the rate constant for the surface reaction. Applying steady state approximation to AS and BS, the following equations can be obtained:

$$\theta_A = \frac{K_A C_A}{1 + K_A C_A + K_B C_B} \quad (3-9)$$

$$\theta_B = \frac{K_B C_B}{1 + K_A C_A + K_B C_B} \quad (3-10)$$

Where K_A and K_B are the adsorption constants of glycerol and H₂, respectively. Thus, the rate law can be rewritten as:

$$r = kC_S^2 \frac{K_A C_A K_B C_B}{(1 + K_A C_A + K_B C_B)^2} \quad (3-11)$$

As indicated by the reaction results, H₂ has high adsorption on Cu surface and glycerol hardly adsorbed under reaction conditions ($K_A C_A \ll K_B C_B$), so:

$$r = kC_S^2 \frac{K_A C_A}{K_B C_B} \quad (3-12)$$

Assume that the solution is ideal mixture and concentration of H₂ in reaction solution follows the Henry's law [9]:

$$C_B = H_{H_2} * p_{H_2} \quad (3-13)$$

where H_{H_2} is the Henry's law constant of H₂, p_{H_2} is the pressure of the H₂ gas. Finally, the rate law can be written as:

$$r = kC_S^2 \frac{K_A C_A}{K_B H_{H_2} p_{H_2}} \quad (3-14)$$

From Equation 3-14, it could be concluded that the reaction order is negative with respect to hydrogen pressure. Therefore, increasing H₂ pressure inhibited the reaction by competitive absorption with glycerol and saturating the Cu surface, as observed from the results of the reaction tests.

Moreover, the HDO product selectivity was almost constant (97.5 to 97.8 C-mol%) with H₂ pressure, suggesting that HDO and the cracking reactions proceeded in parallel. Therefore, the effect of H₂ pressure on the product distribution of glycerol conversion was almost negligible under the reaction conditions tested (0.6–1.2 MPa).

To conclude, decreasing the hydrogen pressure is favored to improve the glycerol conversion and HDO product yield as a result of the less competitive adsorption of glycerol and hydrogen at a lower hydrogen pressure. However, because the reactor used in this study was a batch reactor that cannot refill hydrogen during the reaction, the theoretical maximum conversion would be limited at low hydrogen pressure. Thus, a higher hydrogen pressure is necessary to ensure sufficient hydrogen supply during reaction processes to achieve higher glycerol conversion levels. Therefore, an initial hydrogen pressure of 1.2 MPa was selected for further investigation of the HDO of glycerol, which can guarantee a maximum conversion greater of 100%.

3.3.2.2 Effects of reaction temperature and time

The reaction temperature and reaction time are also key parameters that affect the yield of the HDO products. To investigate the effects of temperature and reaction time on glycerol conversion and product selectivity, HDO of glycerol over Cu@C was carried out at 150, 165, and 180 °C, and the reaction time was systematically varied from 24 to 240 h. The amount of catalyst in the reactor was set at 0.2 g_{Cu}/g_{glycerol} and the initial H₂ pressure was set at 1.2 MPa.

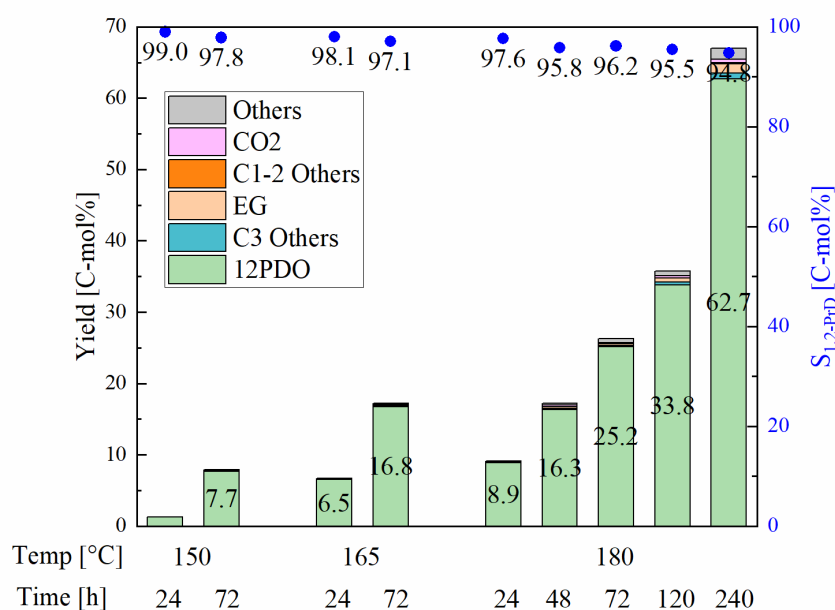


Figure 3.4: Effect of reaction temperature and time on product yield and selectivity of glycerol conversion. (Reactant: 20 g of 15 wt% aqueous glycerol solution, catalyst loading: 0.2 g_{Cu}/g_{glycerol}, reaction temperature: 150–180 °C, reaction time: 24–240 h, initial H₂ pressure: 1.2 MPa)

As shown in **Figure 3.4**, increasing the reaction temperature and reaction time significantly increased glycerol conversion. The glycerol conversions at 150, 165, and 180 °C were respectively 1.9, 7.3, and 16.3 C-mol% at 120 h and 5.3, 14.9, and 33.8 C-mol% at 240 h. The HDO product selectivity was almost constant with time at each reaction temperature, suggesting that the HDO and cracking reactions proceeded in parallel. The HDO product selectivity increased with a decrease in the reaction temperature, indicating that the activation energy of the HDO reaction was smaller than that of the C-C bond cleavage reaction and that the HDO reaction was favored at lower reaction temperatures. The relationship between reaction temperature and selectivity was in good agreement with the results previously reported for glycerol HDO over other Cu catalysts [10].

Given these points, increasing the reaction temperature and extending the reaction time are effective for improving the HDO product yield. However, the required reaction time was long and further optimization of the reaction condition and improvement of the Cu@C catalyst to accelerate the reaction rate are needed. We finally achieved 62.7 C-mol% 1,2-PrD yield from glycerol over

Cu@C catalyst at 180 °C and 1.2 MPa H₂ for 240 h. The prepared Cu@C catalyst exhibited high HDO product selectivity (> 94 C-mol%) for all reaction conditions, which was attributed to the smaller metal particle size of Cu and the inert carbon support (absence of active sites for side reactions).

3.3.3 Effect of Mg addition on catalytic performance of C3 HDO over MgCu@C catalysts

To further improve the catalytic activity of Cu@C, Mg was introduced during the ion-exchange process to prepare bimetallic MgCu@C catalysts. Reaction tests on monometallic Cu catalyst and bimetallic MgCu@C catalysts were carried out at 180 °C under 1.2 MPa H₂ for 24-240 h, and the metal weight of the catalysts used was fixed at 0.2 g_{Metal}/g_{Glycerol} for all catalysts.

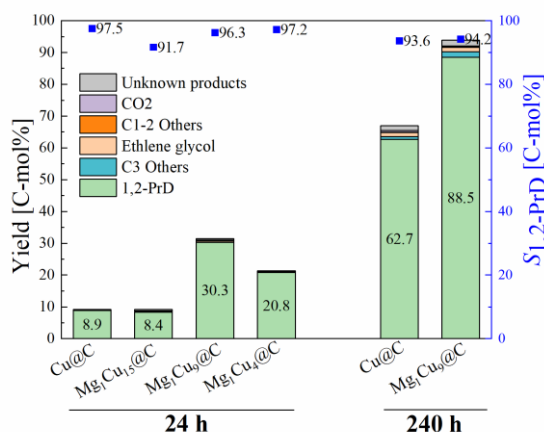


Figure 3.5: Product yield and selectivity of glycerol conversion over MgCu@C catalysts. (Reactant: 20 g of 15 wt% aqueous glycerol solution, catalyst loading: 0.2 g_{Cu}/g_{glycerol}, reaction temperature: 180 °C, reaction time: 24–240 h, initial H₂ pressure: 1.2 MPa)

Table 3.1: Glycerol conversion, selectivity of products, TOF and carbon balance over Cu@C and MgCu@C catalysts. (Reactant: 20 g of 15 wt% glycerol aqueous solution, catalyst loading: 0.2 g_{Metal}/g_{Glycerol}, initial H₂ pressure: 1.2 MPa)

Catalyst	Time [h]	X_{gly} [C-mol%]	Selectivity [C-mol%]						TOF [h ⁻¹]	CB [%]
			1,2-PrD	C3 Others ^a	EG	CO ₂	C1-2 Others ^b	Unknown products ^c		
			Cu@C	24	9.1	97.5	0.1	0.8		
	240	70.1	93.6	1.2	2.1	0.8	0.1	2.3	1.9	96.9
Mg ₁ Cu ₁₅ @C	24	9.1	91.7	2.1	0.9	0.9	0.7	3.8	8.6	101.2
Mg ₁ Cu ₉ @C	24	31.5	96.3	0.4	1.4	0.2	0.3	1.5	5.7	101.4
	240	94.0	94.2	1.8	1.5	0.3	0.1	2.0	2.0	102.8
Mg ₁ Cu ₄ @C	24	21.4	97.1	0.02	0.4	0.6	0.1	1.7	10.2	93.6

^a Sum of selectivities of hydroxyacetone, 2-propanol, and propane

^b Sum of the selectivities of ethanol, methanol, methane, and ethane

^c Sum of selectivities of unidentified products observed by GC-FID

Figure 3.5 and **Table 3.1** summarized the activities of glycerol HDO over reduced MgCu@C and Cu@C catalysts. The conversion of glycerol can be found to have performed successfully on bimetallic MgCu@C catalysts. For all MgCu@C catalysts, 1,2-PrD was obtained as the main HDO product, and other products such as hydroxyacetone, ethylene glycol (EG), and CO₂ were also observed. Furthermore, the tests revealed a significantly different activity between bimetallic MgCu@C and monometallic Cu@C. After 24 h reaction at 180 °C, the conversion of glycerol reached 31.5 C-mol% over bimetallic Mg₁Cu₉@C, while the conversion of glycerol was 9.1 C-mol% over monometallic Cu@C. When the reaction time was increased to 240 h, a glycerol conversion of 94.0 C-mol% was obtained over Mg₁Cu₉@C. The higher catalytic activity of Mg₁Cu₉@C could be partially ascribed to the improved metal dispersion because the exposed Cu surface area of Mg₁Cu₉@C was larger than Cu@C. However, Mg₁Cu₄@C showed higher glycerol conversion than Cu@C though the exposed Cu surface area of Mg₁Cu₄@C (1.38 m²/g) was smaller than that of Cu@C (2.26 m²/g). These results indicated that glycerol conversion is not only dependent on Cu surface area, but may also be related to the promotion effects of Mg species,

reported in previous literature [11–13]. The turnover frequency (TOF) values calculated for the catalysts examined are shown in **Table 3.1**. The TOF values over $\text{Mg}_1\text{Cu}_9@\text{C}$ decreased from 5.7 to 2.0 h^{-1} when the reaction time increased from 24 h to 240 h, which was due to the low substrate concentration after a long reaction time. However, all $\text{MgCu}@\text{C}$ samples showed TOF values higher than $\text{Cu}@\text{C}$ at similar or higher conversion levels after a fixed reaction time of 24 h. The TOF values of 24 h reactions tests over $\text{Cu}@\text{C}$, $\text{Mg}_1\text{Cu}_{15}@\text{C}$, $\text{Mg}_1\text{Cu}_9@\text{C}$, and $\text{Mg}_1\text{Cu}_4@\text{C}$ were 2.3, 8.6, 5.7, and 10.2 h^{-1} , respectively.

Comparing the $\text{MgCu}@\text{C}$ catalysts with different Cu/Mg ratio, $\text{Mg}_1\text{Cu}_9@\text{C}$ and $\text{Mg}_1\text{Cu}_4@\text{C}$ showed similar catalytic activity and selectivity to the hydrogenation of hydroxyacetone, while $\text{Mg}_1\text{Cu}_9@\text{C}$ showed higher conversion of glycerol than $\text{Mg}_1\text{Cu}_4@\text{C}$. These results suggested that the higher HDO activity of $\text{Mg}_1\text{Cu}_9@\text{C}$ than $\text{Mg}_1\text{Cu}_4@\text{C}$ catalysts was probably due to the higher ability to convert glycerol into the dehydrated intermediate, rather than the hydrogenation activity. From the STEM-EDS observation, it can be found that $\text{Mg}_1\text{Cu}_9@\text{C}$ has higher Mg dispersion than $\text{Mg}_1\text{Cu}_4@\text{C}$, which may provide more available Mg sites despite lower Mg loading. Given these points, the higher HDO activity of $\text{Mg}_1\text{Cu}_9@\text{C}$ than $\text{Mg}_1\text{Cu}_{15}@\text{C}$ and $\text{Mg}_1\text{Cu}_4@\text{C}$ can be explained by the higher dispersion of both Mg and Cu species, which provided active sites for the dehydration and hydrogenation step in the HDO processed, respectively.

The selectivities of main HDO product, $S_{1,2\text{-PrD}}$, over $\text{Cu}@\text{C}$, $\text{Mg}_1\text{Cu}_9@\text{C}$, and $\text{Mg}_1\text{Cu}_4@\text{C}$ at $180 \text{ }^\circ\text{C}$ under 1.2 MPa H_2 after 24 h reactions were almost same at 97.5, 96.3, and 97.1 C-mol%, respectively. The high $S_{1,2\text{-PrD}}$ values were maintained over bimetallic $\text{Mg}_1\text{Cu}_9@\text{C}$ and $\text{Cu}@\text{C}$ at higher conversion levels, suggesting that Mg addition did not promote side reactions, such as oligomerization and degradation. The present results are comparable to the results reported in the previous literature [15-20].

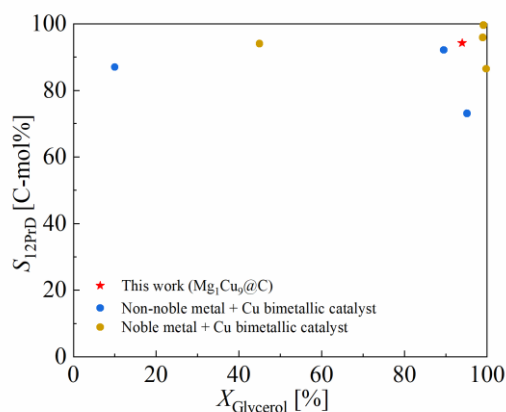


Figure 3.6: Selectivity to 1,2-PrD versus glycerol conversion over $Mg_1Cu_9@C$ and literature data.

Table 3.2: Comparative activity of Cu-based bimetallic catalysts for the HDO of glycerol.

Catalyst	Conditions	Glycerol	1,2-PrD	REF.
		conversion [%]	selectivity [%]	
$Mg_1Cu_9@C$	180 °C, 1.2 MPa, 240 h	94.0	94.2	This work
Co-Cu/TiO ₂	250 °C, 4 MPa, 4 h	95.2	73.0	[14]
Cu-Mg/SiO ₂	210 °C, 4.5 MPa, 24 h	89.5	92.1	[15]
Co-Cu/Al ₂ O ₃	220 °C, 5 MPa	10	87	[16]
Pt-Cu/SiO ₂	200 °C, 4 MPa, 12 h	99.0	95.9	[17]
Pt-Cu/SAA	12 h (In ethanol solution)	99.2	99.6	[18]
Ru-Cu/Al ₂ O ₃	200 °C, 4 MPa, 24 h	45	94	[19]
Ru-Cu/MWCNTs	200 °C, 4.0 MPa, 6 h	99.8	86.5	[20]

Figure 3.6 illustrates the comparative selectivity of bimetallic Cu catalysts for the HDO of glycerol to 1,2-PDO in the aqueous phase, with the details of each catalyst shown in **Table 3.2**. When comparing the catalytic performance in this work with others, the $Mg_1Cu_9@C$ catalyst showed high selectivity to 1,2-PrD under relatively low initial H₂ pressure (1.2 MPa), which is commonly not advantageous for the HDO of glycerol to 1,2-PrD.

3.3.4 Catalyst stability tests for C3 polyol HDO

Previous literature reported that Cu-based catalysts undergo serious deactivation problems in the glycerol HDO reaction [21]. Deactivation behaviors constitute the major obstacle to their industrial application [13]. Thus, the reusability test was performed to elucidate the stability of the $Mg_1Cu_9@C$ catalyst. The recovered catalyst after glycerol HDO was dried overnight at room temperature and reduced in the same manner as the pretreatment for the fresh catalyst. The following glycerol HDO was performed under the same reaction condition at 180 °C under 1.2 MPa H_2 for 24 h, and the metal weight of the catalysts used was fixed at 0.2 $g_{Metal}/g_{Glycerol}$.

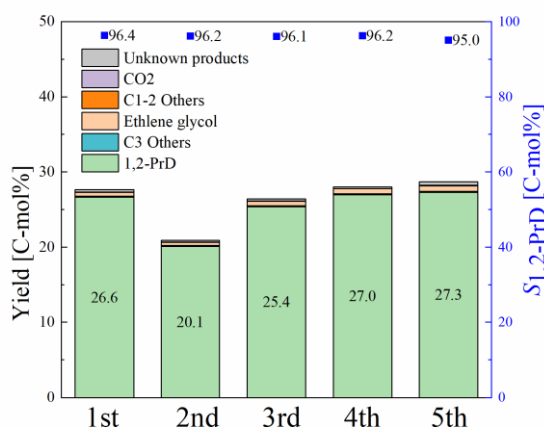


Figure 3.7: Product yield and selectivity of glycerol conversion over $Mg_1Cu_9@C$ catalyst for 5 sequential reaction runs. (Reactant: 20 g of 15 wt% aqueous glycerol solution, catalyst loading: 0.2 $g_{Cu}/g_{glycerol}$, reaction temperature: 180 °C, reaction time: 24 h, initial H_2 pressure: 1.2 MPa)

The product yield and selectivity towards 1,2-PrD data obtained for each recycle experiment are shown in **Figure 3.7**. The results show that the glycerol conversion decreases from 27.6 to 20.9 C-mol% after the first run and recovers to a level of 26.4-28.7 C-mol% in the third - fifth reaction runs. The lower glycerol conversion of the second reaction run was possibly due to experimental or analytic error but not catalyst deactivation, because the following 3 reaction runs showed a similar glycerol conversion compared to the first reaction run. For all reaction runs, the selectivity towards 1,2-PrD was maintained at a high level (>95 C-mol%). These results suggested

that the high activity and product selectivities of $\text{Mg}_1\text{Cu}_9@\text{C}$ were maintained after the use of 5 reaction runs, and the active site for HDO in $\text{MgCu}@\text{C}$ did not change during the reaction, recovery, and regeneration procedures.

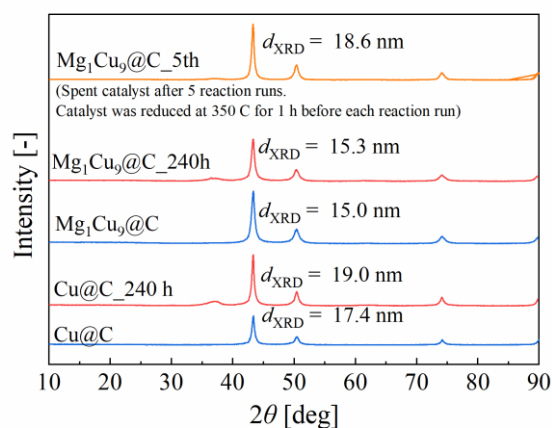


Figure 3.8: XRD patterns of fresh and spent $\text{Cu}@\text{C}$ and $\text{Mg}_1\text{Cu}_9@\text{C}$ catalysts. (Reaction conditions: temperature = 180 °C, initial H_2 pressure = 1.2 MPa, reaction time = 24-240 h.)

In addition, the stability of the metal particles was examined by characterizing spent catalysts. The XRD patterns of the fresh and spent catalysts are shown in **Figure 3.8**. Small metal particle sizes in $\text{Cu}@\text{C}$ and $\text{Mg}_1\text{Cu}_9@\text{C}$ were maintained throughout the reaction tests. The d_{XRD} of $\text{Cu}@\text{C}$ slightly increased from 17.4 to 19.0 nm after 240 h reaction time at 180 °C, indicating that the confinement structure of the carbon-supported catalyst prepared from metal-loaded resin is effective in suppressing Cu sintering under hydrothermal reaction conditions. Furthermore, the d_{XRD} of $\text{Mg}_1\text{Cu}_9@\text{C}$ before and after 240 h reaction time at 180 °C were 15.0 and 15.3 nm, respectively, which were almost unchanged during long time reaction. In the case of the $\text{Mg}_1\text{Cu}_9@\text{C}$ catalyst after 5 reaction runs, the d_{XRD} of $\text{Mg}_1\text{Cu}_9@\text{C}$ only slightly increased from 15.0 to 18.6 nm. Considering that the $\text{Mg}_1\text{Cu}_9@\text{C}$ catalyst used in the reusability test was recovered and reduced several times, it can be concluded that $\text{Mg}_1\text{Cu}_9@\text{C}$ showed high stability during reaction as well as pretreatment procedures.

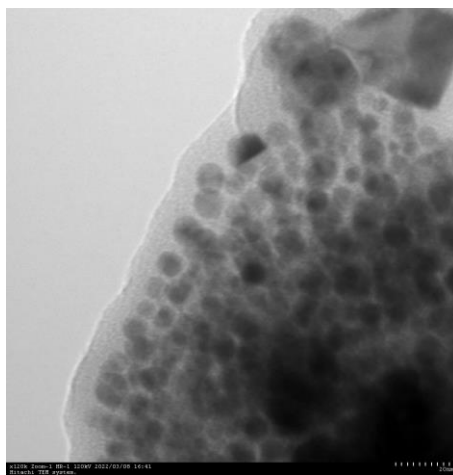


Figure 3.9: TEM image for spent $Mg_1Cu_9@C$ catalyst. (Reaction conditions: temperature = 180 °C, initial H_2 pressure = 1.2 MPa, reaction time = 240 h.)

This finding is in agreement with the results of the TEM observation. As shown in **Figure 3.9**, the uniformly dispersed metal particles were maintained in $Mg_1Cu_9@C$ after a reaction time of 240 h at 180 °C. The d_{TEM} of 240 h spent $Mg_1Cu_9@C$ was 12.4 nm, which is almost the same as the fresh catalyst (12.5 nm). The high stability of the metal particles in the $Mg_1Cu_9@C$ catalyst suggested that the high sintering resistance of the original $Cu@C$ sample was maintained after the addition of Mg and the potential of $MgCu@C$ catalysts for industrial application.

3.3.5 Insight into the reaction mechanism of C3 polyol HDO over $Cu@C$ and $MgCu@C$

To better understand the difference in activity between $Cu@C$ and $MgCu@C$, reaction pathway and mechanism studies on glycerol HDO were carried out. Two main reaction mechanisms are proposed for the HDO of glycerol to 1,2-PrD: the dehydration-hydrogenation mechanism (**Figure 3.10 (a)**) and the dehydrogenation-dehydration-hydrogenation mechanism (**Figure 3.10 (b)**) [22]. The dehydration-hydrogenation mechanism composed of the dehydration of glycerol to hydroxyacetone and the subsequent hydrogenation step of hydroxyacetone to 1,2-PrD [23]. The mechanism of dehydrogenation-dehydration-hydrogenation starts with the dehydrogenation of glycerol to glyceraldehyde and is then dehydrated to the intermediate enol, which is then hydrogenated to hydroxyacetone and finally converted to 1,2-PrD [24]. In HDO reactions of

glycerol on Cu@C and MgCu@C catalysts, hydroxyacetone was obtained with a small amount, and other dehydrogenation or dehydration intermediates, such as glyceraldehyde and pyruvaldehyde, were not detected. From these results, we proposed that the HDO of glycerol over Cu@C and MgCu@C follows the dehydration-hydrogenation mechanism, where hydroxyacetone is produced from glycerol dehydration and further hydrogenated into 1,2-PrD.

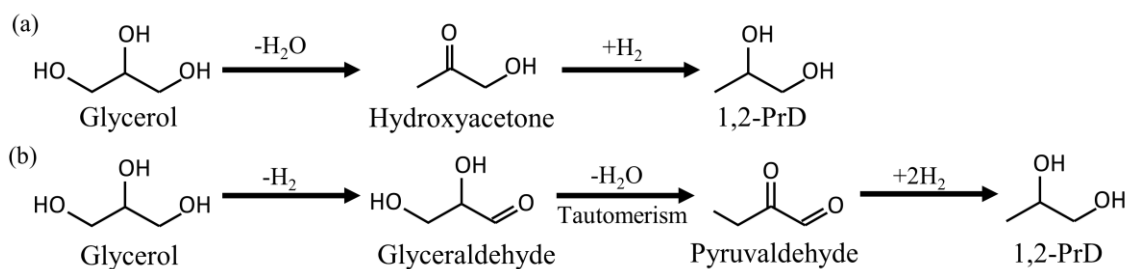


Figure 3.10: Possible reaction pathways of glycerol transformation under hydrogen over Cu-based catalysts. (a) the dehydration-hydrogenation mechanism. (b) the dehydrogenation-dehydration-hydrogenation mechanism

To verify the reaction mechanism, HDO of hydroxyacetone was carried out over Cu@C, Mg₁Cu₉@C, and Mg₁Cu₄@C catalysts in H₂ atmosphere in the aqueous phase. **Table 3.3** shows the yield of 1,2-PrD, product selectivity, and carbon balance obtained in each experiment.

Table 3.3: Yield of 1,2-PrD, selectivity of products, and carbon balance over Cu@C and Mg₁Cu₉@C catalysts. (Reactant: 20 g of 15 wt% hydroxyacetone aqueous solution, catalyst loading: 0.2 g_{Metal}/g_{Hydroxyacetone}, initial H₂ pressure: 1.2 MPa, reaction temperature: 180 °C, reaction time: 24 h)

Catalyst	$Y_{1,2-PrD}$ [C- mol%]	Selectivity [C-mol%]						CB [%]
		1,2- PrD	C3 Others ^a	EG	CO ₂	C1-2 Others ^b	Unknown products ^c	
Cu@C	96.4	93.8	trace	0.1	0.1	trace	5.9	104.1
Mg ₁ Cu ₉ @C	81.7	85.4	0.1	0.4	0.2	0.9	12.9	96.8
Mg ₁ Cu ₄ @C	82.5	85.0	0.2	0.6	0.5	1.2	12.5	97.9

^a Sum of selectivities of propanol and propane

^b Sum of selectivities of ethanol, methanol, methane, and ethane

^c Sum of selectivities of unidentified products observed by GC-FID

The results show that the hydrogenation of the C=O bond in hydroxyacetone was highly favorable and the production of 1,2-PrD was dominant over Cu@C and MgCu@C. The 1,2-PrD yields were 96.4, 81.7, and 82.5 C-mol% over Cu@C, Mg₁Cu₉@C, and Mg₁Cu₄@C, respectively, and the selectivities to 1,2-PrD were 93.8, 85.4, and 85.0 C-mol% over Cu@C, Mg₁Cu₉@C, and Mg₁Cu₄@C respectively. These results suggest that hydroxyacetone produced by glycerol dehydration can immediately convert to 1,2-PrD over Cu@C and MgCu@C, which is in accordance with the dehydration-hydrogenation mechanism. Furthermore, monometallic Cu@C showed higher catalytic activity for hydroxyacetone hydrogenation to 1,2-PrD than bimetallic MgCu@C, indicating that the addition of Mg species slightly decreased the hydrogenation activity of the Cu catalyst. On the other hand, bimetallic Mg₁Cu₉@C and Mg₁Cu₄@C showed a higher conversion than Cu@C in the glycerol HDO to 1,2-PrD, which involves both the dehydration step and the hydrogenation step. Since the dehydration reaction is usually an unfavorable step in the diluted glycerol aqueous solution, it is considered a rate determining step of glycerol conversion [26]. It was well accepted that dehydration of glycerol is favorable over the acidic and/or basic sites of the catalyst [12,25]. The CO₂-TPD profiles of Cu@C and Mg₁Cu₉@C clearly showed an enhancement

in the basicity of the catalysts after the addition of Mg. From these considerations, we envisaged that the addition of Mg to Cu catalysts promoted the dehydration of glycerol to hydroxyacetone by increasing the basicity of the catalyst and the produced hydroxyacetone was then immediately converted into 1,2-PrD.

Furthermore, the by-products obtained from hydroxyacetone over Cu@C and MgCu@C catalysts were mainly unknown compounds that cannot be identified by GC-MS. The main degradation products obtained from glycerol (i.e., EG and CO₂) were only produced with small amounts (< 0.5 C-mol% selectivity) from hydroxyacetone over Cu@C and MgCu@C. In addition, the selectivity for 1,2-PrD was almost constant with time in the glycerol conversion reaction tests, indicating that the HDO and cracking reactions proceeded in parallel. Therefore, these results suggest that EG and CO₂ were probably not produced from hydroxyacetone or 1,2-PrD, but directly from glycerol.

To conclude, the HDO reactions over Cu@C and MgCu@C proceed through the dehydration of glycerol to hydroxyacetone followed by the hydrogenation of hydroxyacetone to 1,2-PrD, while the cracking reactions proceed via the cleavage of terminal C-C bonds in glycerol.

3.4 Conclusions

The catalytic performance of the materials was studied for the hydrodeoxygenation (HDO) of glycerol to produce value-added C3 diols. The carbon-supported Cu catalysts prepared from the ion-exchange resin exhibited a higher catalytic performance for the HDO of glycerol compared to the Cu-based catalysts prepared by impregnation methods (Cu/AC, Cu/SiO₂, and Cu/Al₂O₃) due to its high metal dispersion. A glycerol conversion of 70.1 C-mol% and a selectivity towards 1,2-PrD of 93.6 C-mol% were obtained at 180 °C under 1.2 MPa H₂ for 240 h with a catalyst loading of 0.2 g_{Cu}/g_{Glycerol}.

To further improve the catalytic performance of Cu@C, Mg was added as additives. Among the Mg-added Cu catalysts, the Mg₁Cu₉@C catalyst showed better catalytic activity for the HDO of

Study on Hydrodeoxygenation of Biomass-Derived Polyols to Value-Added Chemicals on Carbon-Supported Metal Catalyst

Weican Wang

glycerol due to the high dispersion of both Mg and Cu species. The maximum glycerol conversion in this study was achieved at 94.0% C-mol with 94.2% C-mol selectivity toward 1,2-PrD over the Mg₁Cu₉@C catalyst at 180 °C under 1.2 MPa H₂ for 240 h with a catalyst loading of 0.2 g_{Cu}/g_{Glycerol}. Furthermore, no obvious metal sintering was observed in Cu@C and MgCu@C after a 240 h reaction, indicating the high stability of the catalysts prepared from the metal-loaded resin. The reusability test of Mg₁Cu₉@C also demonstrated that there was no obvious catalyst deactivation after 5 reaction runs.

The conversion of glycerol to 1,2-PrD over Cu@C and MgCu@C was supposed to proceed with the dehydration-hydrogenation mechanism, where glycerol was first dehydrated to hydroxyacetone and then hydroxyacetone was hydrogenated to 1,2-PrD. Reaction tests of the hydrogenation of hydroxyacetone revealed that the addition of Mg species to Cu catalysts enhanced catalytic activity possibly by promoting the dehydration step on the introduced base sites.

References

- [1] T. Werpy, G. Petersen, *Top Value Added Chemicals from Biomass: Volume I -- Results of Screening for Potential Candidates from Sugars and Synthesis Gas*, 2004. <https://doi.org/10.2172/15008859>.
- [2] S. Bagheri, N.M. Julkapli, W.A. Yehye, Catalytic conversion of biodiesel derived raw glycerol to value added products, *Renew. Sustain. Energy Rev.* 41 (2015) 113–127. <https://doi.org/10.1016/j.rser.2014.08.031>.
- [3] J.B. Restrepo, C.D. Paternina-Arboleda, A.J. Bula, 1,2—Propanediol Production from Glycerol Derived from Biodiesel's Production: Technical and Economic Study, *Energies.* 14 (2021) 5081. <https://doi.org/10.3390/en14165081>.
- [4] B. Mallesham, P. Sudarsanam, B.V.S. Reddy, B.M. Reddy, Development of cerium promoted copper–magnesium catalysts for biomass valorization: Selective hydrogenolysis of bioglycerol, *Appl. Catal. B Environ.* 181 (2016) 47–57. <https://doi.org/10.1016/j.apcatb.2015.07.037>.
- [5] H. Mitta, N. Devunuri, J. Sunkari, S. Mutyala, P. Balla, V. Perupogu, A highly active dispersed copper oxide phase on calcined Mg₉Al₂.7-Ga₂.3O₂ catalysts in glycerol hydrogenolysis, *Catal. Today.* 375 (2021) 204–215. <https://doi.org/10.1016/j.cattod.2020.02.032>.
- [6] J. Shan, H. Liu, K. Lu, S. Zhu, J. Li, J. Wang, W. Fan, Identification of the dehydration active sites in glycerol hydrogenolysis to 1,2-propanediol over Cu/SiO₂ catalysts, *J. Catal.* 383 (2020) 13–23. <https://doi.org/10.1016/j.jcat.2019.12.032>.
- [7] R.B. Mane, A.M. Hengne, A.A. Ghalwadkar, S. Vijayanand, P.H. Mohite, H.S. Potdar, C.V. Rode, Cu:Al Nano Catalyst for Selective Hydrogenolysis of Glycerol to 1,2-Propanediol, *Catal. Lett.* 135 (2010) 141–147. <https://doi.org/10.1007/s10562-010-0276-5>.
- [8] Principles of Heterogeneous Catalysis, in: *React. Solid Surf.*, John Wiley & Sons, Ltd, 2009: pp. 103–121. <https://doi.org/10.1002/9780470535295.ch5>.
- [9] Phase Equilibrium Principles, in: *Thermodyn. Pract. Eng.*, John Wiley & Sons, Ltd, 2009: pp. 201–230. <https://doi.org/10.1002/9780470451595.ch11>.
- [10] T. Gabrysch, M. Muhler, B. Peng, The kinetics of glycerol hydrodeoxygenation to 1,2-propanediol over Cu/ZrO₂ in the aqueous phase, *Appl. Catal. Gen.* 576 (2019) 47–53. <https://doi.org/10.1016/j.apcata.2019.03.001>.
- [11] C.-J. Yue, L.-P. Gu, Y. Su, S.-P. Zhu, Selective hydrogenolysis of glycerol to 1,2-propanediol over MgO-nested Raney Cu, *React. Kinet. Mech. Catal.* 111 (2014) 633–645. <https://doi.org/10.1007/s11144-013-0670-2>.
- [12] N.N. Pandhare, S.M. Pudi, P. Biswas, S. Sinha, Selective Hydrogenolysis of Glycerol to 1,2-Propanediol over Highly Active and Stable Cu/MgO Catalyst in the Vapor Phase, *Org. Process Res. Dev.* 20 (2016) 1059–1067. <https://doi.org/10.1021/acs.oprd.6b00110>.
- [13] S.M. Pudi, P. Biswas, S. Kumar, Selective hydrogenolysis of glycerol to 1,2-propanediol over highly active copper–magnesia catalysts: reaction parameter, catalyst stability and mechanism study,

- J. Chem. Technol. Biotechnol. 91 (2016) 2063–2075. <https://doi.org/10.1002/jctb.4802>.
- [14] W. Mondach, S. Chanklang, P. Somchuea, T. Witoon, M. Chareonpanich, K. Faungnawakij, H. Sohn, A. Seubsai, Highly efficient TiO₂-supported Co–Cu catalysts for conversion of glycerol to 1,2-propanediol, *Sci. Rep.* 11 (2021) 23042. <https://doi.org/10.1038/s41598-021-02416-7>.
- [15] P. Kumar, A.K. Shah, J.-H. Lee, Y.H. Park, U.L. Štangar, Selective Hydrogenolysis of Glycerol over Bifunctional Copper–Magnesium-Supported Catalysts for Propanediol Synthesis, *Ind. Eng. Chem. Res.* 59 (2020) 6506–6516. <https://doi.org/10.1021/acs.iecr.9b06978>.
- [16] C. Sepúlveda, K. Cruces, J. Gajardo, J. Seguel, R. García, D. Salinas, J.L.G. Fierro, I.T. Ghampson, R. Serpell, N. Escalona, The promoter effect of Co on the catalytic activity of the Cu oxide active phase supported on Al₂O₃ in the hydrogenolysis of glycerol, *New J. Chem.* 43 (2019) 15636–15645. <https://doi.org/10.1039/C9NJ03534F>.
- [17] Y. Kang, X. Bu, G. Wang, X. Wang, Q. Li, Y. Feng, A Highly Active Cu–Pt/SiO₂ Bimetal for the Hydrogenolysis of Glycerol to 1,2-Propanediol, *Catal. Lett.* 146 (2016) 1408–1414. <https://doi.org/10.1007/s10562-016-1766-x>.
- [18] X. Zhang, G. Cui, H. Feng, L. Chen, H. Wang, B. Wang, X. Zhang, L. Zheng, S. Hong, M. Wei, Platinum–copper single atom alloy catalysts with high performance towards glycerol hydrogenolysis, *Nat. Commun.* 10 (2019) 5812. <https://doi.org/10.1038/s41467-019-13685-2>.
- [19] A.V.H. Soares, J.B. Salazar, D.D. Falcone, F.A. Vasconcellos, R.J. Davis, F.B. Passos, A study of glycerol hydrogenolysis over Ru–Cu/Al₂O₃ and Ru–Cu/ZrO₂ catalysts, *J. Mol. Catal. Chem.* 415 (2016) 27–36. <https://doi.org/10.1016/j.molcata.2016.01.027>.
- [20] Z. Wu, Y. Mao, X. Wang, M. Zhang, Preparation of a Cu–Ru/carbon nanotube catalyst for hydrogenolysis of glycerol to 1,2-propanediol via hydrogen spillover, *Green Chem.* 13 (2011) 1311. <https://doi.org/10.1039/c0gc00809e>.
- [21] C. Montassier, J.M. Dumas, P. Granger, J. Barbier, Deactivation of supported copper based catalysts during polyol conversion in aqueous phase, *Appl. Catal. Gen.* 121 (1995) 231–244. [https://doi.org/10.1016/0926-860X\(94\)00205-3](https://doi.org/10.1016/0926-860X(94)00205-3).
- [22] E.S. Vasiliadou, A.A. Lemonidou, Glycerol transformation to value added C₃ diols: reaction mechanism, kinetic, and engineering aspects, *WIREs Energy Environ.* 4 (2015) 486–520. <https://doi.org/10.1002/wene.159>.
- [23] S. Sato, M. Akiyama, R. Takahashi, T. Hara, K. Inui, M. Yokota, Vapor-phase reaction of polyols over copper catalysts, *Appl. Catal. Gen.* 347 (2008) 186–191. <https://doi.org/10.1016/j.apcata.2008.06.013>.
- [24] C. Montassier, J.C. Ménézo, L.C. Hoang, C. Renaud, J. Barbier, Aqueous polyol conversions on ruthenium and on sulfur-modified ruthenium, *J. Mol. Catal.* 70 (1991) 99–110. [https://doi.org/10.1016/0304-5102\(91\)85008-P](https://doi.org/10.1016/0304-5102(91)85008-P).
- [25] S. Basu, A.K. Sen, A Review on Catalytic Dehydration of Glycerol to Acetol, *ChemBioEng Rev.* n/a (n.d.). <https://doi.org/10.1002/cben.202100009>.

4. Conversion of C4 polyol to value-added diols over carbon-supported metal catalysts

4.1 Introduction

Erythritol (*meso*-1,2,3,4-butanetetraol; $C_4H_6(OH)_4$) is a major biomass-derived polyol produced by fermentation processes with glucose and sucrose derived from starch [1]. It can be used as a raw material for the production of butanediols, tetrahydrofuran, and butane dienes [1,2]. Similarly to C3 polyol, erythritol can be converted to value-added chemicals via HDO over Cu-based catalysts. The corresponding diol components converted from C4 polyols, such as 1,2-butanediol, 1,3-butanediol, and 1,4-butanediol, are widely used as building blocks in the chemical industry [3].

In this chapter, carbon-supported Cu catalysts (Cu@C and MgCu@C) were prepared by the ion exchange of metal ions onto a weakly acidic cation-exchange resin, followed by carbonization. The prepared catalyst was applied to the HDO of erythritol to butanediols under mild reaction conditions ($T \leq 180$ °C, $p_{H_2} \leq 1.8$ MPa). The effects of reaction temperature, reaction time, and hydrogen pressure on erythritol HDO over the prepared Cu@C were investigated. In addition, the reaction mechanism over the prepared Cu@C catalyst was also studied to gain further understanding of erythritol HDO.

4.2 Experimental

4.2.1 Materials

All chemicals were used without further purification. Meso-erythritol (97%) and distilled water were purchased from FUJIFILM Wako Pure Chemical Ltd., Japan. 1,5-entanediol (97%) was purchased from Tokyo Chemical Industry CO., LTD., Japan. The commercial catalyst Cu chromite was purchased from Sigma-Aldrich, Japan. Other Cu-based catalysts (Cu@C, MgCu@C, Cu/AC, Cu/SiO₂) were prepared according to the method described in **Chapter 2**.

Table 4.1: Properties of the prepared monometallic Cu-based catalysts.

Catalyst	Mg ₁ Cu ₉ @C	Cu@C	Cu/AC	Cu/SiO ₂	Cu chromite
Metal loading [wt%]	56.5	66.9	6.5	15 ^a	45.5 ^a
BET surface area [m ² /g _{cat}]	129	119	1250	66	28
Mean metal particle size; d_{XRD} [nm]	15.0	17.4	22.7	35.3	20.2
d_{TEM} [nm]	12.5	14.9	12.8	40.5	96.9
Geometric Cu surface area; $S_{\text{TEM}}^{\text{a}}$ [m ² /g]	34.1	30.2	3.4	2.5	3.1
Accessible Cu surface area; $S_{\text{N}_2\text{O}}^{\text{c}}$ [m ² /g]	2.49	2.26	— ^d	0.60	n. d.
$S_{\text{N}_2\text{O}} / S_{\text{TEM}}$ [%]	7.3	7.9	— ^d	24.0.	n. d.

^a Nominal value

^b Calculated by d_{TEM} .

^c Calculated by N₂O titration.

^d The amount of adsorbed N₂O was too small to calculate $S_{\text{N}_2\text{O}}$.

Information about the catalysts used in this chapter is summarized in **Table 4.1**. Which is different from the Cu/AC catalyst used in **Chapter 3**, the designed Cu loading of the Cu/AC catalyst used in this chapter was reduced to 5 wt% to improve metal dispersion, and the actual Cu loading measured by TG was 6.5 wt%. Accordingly, the d_{XRD} and d_{TEM} of Cu/AC decreased from 27.7 and 22.8 nm to 22.7 and 12.8 nm, respectively. However, the new Cu/AC catalyst still has a very small amount of surface area in the N₂O titration test, suggesting that the poisoning effects of sulfur contents on support still exists.

4.2.2 Catalytic reaction test

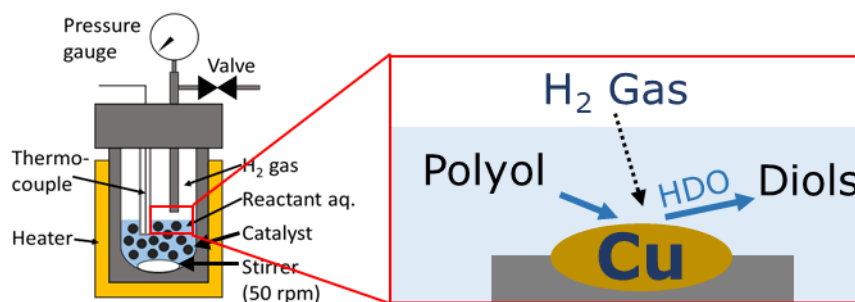


Figure 4.1: Reactor scheme of the Teflon-sealed stainless-steel batch reactor.

The liquid phase HDO of erythritol was performed in a 200 ml Teflon-sealed stainless-steel batch reactor (HIRO Corp., Japan, Figure 4.1). Before the reaction test, the prepared catalyst was reduced in 10% H₂/N₂ flow at 350 °C for 1 h, then ground into powder and sieved into diameters less than 100 μm. Typically, 30 g of 15 wt% polyol aqueous solution and a predetermined amount of catalyst were introduced into the reactor. The reactor was flushed with Ar gas for 3 times to purge out the remaining air, sequentially pressurized with H₂ and heated to the designed temperature. The time the reactor reached the designed temperature was taken as the starting time of the reaction. After the desired reaction time, the reactor was quenched in an ice bath to terminate the reaction. The gaseous phase products in the reactor were purged out by Ar gas and collected in a gasbag. The gaseous products were analyzed using a GC-2014 gas chromatograph (Shimadzu Co. Ltd., Japan) equipped with a TCD and a Porapak-Q column (GL Sciences Inc., Japan). The liquid products and the catalysts were separated by centrifugation and filtration. The compounds in the liquid samples were identified by a GC-2010 gas chromatograph (Shimadzu Co. Ltd., Japan) equipped with a DB-WAX column (Agilent Technologies Inc., Japan) and a Parvum 2 mass spectrometer (Shimadzu Co. Ltd., Japan). The identified liquid products were quantified using a GC-2014 gas chromatograph equipped with a DB-WAX column and a flame ionization detector (FID) using 1,5-pentanediol as internal standard. Components observed by GC-FID but could not be identified by GC-MS products were labelled “Others” in the following figures and tables. The conversion of reactant (X), product

yield (Y_i), product selectivity (S_i), carbon balance (CB), and turnover frequency (TOF) were calculated according to the following equations, respectively:

$$X [\text{C-mol}\%] = \frac{\sum \text{mol of product carbon atoms}}{\text{mol of carbon atoms charged into reactor}} \times 100\% \quad (4-1)$$

$$Y_i [\text{C-mol}\%] = \frac{\text{mol of carbon atoms in } i}{\text{mol of carbon atoms charged into reactor}} \times 100\% \quad (4-2)$$

$$S_i [\text{C-mol}\%] = \frac{\text{mol of carbon atoms in } i}{\sum \text{mol of product carbon atoms}} \times 100\% \quad (4-3)$$

$$CB [\%] = \frac{\text{mol of carbon atoms recovered after reaction}}{\text{mol of carbon atoms in initial reactant}} \times 100\% \quad (4-4)$$

$$TOF [\text{h}^{-1}] = \frac{\text{mol of the converted reactant}}{\text{mol of Cu atoms on accessible surface} \times \text{Reaction time}} \quad (4-5)$$

where Y_{BuT} and S_{BuT} denote the sum of the yields and the sum of the selectivities of all butanetriol isomers. Similarly, Y_{BuD} and S_{BuD} denote the sum of the yields and the sum of the selectivities of all butanediols isomers. Y_{HDO} indicates the sum of the yields of the HDO products, including all the butanetriols, butanediols, butanols, and butane. The unidentified products, labelled as “Others” in following figures and tables, were components which was observed by the GC-FID but could not be identified by the GC-MS. Threitol, which is a stereoisomer of erythritol, was obtained for all HDO test of erythritol while it was considered an unconverted reactant because threitol can be converted to butanediols by HDO, similar to erythritol [4].

4.3 Results and discussion

4.3.1 Effects of catalyst preparation methods and supports on the catalytic performance of C4 HDO

First, to compare the activity of the prepared monometallic Cu-based catalysts for erythritol HDO, reaction tests were conducted at 180 °C under 1.8 MPa H₂ for 24 h. The ratio of the amount of Cu and the amount of the reactant in the reactor was fixed at 0.04 g_{Cu}/g_{erythritol} for all prepared catalysts.

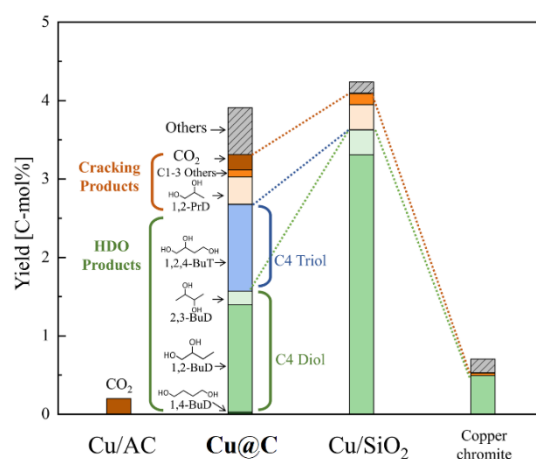


Figure 4.2: Product yields with the prepared Cu based catalysts. (Reactant: 30 g of 15 wt% aqueous erythritol solution; catalyst loading: 0.04 g_{Cu}/g_{erythritol}; reaction temperature: 180 °C; reaction time: 24 h, initial H₂ pressure: 1.8 MPa)

As shown in **Figure 4.2** and **Table 4.2**, the erythritol conversion over Cu@C reached 3.91 C-mol% and TOF value of 4.0 h⁻¹. The desired reaction, HDO of erythritol without C-C bond cleavage, proceeded over the Cu@C catalyst to produce 1,2,4-butanetriol (1,2,4-BuT), 1,2-butanediol (1,2-BuD), 2,3-butanediol (2,3-BuD), and 1,4-butanediol (1,4-BuD), and the HDO product yield was 2.68 C-mol%. The yield of the HDO products increased in the following order: 1,2-BuD (1.37 C-mol%) > 1,2,4-BuT (1.11 C-mol%) > 2,3-BuD (0.17 C-mol%) > 1,4-BuD (0.03 C-mol%). The HDO products mainly possessed vicinal hydroxyl groups. The other HDO products, 1,2-propandiol (1,2-PrD), CO₂, ethylene glycol, monoalcohol, and alkanes were concomitantly generated at small

yields. Cyclic product via dehydration including 1,4-anhydroerythritol was not detected. Furthermore, the carbon recovery for Cu@C was almost 100 %, indicating that the oligomerized products and highly oxygenated compounds that could not be detected by GC were not produced. Therefore, the Cu@C prepared in this study was able to remove part of the hydroxyl groups of C4 polyols with high selectivity. In contrast, using Cu/AC as the catalyst, the erythritol conversion was only 0.20 C-mol% and the main product was CO₂. The low activity of Cu/AC was attributed to the poisoning effects of sulfur contents, as discussed in **Chapter 2**. The erythritol conversion over Cu/SiO₂ was comparable to that of Cu@C and BuDs and BuTs were mainly obtained for these two catalysts. The carbon recovery for Cu/SiO₂ was 79 C-mol%, implying that the formation of undetectable compounds by GC, such as the oligomers of erythritol and highly oxygenated compounds. The conversion of erythritol over Cu chromite was small. Therefore, the prepared Cu@C exhibited the high HDO activity.

Study on Hydrodeoxygenation of Biomass-Derived Polyols to Value-Added Chemicals on Carbon-Supported Metal Catalyst

Weican Wang

Table 4.2: Effect of the prepared catalysts on erythritol conversion, yield of products, BuD and HDO selectivity, and carbon recovery. (Reactant: 30 g of 15 wt% erythritol aqueous solution, catalyst loading: 0.04 g_{Cu}/g_{erythritol}, initial H₂ pressure: 1.8 MPa, reaction temperature: 180 °C, reaction time: 24 h)

Catalyst		Cu@C	Cu/AC	Cu/SiO ₂	Cu chromite
$X_{\text{erythritol}}$ [C-mol%] ^{*a}		3.91	0.20	4.24	0.70
Epimerization					
Y_{threitol} [C-mol%]		32.89	0	9.86	3.79
Hydrodeoxygenation					
Y_{HDO} [C-mol%]		2.68	0.00	3.63	0.49
Breakdown of products	1,2,4-BuT	1.11	0	0	0
	1,2,3-BuT	0	0	0	0
	1,2-BuD	1.37	0	3.31	0.49
	2,3-BuD	0.17	0	0.32	0
	1,4-BuD	0.03	0	0	0
	Butanols ^{*b}	0	0	0	0
	Butane	0.00	0.00	0.00	0.00
Cracking					
Y_{cracking} [C-mol%]		0.63	0.20	0.47	0.04
Breakdown of products	Glycerol	0	0	0.06	0.01
	1,2-PrD	0.35	0.00	0.32	0
	Ethylene glycol	0.07	0.00	0	0
	C1-3 alcohols ^{*c}	0.02	0.00	0.03	0
	C1-3 alkanes ^{*d}	0.00	0.00	0.05	0.02
	CO ₂	0.20	0.20	0.01	0.01
Y_{others} [C-mol%] ^{*e}		0.60	0	0.14	0.17
Y_{BuD} [C-mol%]		1.57	0	3.63	0.5
S_{HDO} [C-mol%]		68.5	0.00	85.6	70.1
S_{BuD} [C-mol%]		40.1	0.37	84.6	70.1
CB [C-mol%]		104.1	79.6	85.1	78.7

*a Threitol was regarded as unconverted reactant

*b Sum of yields of 1-butanol and 2-butanol

*c Sum of yields of 1-propanol, 2-propanol, ethanol, and methanol

*d Sum of yields of propane, ethane, and methane

*e Unidentified products observed by GC-FID

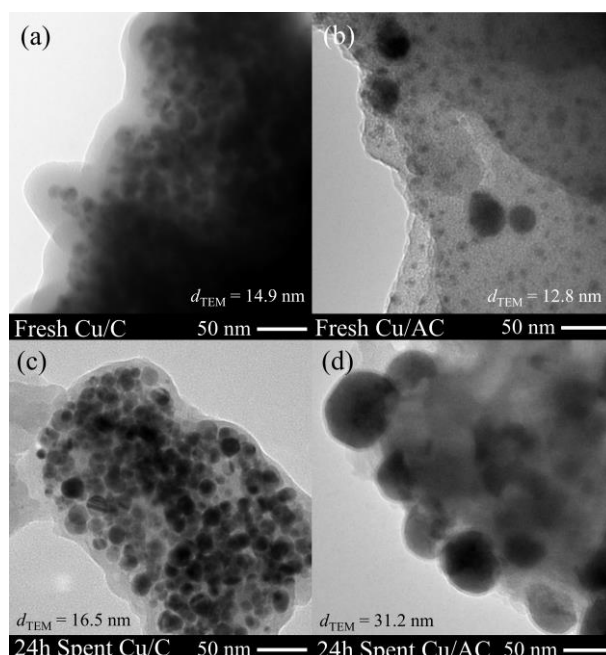


Figure 4.3: TEM images of the prepared Cu based catalysts: (a)fresh Cu/C, (b)fresh Cu/AC, (c) spent Cu/C, and spent Cu/AC. The fresh catalysts were pretreated in H₂ at 350 °C for 1 h and the spent catalysts were the samples after erythritol HDO in 1.8 MPa H₂ at 180 °C for 24 h.

Additionally, the stability of Cu was determined by characterizing the spent catalyst. As shown in **Figure 4.3**, The Cu particle size of the spent Cu@C after 24 h reaction observed by TEM was almost comparable to that of the fresh Cu@C. Thus, small Cu particles in Cu@C were successfully maintained throughout the HDO reaction. In the case of Cu/AC, the Cu particle size of the spent catalyst increased from 22.7 to 30.7 nm, indicating that further agglomeration occurred during the reaction. Therefore, the Cu@C catalyst realized high activity and high stability of Cu nanoparticles for HDO conversion of lager molecule polyol as in the case of C3 polyol. As discussed in **Chapter 3**, the difference in the sintering resistance of Cu between Cu@C and other catalysts was attributed to the confinement structure of Cu@C, where the Cu particles were immobilized in the carbon support. Given these points, Cu@C showed high activity for HDO of erythritol, and higher stability and carbon recovery than other Cu catalysts prepared with different supports, which demonstrated that carbon-supported Cu catalysts prepared by the ion-exchange resin method were also promising catalysts for effective conversion of C4 or larger polyols.

4.3.2 Effects of Mg addition on catalytic performance of C4 HDO

In **Chapter 3**, the $\text{Mg}_1\text{Cu}_9@\text{C}$ bimetallic catalysts showed improved catalytic activity for glycerol HDO compared to the monometallic $\text{Cu}@\text{C}$ catalyst. Then, C4 polyol (erythritol) HDO reaction tests were carried out on $\text{Mg}_1\text{Cu}_9@\text{C}$ catalyst. Reaction tests were carried out at 180 °C under an initial H_2 pressure of 1.8 MPa for 24-360 h. The ratio between the amount of metal and the amount of reactant in the reactor was fixed at 0.2 $\text{g}_{\text{Cu}}/\text{g}_{\text{Erythritol}}$.

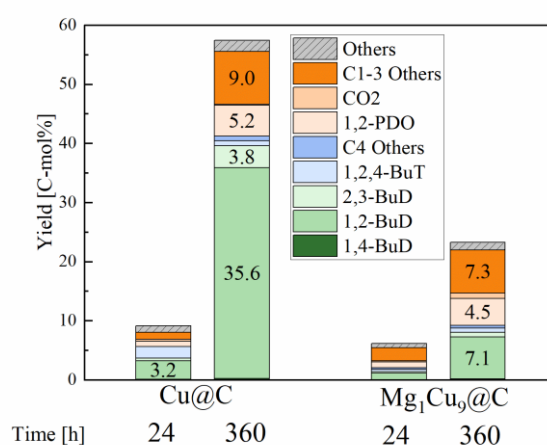


Figure 4.4: Effect of Mg addition on product yields. (Reactant: 30 g of 15 wt% aqueous erythritol solution, catalyst loading: 0.2 $\text{g}_{\text{Cu}}/\text{g}_{\text{erythritol}}$, reaction temperature: 180 °C, reaction time: 24-360 h, initial H_2 pressure: 1.8 MPa)

Study on Hydrodeoxygenation of Biomass-Derived Polyols to Value-Added Chemicals on Carbon-Supported Metal Catalyst
Weican Wang

Table 4.2: Erythritol conversion, yield of products, selectivity of products, and carbon balance over Cu@C and Mg₁Cu₉@C. (Reactant: 20 g of 15 wt% erythritol aqueous solution, catalyst loading: 0.2 g_{Metal}/g_{Erythritol}, initial H₂ pressure: 1.8 MPa, reaction temperature: 180 °C, reaction time: 24-360 h)

Catalyst		Cu@C		Mg ₁ Cu ₉ @C	
Reaction time [h]		24	360	24	360
$X_{\text{erythritol}}$ [C-mol%] ^{*a}		8.27	52.27	5.01	18.75
Epimerization					
Y_{threitol} [C-mol%]		42.19	31.81	12.59	22.20
Hydrodeoxygenation					
Breakdown of products	Y_{HDO} [C-mol%]	5.64	41.28	2.07	9.26
	1,2,4-BuT	1.95	0.83	0.41	0.73
	1,2,3-BuT	0	0	0.22	0.46
	1,2-BuD	3.16	35.63	1.15	7.09
	2,3-BuD	0.41	3.77	0.27	0.78
	1,4-BuD	0.11	0.26	0.02	0.19
	Butanols ^{*b}	0	0.65	0	0.01
	Butane	0.01	0.14	0	0
Cracking					
Breakdown of products	Y_{cracking} [C-mol%]	1.52	9.13	2.45	8.23
	Glycerol	0.13	1.93	0	0.23
	1,2-PrD	0.92	5.20	0.97	4.54
	Ethylene glycol	0.06	1.52	0.95	2.18
	C1-3 alcohols ^{*c}	0.06	0.30	0.32	0.37
	C1-3 alkanes ^{*d}	trace	trace	trace	trace
	CO ₂	0.35	0.18	0.21	0.91
$Y_{\text{Unknown products}}$ [C-mol%] ^{*e}		1.11	1.86	0.65	1.26
Y_{BuD} [C-mol%]		3.68	39.66	1.44	8.06
S_{HDO} [C-mol%]		68.2	79.0	41.3	49.4
S_{BuD} [C-mol%]		44.5	75.9	28.7	43.0
Carbon balance [%]		90.3	94.6	81.9	91.6

*a Threitol was regarded as an unconverted reactant

*b Sum of yields of 1-butanol and 2-butanol

*c Sum of yields of 1-propanol, 2-propanol, ethanol, and methanol

*d Sum of yields of propane, ethane, and methane

*e Unidentified products observed by GC-FID

As shown in **Figure 4.4** and **Table 4.2**, $\text{Mg}_1\text{Cu}_9@\text{C}$ exhibited catalytic activity against erythritol HDO. The erythritol conversion reached 5.01 and 18.75 C-mol% after 24 and 360 h of reaction, respectively. The major HDO products were butanetriols (BuT) and butanediols (BuD). In the 360 h reaction, the yield of the HDO products increased in the following order: 1,2-BuD (7.09 C-mol%) > 2,3-BuD (0.78 C-mol%) > 1,2,4-BuT (0.73 C-mol%) > 1,2,3-BuT (0.46 C-mol%) > 1,4-BuD (0.19 C-mol%). Other HDO products (butanols and butane) were also obtained. These results demonstrated that $\text{Mg}_1\text{Cu}_9@\text{C}$ was able to selectively remove -OH groups in erythritol to produce value-added C4 diols.

However, the conversion of erythritol over $\text{Mg}_1\text{Cu}_9@\text{C}$ was considerably lower than that over $\text{Cu}@\text{C}$ catalyst. After 360 h of reaction, $X_{\text{Erythritol}}$ over $\text{Mg}_1\text{Cu}_9@\text{C}$ only reached 18.75 C-mol% while $X_{\text{Erythritol}}$ over $\text{Cu}@\text{C}$ was 52.27 C-mol%. Compared to the HDO product yield obtained over the $\text{Cu}@\text{C}$ catalyst, the HDO product yield decreased from 41.28 to 9.45 C-mol% over the $\text{Mg}_1\text{Cu}_9@\text{C}$ catalyst after 360 h of reaction. The difference in the effects of the addition of Mg on the catalytic performance of HDO C3 and C4 polyols was also supported by the distribution of the cracking product over $\text{Cu}@\text{C}$ and $\text{Mg}_1\text{Cu}_9@\text{C}$. In the 360-h reaction test over $\text{Cu}@\text{C}$, the yields of major cracking products increased in the following order: 1,2-PrD (5.20 C-mol%) > glycerol (1.93 C-mol%) > EG (1.52 C-mol%). In the case of $\text{Mg}_1\text{Cu}_9@\text{C}$, this order was changed to 1,2-PrD (4.54 C-mol%) > EG (2.18 C-mol%) > glycerol (0.23 C-mol%). The lower yield of glycerol and higher yield of 1,2-PrD over $\text{Mg}_1\text{Cu}_9@\text{C}$ were probably due to the higher ability of $\text{Mg}_1\text{Cu}_9@\text{C}$ to convert glycerol to 1,2-PrD compared with $\text{Cu}@\text{C}$. A possible explanation for the opposite effect of Mg addition on the HDO of C3 and C4 polyols is that the main reaction mechanisms are different between the C3 and C4 HDO over these catalysts. As discussed in **Chapter 3**, the HDO of C3 polyol possibly follows the dehydration-hydrogenation mechanism, which is more favored over bimetallic $\text{MgCu}@\text{C}$ catalysts. In the case of C4 HDO, this process may be less favored when Mg was added to the Cu catalyst. Therefore, $\text{Cu}@\text{C}$ was considered a more effective catalyst for C4 HDO and was selected for further investigation of HDO of erythritol.

4.3.3 Optimization of the C4 polyol HDO reaction conditions over Cu@C

4.3.3.3 Effects of hydrogen pressure on C4 polyol HDO over Cu@C

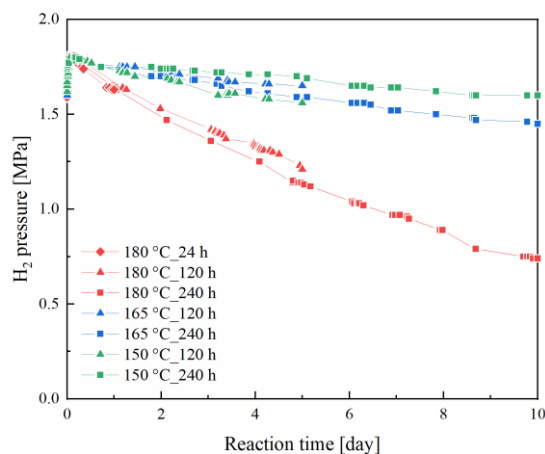


Figure 4.5: Hydrogen pressure change during the erythritol HDO over Cu@C.

Because the HDO of erythritol was carried out in a batch reactor, the hydrogen pressure widely changed with reaction time, as shown in **Figure 4.5**. To understand the reaction pathway of erythritol HDO, the effect of H₂ pressure must be determined. Thus, the effect of initial hydrogen pressure on the product yield and selectivity for the erythritol HDO reaction over Cu@C was investigated. The hydrogen pressure ranged from 0.3 to 1.8 MPa, and the selected ratio of the amount of metal in the catalyst to the amount of reactant was 0.2 g_{Cu}/g_{erythritol}. For all the experiments, the hydrogen gas remained after 24 h reaction; hence, the erythritol reaction proceeded throughout the reaction period.

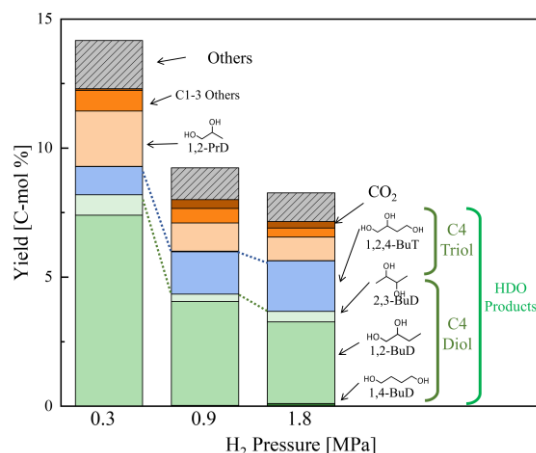


Figure 4.6: Effect of H₂ pressure on product yields. (Reactant: 30 g of 15 wt% aqueous erythritol solution, catalyst loading: 0.2 g_{Cu}/g_{erythritol}, reaction temperature: 180 °C, reaction time: 24 h, initial H₂ pressure: 0.3–1.8 MPa)

As shown in **Figure 4.6**, the erythritol conversion and the yield of HDO product were 14.2 C-mol% and 9.3 C-mol%, respectively, at an initial pressure of 0.3 MPa and 9.2 C-mol% and 6.0 C-mol% at H₂ pressures above 0.9 MPa. The slight decrease in erythritol conversion with H₂ pressure can also be attributed to the competitive adsorption of erythritol and hydrogen, which is consistent with the finding of C₃ HDO over Cu@C in **Chapter 3**. Because the prepared Cu@C catalyst only possess Cu sites, the competitive adsorption of H₂ and erythritol could be observed for Cu@C. Moreover, the HDO product selectivity was almost constant (65 to 68 C-mol%) with H₂ pressure, suggesting that HDO and the cracking reactions of erythritol proceeded in parallel. Therefore, the effect of H₂ pressure on the selectivity of erythritol conversion was almost negligible under the reaction conditions tested. In this regard, the reaction pathway and the mechanism of C₄ HDO could be discussed on the basis of the change in product yield with reaction time.

Given these points, high hydrogen pressure is not preferred to improve the C₄ HDO reaction rate due to competitive adsorption over Cu sites. However, to achieve high HDO product yield, higher hydrogen pressure is still necessary to guarantee hydrogen supply. Thus, a H₂ pressure 1.8 MPa was applied for the further investigation of C₄ HDO.

4.3.3.2 Effects of reaction temperature and time C4 polyol HDO over Cu@C

The HDO of erythritol over Cu@C produced not only BuDs but also BuTs and C1–C3 products. The HDO reactions can proceed in series and the HDO products can participate in cracking reactions. Therefore, the reaction temperature and reaction time are key parameters that affect the HDO yield. To investigate the effects temperature and reaction time on erythritol conversion and product selectivity, the HDO of erythritol over Cu@C was carried out at 150, 165, and 180 °C, and the reaction time was systematically varied from 24 to 240 h. The amount of catalyst in the reactor was set at 0.2 g_{Cu}/g_{erythritol} and the initial H₂ pressure was fixed at 1.8 MPa.

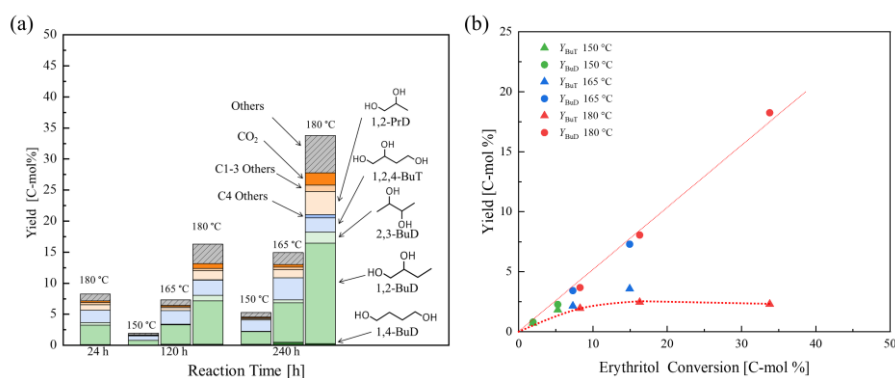


Figure 4.7: (a) Effect of reaction temperature and time on erythritol conversion, BuD yield, and selectivity. (b) Product yield against erythritol conversion over Cu@C. (Reactant: 30 g of 15 wt% aqueous erythritol solution, catalyst loading: 0.2 g_{Cu}/g_{erythritol}, reaction temperature: 150–180 °C, reaction time: 24–240 h, initial H₂ pressure: 1.8 MPa)

As shown in **Figure 4.7**, increasing the reaction temperature and reaction time significantly increased the conversion of erythritol. The erythritol conversions at 150, 165, and 180 °C were respectively 1.9, 7.3, and 16.3 C-mol% at 120 h and 5.3, 14.9, and 33.8 C-mol% at 240 h. The HDO product selectivity was almost constant with time at each reaction temperature, suggesting that the HDO and the cracking reactions proceeded in parallel. The HDO product selectivity increased with a decrease in the reaction temperature, indicating that the activation energy of the HDO reaction was smaller than that of the C-C bond cleavage reaction and that the HDO reaction was favored at lower reaction temperatures. The relationship between reaction temperature and selectivity was in

good agreement with the finding in **Chapter 3** and the previously reported results for glycerol HDO over other Cu catalysts [5]. The TOF values were ranged from 0.08–1.7 h⁻¹ and increased with the reaction temperature. The TOF value of erythritol HDO at catalyst loading of 0.2 g_{Cu}/g_{erythritol} and 180 °C for 24 h (1.7 h⁻¹) was smaller than that at catalyst loading of 0.2 g_{Cu}/g_{erythritol} and same reaction temperature and time (4.0 h⁻¹). This difference in the TOF value could be because the diffusion resistance of the reactants to the Cu surface of Cu@C affected the reaction rate. The majority of the Cu metal of Cu@C was inside the micropores, and the reactants could access the Cu surface from the bulk aqueous phase through small pores slowly.

Focusing on the selectivity of the HDO products, the BuD selectivity increased with the reaction time, whereas the BuT selectivity was almost constant at erythritol conversions above 20 C-mol%, as shown in **Figure 4.7(b)**. Butanols and butane were produced with low yields as shown in **Table 4.3**. These results indicated that the HDO of erythritol to BuT and HDO of BuT to BuD proceeded sequentially, while further HDO of BuD to butanol hardly proceeded, which was attributed to the reaction mechanism of HDO. Detail discussions of the reaction pathways and mechanisms of C4 polyol are given in **Section 4.3.4**.

We finally achieved 39.66 C-mol% BuD yield from erythritol over Cu@C catalyst at 180 °C and 1.8 MPa H₂ for 360 h. The prepared Cu@C catalyst exhibited high BuD selectivity (> 40 C-mol%) for all reaction conditions, which was ascribed to the smaller metal particle size of Cu and the inert carbon support (absence of active sites for side reactions). The obtained BuD selectivity was higher than that reported in the literature using Cu based catalyst (38.6 C-mol% for Cu/CaO-Al₂O₃, reaction temperature 230 °C, and hydrogen pressure at 2.8 MPa [6]), which could be because of the use of inert carbon support. On the other hand, the obtained 1,2-butanediol (16.2 C-mol%) was still lower than that obtained by using ReO_x-Pd/CeO₂ catalyst and 1,4-dioxane solvent (77 C-mol% [7]) and further optimization of the reaction condition and improvement of Cu@C catalyst to accelerate the access of the reactants to Cu surface are still needed.

Table 4.3: Effect of reaction temperature on erythritol conversion, yield of products, BuD and HDO selectivity, TOF and carbon balance over Cu@C. (Reactant: 30 g of 15 wt% erythritol aqueous solution, catalyst loading: 0.2 g_{Cu}/g_{erythritol}, initial H₂ pressure: 1.8 MPa)

Temperature[°C]		150		165		180		
Time [h]		120	240	120	240	24	120	240
$X_{\text{erythritol}}$ [C-mol%] ^{*a}		1.94	5.26	7.30	14.94	8.27	16.29	33.79
Epimerization								
Y_{threitol} [C-mol%]		37.17	50.04	46.36	49.25	42.19	37.78	34.22
Hydrodeoxygenation								
Y_{HDO} [C-mol%]		1.53	4.09	5.58	10.89	5.64	10.55	21.06
Breakdown of products	1,2,4-BuT	0.72	1.82	2.15	3.58	1.96	2.46	2.31
	1,2,3-BuT	0	0	0	0	0	0	0
	1,2-BuD	0.76	2.02	3.15	6.34	3.16	6.99	16.19
	2,3-BuD	0.00	0.07	0.13	0.46	0.41	0.92	1.78
	1,4-BuD	0.04	0.18	0.15	0.50	0.11	0.15	0.28
	Butanols ^{*b}	0	0	0	0	0	0	0.35
	Butane	0.01	0.00	0.01	0.01	0.01	0.03	0.15
Cracking								
Y_{cracking} [C-mol%]		0.17	0.43	0.83	2.09	1.51	2.60	6.71
Breakdown of products	Glycerol	0	0.06	0.10	0.20	0.13	0.18	0.25
	1,2-PrD	0.05	0.17	0.48	1.30	0.92	1.46	3.71
	Ethylene glycol	0	0	0	0.04	0.06	0.46	1.41
	C1-3 alcohols ^{*c}	0.02	0.08	0.07	0.16	0.06	0.10	0.32
	C1-3 alkanes ^{*d}	0.00	0.00	0.00	0.00	0.00	0.00	0.00
	CO ₂	0.09	0.12	0.17	0.39	0.35	0.39	1.01
Y_{others} [C-mol%] ^{*e}		0.24	0.73	0.89	1.96	1.11	3.15	6.02
Y_{BuD} [C-mol%]		0.72	2.27	3.43	7.30	3.68	8.06	18.25
S_{HDO} [C-mol%]		78.8	77.8	76.5	72.9	68.2	64.7	62.3
S_{BuD} [C-mol%]		41.5	43.2	47.0	48.8	44.5	49.5	54.0
TOF [h ⁻¹]		0.08	0.11	0.30	0.31	1.71	0.67	0.70
CB [C-mol%]		102.2	84.6	94.2	85.2	90.3	85.7	80.9

*a Threitol was regarded as unconverted reactant

*b Sum of yields of 1-butanol and 2-butanol

*c Sum of yields of 1-propanol, 2-propanol, ethanol, and methanol

*d Sum of yields of propane, ethane, and methane

*e Unidentified products observed by GC-FID

4.3.4 Insight into the erythritol HDO pathway and mechanism over Cu@C.

To gain a deeper understanding of the erythritol conversion over the Cu@C catalyst, an investigation of the reaction pathway and mechanism was undertaken. Focusing on the HDO reaction of erythritol to BuDs, the reaction proceeded in series via BuTs. To elucidate the successive HDO reactions, we plotted the yields of BuTs and BuDs against erythritol conversion. As shown in **Figure 4.7(b)**, the yield of BuTs increased with increasing erythritol conversion to 15 C-mol% and then decreased slightly. In contrast, the BuD yield monotonically increased with erythritol conversion. These trends in the yield against the conversion were generally observed in series reactions in which erythritol was first converted to BuTs as an intermediate and then BuTs were further converted to BuDs as the final product. Only a small amount of butanol was obtained during the erythritol conversion at 180 °C and 1.2 MPa H₂ for 240 h, suggesting that BuDs were stable under the reaction conditions tested over Cu@C; therefore, BuDs behaved as the final product of the successive HDO of erythritol.

The detailed HDO reaction network of erythritol over Cu@C was investigated. During the HDO of erythritol, three types of BuDs, 1,2-BuD, 2,3-BuD, and 1,4-BuD were produced. To elucidate which reaction pathway mainly proceeded to form BuDs in erythritol HDO over Cu@C, HDO reactions of 1,2,4-BuT and 1,2,3-BuT were carried out over Cu@C at 180 °C and 1.8 MPa H₂ for 24 h. As shown in **Figure 4.8**, the conversions reached approximately 10 C-mol% for erythritol, 1,2,3-BuT, and 1,2,4-BuT after 24 h. 1,2-BuD and 1,4-BuD were mainly obtained from 1,2,4-BuT, and 1,2-BuD and 2,3-BuD were mainly obtained from 1,2,3-BuT. Formation of 1,3-BuD was not observed with either reactant.

Study on Hydrodeoxygenation of Biomass-Derived Polyols to Value-Added Chemicals on Carbon-Supported Metal Catalyst
Weican Wang

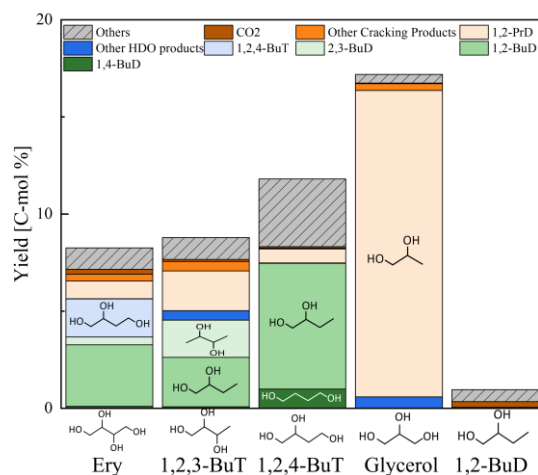


Figure 4.8: Product yields for the HDO of erythritol and 1,2,3-BuT, 1,2,4-BuT, glycerol, and 1,2-PrD over Cu@C. (Reactant solution: 30 g and 15 wt%, catalyst loading: 0.2 g_{Cu}/g_{Substrate}, reaction temperature: 180 °C, reaction time: 24 h, initial H₂ pressure: 1.8 MPa)

The presence of 2,3-BuD in erythritol HDO indicates the formation of 1,2,3-BuT as an intermediate, although it was not detected. Therefore, the amount of 1,2,3-BuT produced from erythritol was likely small, and 1,2,3-BuT was almost completely converted to BuDs in the HDO of erythritol. The selectivity of 2,3-BuD (5.0 C-mol%) from erythritol was smaller than that from 1,2,3-BuT (16.3 C-mol%). Therefore, the formation of 1,2,4-BuT was more likely than 1,2,3-BuT from erythritol over Cu@C. Because 1,2-BuD was formed with high selectivity (54.1 C-mol%) from 1,2,4-BuT, 1,2-BuD was the main BuD product from erythritol. Furthermore, the HDO of glycerol and 1,2-PrD was performed under the same conditions as that of BuT. The HDO of 1,2-PrD slightly proceeded over Cu@C, and the high conversion of glycerol was attributed to the smaller molecule size of glycerol that could more easily access the Cu surface. In summary, the HDO reaction network is illustrated in **Figure 4.9**. The main HDO reaction of erythritol over Cu@C was the production of 1,2-BuD via 1,2,4-BuT.

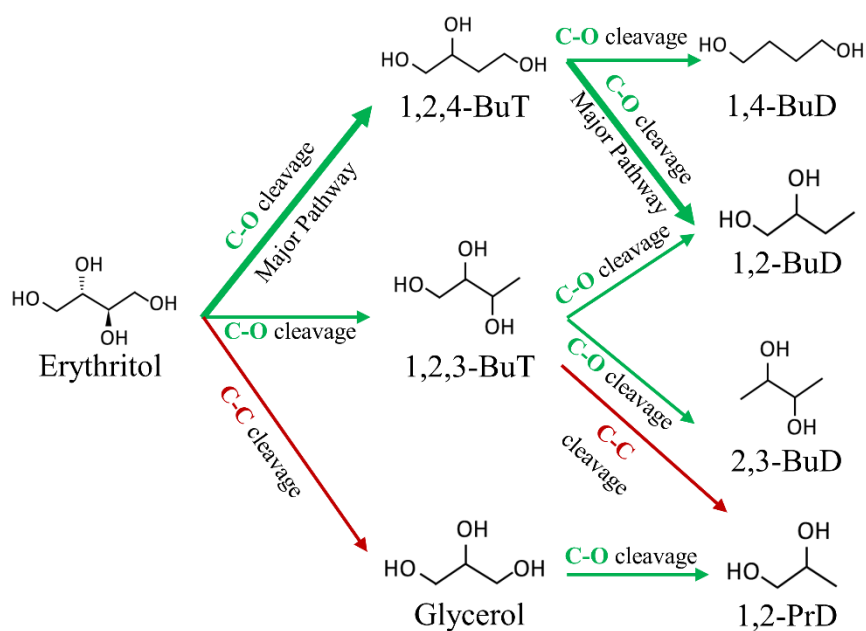


Figure 4.9: Reaction network of erythritol HDO over Cu@C.

As the reaction network was confirmed, the HDO reaction mechanism was finally investigated. Most HDO products from erythritol and glycerol over Cu@C possessed vicinal hydroxyl groups, except for 1,4-BuD, and the HDO of diols rarely proceeded. The HDO of polyols are generally explained by the dehydration-hydrogenation mechanism and the dehydrogenation-dehydration-hydrogenation mechanism as discussed in **Chapter 3**. These reaction mechanisms can explain that the formation of 1,2,4-BuT is more likely to occur as the protonated intermediate of 1,2,4-BuT is more stable and likely to form than that of 1,2,3-BuT. However, these mechanisms cannot explain the selective production of 1,2-BuD from 1,2,4-BuT. In addition to the finding that the addition of Mg to Cu@C showed opposite effects on HDO of C3 and C4 polyols, we envisaged that the HDO reaction of C4 polyols follows different mechanisms with HDO of C3 polyol.

In this work, we suggest that the vicinal hydroxyl groups in erythritol were involved in a stable adsorption state on the Cu surface, and the HDO reaction proceeded between the hydroxyl groups that were not involved in the adsorption and the hydrogen atoms on the Cu metal surface. Kühne et al. proposed a similar reaction pathway for the HDO of mannitol over Raney Cu in which the main

products were hexanetriols and hexanetraols possessing terminal vicinal hydroxyl groups [8]. The following HDO reaction mechanism was concluded: Two adjacent hydroxyl groups in the reactant were adsorbed on the Cu metal surface to form a stable adsorption state, and the hydroxyl groups that were not involved in the adsorption reacted with the hydrogen atoms on the Cu surface. In this mechanism, neither HDO nor cracking of the hydroxyl groups involved in the adsorption on the Cu surface proceeded. Although a detailed investigation is still necessary to confirm the reaction mechanism of the HDO over Cu surface, we considered that the mechanism reported by Khüne et al. could be applied to our reaction because of the similarities in the reactants and catalysts. The difference in selectivity between 1,2,3-BuT and 1,2,4-BuT was likely due to the proximity between the adsorbed hydroxyl groups on the Cu surface and those involved in the HDO reaction. Because of the small pore size of the prepared Cu@C, the terminal vicinal hydroxyl groups were able to access the Cu metal surface more easily than the internal vicinal hydroxyl groups.

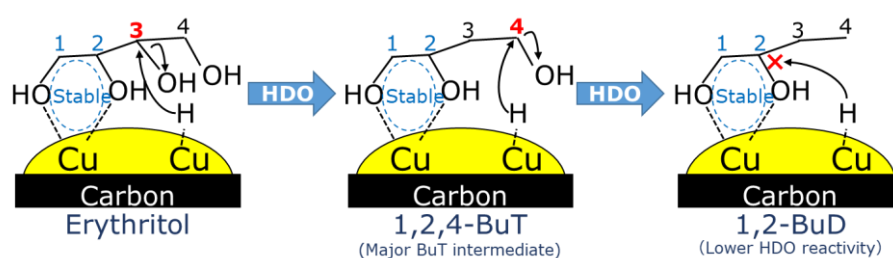


Figure 4.10: Reaction mechanism of C4 HDO over Cu@C. The major reaction pathway was the production of 1,2-BuD from erythritol via 1,2,4-BuT.

Based on the principles above, the reaction between the hydroxyl groups adjacent to those adsorbed on the Cu metal surface and the hydrogen atoms was more likely, resulting in a higher selectivity for 1,2,4-BuT from erythritol than that for 1,2,3-BuT. Similarly, the selectivity for 1,2-BuD was greater than that for 2,3-BuD due to the higher accessibility of the terminal vicinal hydroxyl groups compared to that of the internal hydroxyl groups. From 1,2,4-BuT, 1,2-BuD was selectively formed because the adsorption state of 1,2,4-BuT was limited to the 1- and 2-hydroxyl groups at adjacent positions. The further HDO of 1,2-BuD hardly proceeded because 1,2-BuD did

not possess the hydroxyl groups that were not involved in the stable adsorption state.

In addition to the desired HDO products, 1,2-PrD, CO₂ and a small amount of glycerol were obtained as by-products of erythritol conversion, suggesting that the cleavage of the terminal C-C bond of erythritol proceeded. 1,2-PrD was formed from 1,2,3-BuT with concomitant formation of CO₂ and glycerol, while almost no cracking products were obtained from 1,2,4-BuT. These results suggest that 1,2-PrD can be obtained by HDO and decarbonization of the terminal C-OH moiety of erythritol via 1,2,3-BuT or glycerol. Although the difference between the active sites for HDO and C-C cleavage has not been completely elucidated, one of the possible differences is the Cu surface coordination; the Cu atoms on unsaturated coordination sites (edge, step, and corner) are considered to exhibit Lewis acidity. Hence, we envisaged that the HDO reaction proceeded on the Cu plane surface, while the cleavage of C-C proceeded on the edges of the Cu surface [9,10].

4.4 Conclusion

For the selective HDO of biomass-derived C4 polyols into useful chemicals at low hydrogen pressures, carbon-supported Cu nanoparticle catalysts (Cu@C and MgCu@C) were applied. Among the investigated monometallic Cu-based catalysts, Cu@C prepared from ion-exchange resin showed comparable activity to that of Cu/SiO₂ and significantly higher than Cu/AC and Cu chromite at 180 °C and 1.8 MPa H₂. Furthermore, the size of Cu particles in Cu@C was maintained after the HDO reaction, while the agglomeration of Cu particles was observed for Cu/AC. The higher activity and stability of Cu@C were due to the higher Cu metal surface area and hydrothermal stability, which was likely due to the Cu metal particles embedded in the carbon support.

The effects of reaction conditions on the HDO of erythritol over Cu@C were investigated. The HDO selectivity increased with a decrease in the reaction temperature, whereas the selectivity for BuDs in the HDO products decreased. The higher HDO selectivity at lower reaction temperatures was ascribed to the smaller activation energy of the HDO reaction compared with that of the C-C bond cleavage reaction. A slight decrease in erythritol conversion was observed with an increase in H₂ pressure, suggesting that competitive adsorption of H₂ and erythritol on the Cu surface. While the effect of H₂ pressure on the product selectivity was almost negligible. The highest BuD yield of 39.7 C-mol% was realized for the erythritol conversion over the Cu@C catalyst at 180 °C and 1.2 MPa H₂ for 360 h.

On the contrary of C3 HDO, the addition of Mg to the Cu catalyst showed negative effects on the HDO of C4 polyol. An erythritol conversion of 18.75 C-mol% was achieved over Mg₁Cu₉@C with a selectivity to C4 diols of 43.0 C-mol at 180 °C under 1.2 MPa H₂ after 360 h reaction. The difference effects of Mg addition to Cu catalyst in C3 and C4 polyol HDO indicated that the HDO reactions of C3 and C4 polyol HDO may follow different mechanisms. Thus, the reaction pathway and the mechanisms of HDO of erythritol were examined. In the HDO of erythritol over Cu@C, 1,2-BuD was obtained with the highest yield, which was produced by a sequential HDO via 1,2,4-

Study on Hydrodeoxygenation of Biomass-Derived Polyols to Value-Added Chemicals on Carbon-Supported Metal Catalyst

Weican Wang

BuT. The BuDs with vicinal hydroxyl groups were favorably formed over the prepared Cu@C because the vicinal hydroxyl groups in the reactant were adsorbed on the Cu plain surface to form a stable adsorption state, and cleavage of the closest C-O bond was more likely to occur, as reported in the literature [6].

References

- [1] Y. Nakagawa, T. Kasumi, J. Ogihara, M. Tamura, T. Arai, K. Tomishige, Erythritol: Another C4 Platform Chemical in Biomass Refinery, *ACS Omega*. 5 (2020) 2520–2530. <https://doi.org/10.1021/acsomega.9b04046>.
- [2] K. Tomishige, Y. Nakagawa, M. Tamura, Production of Diols from Biomass, in: Z. Fang, R.L. Smith, X. Qi (Eds.), *Prod. Platf. Chem. Sustain. Resour.*, Springer Singapore, Singapore, 2017: pp. 343–373. https://doi.org/10.1007/978-981-10-4172-3_11.
- [3] H. Gräfe, W. Körnig, H.-M. Weitz, W. Reiß, G. Steffan, H. Diehl, H. Bosche, K. Schneider, H. Kieczka, Butanediols, Butenediol, and Butynediol, in: *Ullmanns Encycl. Ind. Chem.*, American Cancer Society, 2000. https://doi.org/10.1002/14356007.a04_455.
- [4] E.S. Vasiliadou, A.A. Lemonidou, Glycerol transformation to value added C3 diols: reaction mechanism, kinetic, and engineering aspects, *WIREs Energy Environ.* 4 (2015) 486–520. <https://doi.org/10.1002/wene.159>.
- [5] T. Gabrysch, M. Muhler, B. Peng, The kinetics of glycerol hydrodeoxygenation to 1,2-propanediol over Cu/ZrO₂ in the aqueous phase, *Appl. Catal. Gen.* 576 (2019) 47–53. <https://doi.org/10.1016/j.apcata.2019.03.001>.
- [6] X. Jin, J. Shen, W. Yan, M. Zhao, P.S. Thapa, B. Subramaniam, R.V. Chaudhari, Sorbitol Hydrogenolysis over Hybrid Cu/CaO-Al₂O₃ Catalysts: Tunable Activity and Selectivity with Solid Base Incorporation, *ACS Catal.* 5 (2015) 6545–6558. <https://doi.org/10.1021/acscatal.5b01324>.
- [7] N. Ota, M. Tamura, Y. Nakagawa, K. Okumura, K. Tomishige, Performance, Structure, and Mechanism of ReO_x-Pd/CeO₂ Catalyst for Simultaneous Removal of Vicinal OH Groups with H₂, *ACS Catal.* 6 (2016) 3213–3226. <https://doi.org/10.1021/acscatal.6b00491>.
- [8] B. Kühne, H. Vogel, R. Meusinger, S. Kunz, M. Kunz, Mechanistic study on –C–O– and –C–C– hydrogenolysis over Cu catalysts: identification of reaction pathways and key intermediates, *Catal. Sci. Technol.* 8 (2018) 755–767. <https://doi.org/10.1039/C7CY02426F>.
- [9] N. Scotti, E. Finocchio, C. Evangelisti, M. Marelli, R. Psaro, N. Ravasio, F. Zaccheria, Some insight on the structure/activity relationship of metal nanoparticles in Cu/SiO₂ catalysts, *Chin. J. Catal.* 40 (2019) 1788–1794. [https://doi.org/10.1016/S1872-2067\(19\)63392-9](https://doi.org/10.1016/S1872-2067(19)63392-9).
- [10] N. Scotti, M. Dangate, A. Gervasini, C. Evangelisti, N. Ravasio, F. Zaccheria, Unraveling the Role of Low Coordination Sites in a Cu Metal Nanoparticle: A Step toward the Selective Synthesis of Second Generation Biofuels, *ACS Catal.* 4 (2014) 2818–2826. <https://doi.org/10.1021/cs500581a>.

5. Conclusions and perspectives

The scope of this thesis is the investigation of the heterogeneously catalytic hydrodeoxygenation (HDO) of biomass-derived polyols in the aqueous phase under high pressure hydrogen. This catalytic process is very promising for the production of value-added chemicals from renewable biomass-derived feedstocks. The conversion of biomass-derived polyols requires catalysts with high activity, high selectivity, and cheap price, which can be met by the Cu-based catalysts. However, Cu-based catalysts face challenges of low metal dispersion and low stability caused by metal sintering. Thus, the development of a catalytic HDO process with improved Cu catalysts would be a significant breakthrough for the use of renewable feedstocks.

For this purpose, novel carbon-supported Cu catalysts (Cu@C and MgCu@C) were synthesized by using the ion-exchange method. The characteristics of these catalysts were studied and compared with reference catalysts prepared from the impregnation method.

- Cu@C catalysts showed high metal loading (>60 wt%) and high metal dispersion ($d_{\text{TEM}} = 14.9 \text{ nm}$), and high sintering resistance.
- Bimetallic MgCu@C catalysts possessed even higher metal dispersion ($d_{\text{TEM}} < 15 \text{ nm}$) and sintering resistance than Cu@C due to the Mg^{2+} species in the catalyst preventing dissociation and surface diffusion of Cu atoms during preparation.
- Cu/AC, Cu/SiO₂, and Cu/Al₂O₃ prepared by impregnation method showed lower metal dispersion than Cu@C and MgCu@C due to the agglomeration of Cu particles during the preparation and pretreatment processes.

The prepared catalysts were then applied for the conversion of biomass-derived C3-4 polyols.

The major conclusions are summarized in Table 5.1.

Table 5.1: Major result and conclusion of Chapter 3 and Chapter 4.

	Chapter 3	Chapter 4
Catalyst		
Catalyst support	Carbon (Highly inert, avoid side reaction on support)	
Active metal	Cu	
Additive metal	Mg	
Optimized Cu/M ratio	9/1 mol/mol	1/0 mol/mol (No addition)
Reaction configuration		
Reactor	Batch reactor	
Reactant	Glycerol	Erythritol
Temperature	150-180 °C	
H ₂ pressure	0.6-1.2 MPa	0.3-1.8 MPa
Reaction results		
Main HDO product	1,2-PrD	1,2-BuD
Reaction pathway	Via hydroxyacetone	Via 1,2,4-BuT
Reaction mechanism	Dehydration-hydrogenation	S _N 2-like
Effect of Mg addition	Positive (Promote dehydration)	Negative (Possible due to the change to a less favored reaction mechanism)

For both case of C3 and C4 HDO, catalytic performances were studied and optimized by variations of reaction temperature, reaction time, and H₂ pressures. Based on the experimental results of this work the following characteristics of the applied catalysts are presented in the case of C3 and C4 polyols HDO, respectively:

C3 polyol (glycerol) HDO:

- Cu@C showed high activity and selectivity for HDO of C3 polyol, which can be attributed to the high metal dispersion and inert carbon support without active sites for side reactions.
- Increasing reaction temperature in the range of 150-180 °C improved C3 polyol conversion without obvious decreasing of selectivity. Increasing hydrogen pressure suppress the conversion of glycerol due to the competitive adsorption of H₂ and glycerol

over Cu sites.

- The addition of Mg to Cu@C catalysts significantly improved the catalytic performance by promoting the dehydration step at the introduced base sites. The maximum glycerol conversion was achieved over Mg₁Cu₉@C at 94.0% C-mol with 94.2% C-mol selectivity toward 1,2-PrD o at 180 °C under 1.2 MPa H₂ for 240 h.
- The HDO of glycerol follows the dehydration-hydrogenation mechanism. Glycerol is firstly converted to hydroxyacetone and then hydrogenated to 1,2-PrD. The rate-determining step is dehydration reaction, which can be promoted by enhancing the basicity of catalyst derived from Mg species.

C4 polyol (erythritol) HDO:

- Prepared Cu catalysts showed activity to produce C4 diols with vicinal -OH groups from erythritol via HDO. Cu@C exhibited a erythritol conversion of 52.3 C-mol% and a selectivity towards butanediols of 43.0 C-mol% at 180 °C under 1.8 MPa H₂ for 360 h.
- Similar to the C3 polyol HDO, increasing reaction temperature and decreasing hydrogen pressure were found to be effective to improve conversion.
- Mg₁Cu₉@C catalyst showed considerably lower activity for C4 erythritol HDO than Cu@C catalyst. A possible explanation for the opposite effect of Mg addition on the HDO of C3 and C4 polyols is that the main reaction mechanisms are different between the C3 and C4 HDO over these catalysts.
- We proposed that butanediols with vicinal hydroxyl groups were favorably formed over Cu catalysts because the vicinal hydroxyl groups in the reactant were adsorbed on the Cu plain surface to form a stable adsorption state, and cleavage of the closest C-O bond was more likely to occur.

The results of this work demonstrate the feasibility of converting biomass-derived polyol feedstocks to value-added chemicals like diols by the development of novel catalysts and optimization of reaction conditions. The combination of results from this work also provides a

fundamental understanding of catalytic materials and reaction mechanisms of HDO conversion.

This work also shows a major challenge need to be solved to achieve higher HDO product yield. This challenge is the hydrogen supply during reaction in the batch reactor. The HDO reactions over Cu-based catalysts are inhibited under high hydrogen pressure due to the competitive adsorption of H_2 and polyols in aqueous phase, while high hydrogen pressure is required to achieve higher maximum conversion. Thus, this tradeoff between reaction rate and conversion should be taken into consider when using the batch reactor configuration. To solve this problem and achieve both high reaction rate and conversion, modification of reactor configuration can be applied. A gas-liquid solid flow reactor can be a promising candidate(**Figure 5.1**). In this configuration, catalysts are fixed in a flow reactor and continually contact with gas bubbles and liquid flows, making the following ideas possible:

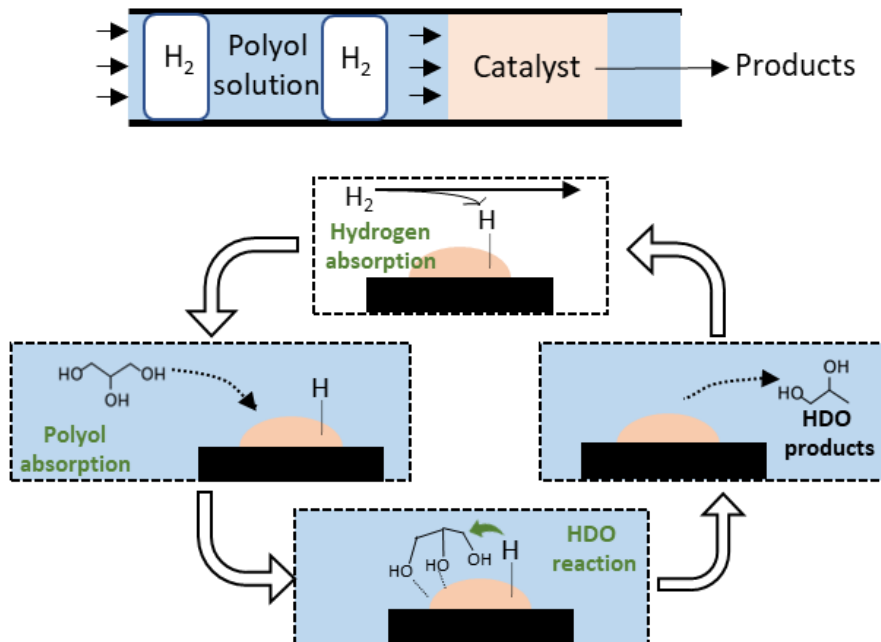


Figure 5.1: Proposed gas-liquid slug flow fixed bed reactor.

- Continuous configuration can ensure the hydrogen supply throughout the reaction as well as keeping the catalyst stability.

Study on Hydrodeoxygenation of Biomass-Derived Polyols to Value-Added Chemicals on Carbon-Supported Metal Catalyst
Weican Wang

- The absorption of hydrogen on catalyst surface occurs in gas bubbles, which provides high H₂ availability under relatively low hydrogen pressure and make it possible to avoid using high operation pressure to solve hydrogen in aqueous phase.
- The competitive adsorption of H₂ and polyol in aqueous phase can be inhibited due to the low hydrogen pressure applied. HDO reaction occurs on catalyst surface in aqueous phase to produce desired HDO products.
- Catalyst repeatedly contacts gas bubbles and liquid flow, promoting the conversion process towards higher polyol conversion.
- Continuous gas-liquid solid slug flow configuration provides a broad range of flow conditions in two-phase flow, which allows the fine tuning of gas and liquid flows to achieve optimal conversions of polyols.

Other methods such as using in situ generated H₂ are also possible options to address higher conversion efficiency. Ultimately, this deeper understanding can be used to inform the design of the next, allowing the field to advance more quickly toward goals such as making large-scale biorefining a reality.

6. Appendix: Effects of active metal species on C3 polyol HDO

6.1 Experimental

6.1.1 Materials

All chemicals were used without further purification. $\text{Cu}(\text{NO}_3)_2 \cdot 3\text{H}_2\text{O}$ (98%), $\text{Ni}(\text{NO}_3)_2 \cdot 6\text{H}_2\text{O}$ (98%), $\text{Co}(\text{NO}_3)_2 \cdot 6\text{H}_2\text{O}$ (98%), and $\text{Mg}(\text{NO}_3)_2 \cdot 6\text{H}_2\text{O}$ (98%), glycerol (97%), and ammonia aqueous solution (28wt%) were purchased from FUJIFILM Wako Pure Chemical Ltd., Japan. DIAION WK-11 ion exchange resin (weakly acidic cation-exchange type, total exchange capacity: 4.3 mEq/g-resin, mean particle size: 620 μm) was purchased from Mitsubishi Chemical Corp., Japan. Activated carbon support (Norit[®] RX3 EXTRA) and $[\text{Ru}(\text{NH}_3)_6]\text{Cl}_2$ (98%) was purchased from Sigma-Aldrich Japan.

6.1.2 Preparation of carbon-supported bimetallic M-Cu (M = Ni, Co, Mg, Zn, Ru) catalysts by using the ion-exchange resin method.

The preparation procedures of bimetallic M-Cu catalyst are generally the same with $\text{MgCu}@C$, as described in Chapter 2. Notably, the ratio of metal ions (Cu^{2+} and M^{2+}) in solution to the theoretical ion exchange capacity of the resin was set at 100% mEq/mEq in the case of Co-Cu, Mg-Cu, Zn-Cu, and Ru-Cu. For Ni-Cu, this ratio was set at 180% mEq/mEq. Moreover, the carbonization temperature of Ru-Cu catalysts was set at 700 °C to reduce Ru ions. The obtained bimetallic catalyst was denoted as $\text{M}_m\text{Cu}_n@C$, where m/n was the nominal molar ratio of M to Cu.

Metal loading, metal ratio, BET surface area, metal particle size, and metal surface area of synthesized bimetallic $\text{MCu}@$ catalysts are presented in **Table 6.1**.

Table 6.1: Properties of the Cu@C and MCu@C catalysts.

Catalyst	Cu@C	Ni ₁ Cu ₁₉ @C	Mg ₁ Cu ₉ @C	Co ₁ Cu ₉ @C	Zn ₁ Cu ₉ @C	Ru ₁ Cu ₉ @C
Cu loading [wt%]	66.9	59.4 ^a	56.5	54.4	51.1 ^a	50.7 ^a
M loading [wt%]	-	2.9 ^a	2.2	5.7	5.8 ^a	9.3 ^a
Cu/M ratio ^b [mol/mol]	-	n.d.	10.3	8.9	n.d.	n.d.
BET surface area [m ² /g _{cat}]	119	n.d.	129	191	129	243
Mean metal particle size; d_{XRD}^c [nm]	17.4	9.8	15.0	14.5	12.2	20.8
d_{TEM} [nm]	14.9	n.d.	12.5	19.5	n.d.	n.d.
Accessible Cu surface area; $S_{N_2O}^d$ [m ² /g]	2.26	n.d.	2.49	7.2	n.d.	n.d.
S_{N_2O} / S_{TEM} [%]	7.5	n.d.	7.3	20.8	n.d.	n.d.

^a Calculated by nominal values

^b Measured by ICP-OES

^c Calculated from XRD diffraction peaks at around 44.3°

^d Calculated by N₂O titration.

6.1.3. Catalytic reaction test

The reaction test procedures using MCu@C catalysts were the same with the case of C3 HDO over Cu@C as described in Chapter 3. Particularly, the reduction pretreatment of RuCu@C catalyst was conducted at 700 °C reduce Ru ions. Reaction conditions were set as follow:

- Reactor: 100 mL batch reactor
- Reactant: 20 g of 15 wt% glycerol aqueous solution
- Catalyst loading: 0.2 g_{metal}/g_{glycerol}
- Initial H₂ pressure: 1.2 MPa at RT
- Reaction temperature: 180 °C
- Reaction time: 24 h

6.2 Results and discussion

Figure 6.1 shows the product yield and selectivity to 1,2-PrD over the prepared monometallic Cu and bimetallic M-Cu (M = Ni, Co, Mg, Zn, Ru) catalysts. The effects of Mg addition were discussed in Chapter 3, which was likely due to the improved metal dispersion, and introduced basic MgO sites that promoting dehydration of glycerol.

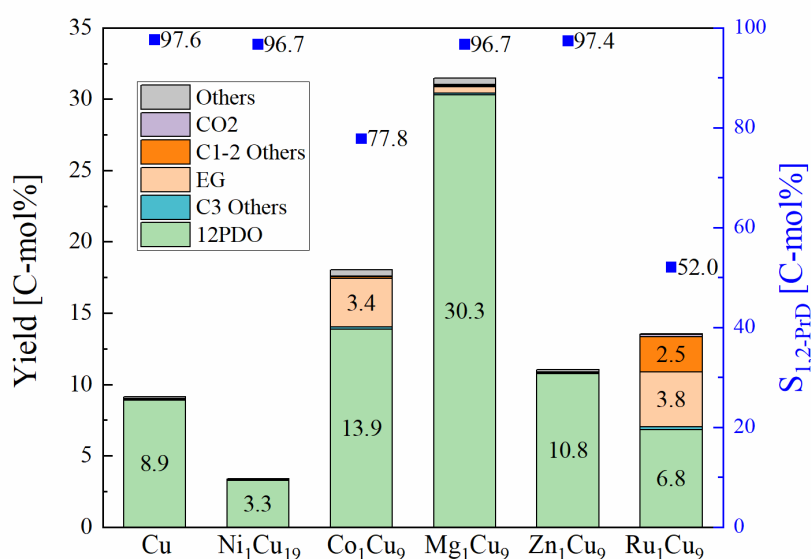


Figure 6.1: Product yields and selectivity to 1,2-PrD with the prepared Cu-based catalysts. (Reactant: 20 g of 15 wt% aqueous glycerol solution; catalyst loading: 0.05 g_{Metal}/g_{glycerol}; reaction temperature: 180 °C; reaction time: 72 h, initial H₂ pressure: 1.2 MPa at RT).

Among other prepared M-Cu bimetallic catalysts, Co-Cu, Zn-Cu, and Ru-Cu bimetallic catalysts showed improved glycerol conversion, and only Ni-Cu catalyst showed decreased catalytic performance. In the case of Ni addition, the yield of 1,2-PrD decreased from 8.9 to 3.3 C-mol%, and the selectivity to 1,2-PrD slightly decreased from 97.6 to 96.7 C-mol%. The negative effects of Ni addition were likely due to the low catalytic activity of Ni atoms to cleavage C-O bonds. It was reported that glycerol dehydration under Ar atmosphere in gas phase will be inhibited when introducing Ni to Cu catalysts, and the product distribution moved to the production of cracking

products [1]. Because the dehydration of glycerol is considered as the rate-determining step of the HDO process, the negative effects of Ni addition were likely due to the inhibited dehydration step of glycerol.

For Co-Cu catalyst, the yield of 1,2-PrD increased from 8.9 to 13.9 C-mol%. The improved conversion and HDO product yield can be ascribed to the enhanced acidity derived from Co oxide species. The hydration of glycerol can be promoted by acid sites, as reported in the literature [2]. However, the enhanced acidity can also cause undesired cracking reactions [3], which lead to lower selectivity towards HDO products.

Over Zn-Cu catalyst, the yield of 1,2-PrD slightly increased to 10.8 C-mol% and the selectivity towards 1,2-PrD maintained at 96.7 C-mol%. Although the characterization data of ZnCu@C was insufficient to conclude the source of this promotion effect, we can propose that the reduced Cu particle size in ZnCu@C was helpful to improve catalytic activity for HDO.

The RuCu@C catalyst was the only catalyst using noble metal in this study. RuCu@C exhibited higher catalytic activity than Cu@C, where glycerol conversion increased from 9.1 C-mol% to approximately 15 C-mol%. However, the selectivity to cracking products significantly increased and the selectivity to desired 1,2-PrD was only 52.0 C-mol%. The phenomena can be explained by the Ru atoms' high activity to cleavage C-C bond, as described above.

In conclusion, the MgCu@C catalyst showed highest catalytic activity and comparable high selectivity to HDO product with original Cu@C. NiCu@C, CoCu@C, and RuCu@C catalysts are not ideal catalysts for polyols HDO due to their low activity and/or selectivity. In this regard, bimetallic MgCu@C catalysts were investigated for the further improvement of polyols conversion processes.

References

- [1] B.C. Miranda, R.J. Chimentão, J. Szanyi, A.H. Braga, J.B.O. Santos, F. Gispert-Guirado, J. Llorca, F. Medina, Influence of copper on nickel-based catalysts in the conversion of glycerol, *Appl. Catal. B Environ.* 166–167 (2015) 166–180. <https://doi.org/10.1016/j.apcatb.2014.11.019>.
- [2] W. Mondach, S. Chanklang, P. Somchuea, T. Witoon, M. Chareonpanich, K. Faungnawakij, H. Sohn, A. Seubsai, Highly efficient TiO₂-supported Co–Cu catalysts for conversion of glycerol to 1,2-propanediol, *Sci. Rep.* 11 (2021) 23042. <https://doi.org/10.1038/s41598-021-02416-7>.
- [3] W. Suprun, M. Lutecki, T. Haber, H. Papp, Acidic catalysts for the dehydration of glycerol: Activity and deactivation, *J. Mol. Catal. Chem.* 309 (2009) 71–78. <https://doi.org/10.1016/j.molcata.2009.04.017>.

List of publications

Partial results of this work have been published, by approval of the Chemical Science and Engineering (represented by Prof. Teruoki Tago), in the following contributions in advance.

Presentations (Presenter)

- (1) W. Wang, K. Nakagawa, H. Fujitsuka, E. Fumoto, T. Yoshikawa, Y. Nakasaka, T. Masuda, T. Tago. Selective production of vicinal-butanediols from erythritol via aqueous phase hydrodeoxygenation over carbon supported Cu catalyst prepared from ion-exchange resin. SCEJ 86th Annual Meeting. K202, Online, Mar. 2021.
- (2) W. Wang, H. Fujitsuka, T. Tago. Improving the selectivity to 1,2-propanediol from glycerol via aqueous phase hydrodeoxygenation by using carbon supported Cu catalyst prepared from ion-exchange resin. 第 128 回触媒討論会, 1J20, Online, Sept. 2021.
- (3) W. Wang, H. Fujitsuka, T. Tago. Hydrodeoxygenation of erythritol over carbon supported Cu catalyst prepared from ion exchange resin. 1st Japan-China Symposium on Catalysis, OP-19, Online, Oct. 2021.
- (4) W. Wang, H. Fujitsuka, T. Tago. Carbon-supported Cu catalyst prepared from ion-exchange resin for selective conversion of glycerol into 1,2-propanediol. 18th Japan-Korea Symposium on Catalysis, Online, Nov. 2021. **(Best presentation award)**

Presentations (Co-author)

- (1) 藤境 大裕, 中川 航司, Wang Weican, 麓 恵里, 吉川 琢也, 中坂 佑太, 増田 隆夫, 多湖 輝興. イオン交換樹脂を前駆体とした炭素担持 Cu 触媒を用いたエリスリトールからのブタンジオール選択合成. 第 126 回触媒討論会, 2I17, Online, Sep. 2020.

Journal Papers

- (1) W. Wang, K. Nakagawa, T. Yoshikawa, T. Masuda, E. Fumoto, Y. Koyama, T. Tago, H. Fujitsuka, Selective aqueous phase hydrodeoxygenation of erythritol over carbon-supported Cu catalyst prepared from ion-exchange resin, *Appl. Catal. Gen.*, **2021**, 619, 118152. <https://doi.org/10.1016/j.apcata.2021.118152> (Chapter 2&3)
- (2) W. Wang, T. Tago, H. Fujitsuka, Hydrodeoxygenation of C3-4 polyols to C3-4 diols over carbon-supported bimetallic MgCu@C catalysts prepared from ion exchange resin, *Catal. Today*, In Press. <https://doi.org/10.1016/j.cattod.2022.06.042> (Chapter 2&4)